Synchronization Stability of Grid-Connected Converters under Grid Faults

Taul, Mads Graungaard

Publication date:
2020

Document Version
Publisher's PDF, also known as Version of record

SYNCHRONIZATION STABILITY OF GRID-CONNECTED CONVERTERS UNDER GRID FAULTS

BY
MADS GRAUNGAARD TAUL

DISSERTATION SUBMITTED 2020

AALBORG UNIVERSITY
DENMARK

Synchronization Stability of Grid-Connected Converters under Grid Faults

Ph.D. Dissertation

Mads Graungaard Taul

Dissertation submitted May 12, 2020

Dissertation submitted: May 12, 2020

PhD supervisor: Prof. Frede Blaabjerg
Aalborg University

Assistant PhD supervisors: Prof. Xiongfei Wang
Aalborg University

Assoc. Prof. Pooya Davari
Aalborg University

PhD committee: Professor Remus Teodorescu (Chair.)
Aalborg University

Professor Florian Dörfler
Swiss Federal Institute of Technology (ETH) Zürich

Professor Bikash C. Pal
Imperial College

PhD Series: Faculty of Engineering and Science, Aalborg University

Department: Department of Energy Technology

ISSN (online): 2446-1636
ISBN (online): 978-87-7210-641-0

Published by:
Aalborg University Press
Langagervej 2
DK – 9220 Aalborg Ø
Phone: +45 99407140
aauf@forlag.aau.dk
forlag.aau.dk

Printed in Denmark by Rosendahls, 2020

Biography

Mads Graungaard Taul

Mads Graungaard Taul received the B.Sc. and M.Sc. degree in Energy Technology with specializing in Electrical Energy Engineering and Power Electronics and Drives from Aalborg University, Denmark, in 2016 and 2019, respectively. In connection with his M.Sc. degree in 2019, he received the 1st prize master's thesis award for excellent and innovative project work by the Energy Sponsor Programme. He was a visiting student researcher at the University of California, Berkeley, at the Department of Electrical Engineering and Computer Science during the period from August 2019 to January 2020. His main research interests include renewable energy sources and grid-connected converters with a particular focus on modeling and control of power electronics-based power systems under grid fault conditions.

Abstract

Modern society sustainment and growth are entirely dependent on a stable and reliable supply of electrical energy that experiences no or very few power outages for an optimal function. The primary purpose of a modern power system is to deliver the requested power in an economical way with an acceptable level of reliability. However, with the unprecedented increase in renewable energy sources and power-electronics-based generation, the overall reliability, and security of supply may be at risk, which implies unacceptable high customer interruption cost. This risk originates due to the fact that the primary frequency response provided by conventional synchronous machines will be significantly reduced or lost with a decreasing system inertia. With the gradual retirement of the synchronous generation, the power system robustness towards large disturbances such as short-circuit grid faults is reduced. To address these challenges, converter-based generators should aim to support the network during abnormal events and provide both frequency and voltage support. Yet, from real-world examples, system instabilities of large wind farms and photovoltaic power plants are reported, occurring due to instabilities in the converter synchronization control. To avoid such undesired events, it is essential that such instabilities can be predicted and accordingly prevented.

Therefore, to achieve a successful transition to a power electronics-based power system with green electricity conversion, models capable of assessing the large-signal synchronization stability of converter-based generation should be developed. This is lacking on the single-converter operation but also for large-scale multi-converter systems. To that end, the computational burden associated with performing a detailed transient stability study of a large-scale study is too time-consuming. Hence, reduced-order, and aggregated models are needed to asses the large-signal synchronization stability on a large scale.

To address these issues, this Ph.D. project proposes models, necessary conditions, and modeling frameworks for large-signal synchronization stability of single-converter and multi-converter systems. Due to the nonlinear dynamics associated with the synchronization process of grid-following converters, nonlinear tools and numerical approximations are presented to estimate the sufficient conditions for transient stability. All models possess high reconstruction accuracies, which are verified

through experimental tests. In this way, using the proposed reduced-order and aggregated models, the control parameters of the synchronization unit can be selected such to provide transient stability given an anticipated worst-case condition.

Since some severe grid faults may imply that no equilibrium point exists for the desired converter operation, control methods are proposed and revisited to address this. These either provide infinite damping of the synchronization dynamics or modify the converter operation to always provide a stable operating point during the fault with associated sufficient damping requirements. Accordingly, by employing the presented models and control methods for enhanced transient instability assessment and prevention, future power electronics-based power systems may be designed and operated to reduce the experienced customer interruption costs and increase the power system security of supply and overall reliability.

Dansk Resumé

En stabil og pålidelig forsyning af elektrisk energi er vigtig for at opretholde et moderne samfund og dets vækst. Derfor er det forventet at det elektriske forsyningssystem opererer pålideligt og oplever få eller ingen strømafbrydelser. Den primære funktion for et moderne el net er at levere den ønskede effekt på en økonomisk måde med et acceptabelt pålidelighedsniveau. Med den hidtil uset stigning i vedvarende energikilder og effektelektronikbaseret el-produktion kan den samlede pålidelighed og forsyningssikkerhed dog bringes i fare, hvilket indebærer høje prisomkostninger når strømmen afbrydes til diverse kunder. Denne risiko opstår da det primære frekvensrespons, der leveres af konventionelle synkrongeneratorer, vil blive væsentligt reduceret med en faldende mængde af den roterende inerti der er i systemet. Med den gradvise udskiftning af synkrongeneratorer, så reduceres elnettets robusthed over for store forstyrrelser, som f.eks. kortslutningsnetsfejl. For at imødekomme disse udfordringer skal konverterbaserede generatorer sigte mod at understøtte elnettet under abnormale tilstande og yde både frekvens- og spændingsstøtte. Dog rapporteres der fra virkelige hændelser om ustabiliteter i store vindmølleparker og solcellesystemer på grund af ustabiliteter i konverterens synkroniseringskontrol. For at undgå sådanne uønskede hændelser, er det vigtigt, at sådanne ustabiliteter kan forudsiges og dernæst forhindres.

For at opnå en vellykket overgang til et grønt elforsyningssystem baseret på effektelektroniske systemer, bør der udvikles matematiske modeller, der er i stand til at forudsige synkroniseringsstabiliteten af konverterbaseret produktion ved kortsutningsfejl. Dette er en mangelvare når der tales om modellering af en enkelt nettilsluttet konverter, men bestemt også når dette udvides til multikonverter-systemer. I forbindelse med dette, er beregningsbyrden forbundet med at udføre en detaljeret stabilitetsundersøgelse af et større system, alt for tidskrævende. Derfor er modeller med reduceret kompleksitet nødvendige for at vurdere synkroniseringsstabilitet i på store sammenkoblede systemer.

For at imødekomme disse problemerstillinger, præsenterer dette ph.d.-projekt modeller, nødvendige betingelser for stabilitet, samt modelleringsmetoder til synkroniseringsstabilitet af enkeltkonverter- og multikonverteringssystemer ved diverse kortslutningsfejl. På grund af den ulineære dynamik, der er forbundet med synkro-

niseringsprocessen for net-følgende konvertere, bruges ulineære værktøjer og numeriske tilnærmelser til at estimere de tilstrækkelige betingelser for transient stabilitet. Alle modeller har høje rekonstruktionsnøjagtigheder, som er verificeret gennem eksperimentelle forsøg. På denne måde kan man ved brug af de foreslåede modeller med reduceret kompleksitet, bestemme de styreparametrene for synkroniseringsenheden således, at den giver transient stabilitet i betragtning af en forventet worst-case-tilstand.

Da nogle alvorlige netfejl kan medføre at der ikke findes et ligevægtspunkt for den ønskede konverterdrift, foreslås og revideres styremetoder for enten at sikre en uendelig dæmpning af synkroniseringsdynamikken eller ændre konverterdriften således at der altid findes et stabilt driftspunkt under fejlen med tilhørende tilstrækkelige dæmpningsdynamik. Ved at anvende de præsenterede modeller og kontrolmetoder til forbedret stabilitetsvurdering og forebyggelse af ustabilitet, kan fremtidige effektelektronikbaserede systemer designes og betjenes således, at omkostninger forbundet med elafbrydelse af kunderne reduceres og forsyningssikkerhed foruden den samlede pålidelighed af elsforsyningsystemet forøges.

Contents

Thesis Details

Thesis Title:	Synchronization Stability of Grid-Connected Converters under Grid Faults
Ph.D. Student:	Mads Graungaard Taul
Supervisors:	Prof. Frede Blaabjerg, Aalborg University
	Prof. Xiongfei Wang, Aalborg University Assoc. Prof. Pooya Davari, Aalborg University

The main part of the dissertation is based on the following publications:

Publications in Refereed Journals

[J1] **M. G. Taul**, X. Wang, P. Davari, and F. Blaabjerg, "An Overview of Assessment Methods for Synchronization Stability of Grid-Connected Converters Under Severe Symmetrical Grid Faults," in *IEEE Trans. Power Electron.*, vol. 34, no. 10, pp. 9655-9670, Oct. 2019.

[J2] **M. G. Taul**, X. Wang, P. Davari, and F. Blaabjerg, "Robust Fault Ride-Through of Converter-based Generation during Severe Faults with Phase Jumps," in *IEEE Trans. Ind. Appl.*, vol. 56, no. 1, pp. 570-583, Jan.-Feb. 2020.

[J3] **M. G. Taul**, X. Wang, P. Davari, and F. Blaabjerg, "Current Limiting Control with Enhanced Dynamics of Grid-Forming Converters during Fault Conditions," in *IEEE Journal Emerg. Sel. Topics Power Electron.*, vol. 8, no.2, pp. 1062-1073, June 2020.

[J4] **M. G. Taul**, S. Golestan, X. Wang, P. Davari, and F. Blaabjerg, "Modeling of Converter Synchronization Stability under Grid Faults: The General Case," under review in *IEEE Trans. Power Electron.*, 2020.

[J5] **M. G. Taul**, X. Wang, P. Davari, and F. Blaabjerg, "Modeling of Large-Signal Synchronization Stability of Multi-Converter Systems," under review in *IEEE Journal Emerg. Sel. Topics Power Electron.*, 2020.

Publications in Refereed Conferences

[C1] **M. G. Taul**, X. Wang, P. Davari, and F. Blaabjerg, "Grid Synchronization of Wind Turbines during Severe Symmetrical Faults with Phase Jumps," in *Proc IEEE ECCE*, Portland, OR, USA, 2018, pp. 38-45.

[C2] **M. G. Taul**, X. Wang, P. Davari, and F. Blaabjerg, "An Efficient Reduced-Order Model for Studying Synchronization Stability of Grid-Following Converters during Grid Faults," in *Proc. IEEE COMPEL*, Toronto, ON, Canada, 2019, pp. 1-7.

[C3] **M. G. Taul**, X. Wang, P. Davari, and F. Blaabjerg, "Systematic Approach for Transient Stability Evaluation of Grid-Tied Converters during Power System Faults," in *Proc. IEEE ECCE*, Baltimore, MD, USA, 2019, pp. 5191-5198.

[C4] **M. G. Taul**, R. E. Betz, and F. Blaabjerg, "Rapid Impedance Estimation Algorithm for Mitigation of Synchronization Instability of Paralleled Converters under Grid Faults," accepted for *Proc. IEEE EPE*, Lyon, France, 2020.

[C5] **M. G. Taul**, X. Wang, P. Davari, and F. Blaabjerg, "Frequency-Locked Frequency-Adaptive Loops for Enhanced Synchronization Stability of Grid-Following Converters during Grid Faults," submitted to *Proc. IEEE COMPEL*, Aalborg, Denmark, 2020.

Relevant Co-author Publication

[O1] R. E. Betz and **M. G. Taul**, "Identification of Grid Impedance During Severe Faults," in *Proc. IEEE ECCE*, Baltimore, MD, USA, 2019, pp. 1076-1082.

This dissertation has been submitted for assessment in partial fulfillment of the Ph.D. degree. Based on the publications shown above, the thesis serves as a summary of those, highlighting the primary outcome of the Ph.D. project. Parts of the results are used directly or indirectly in the extended summary of the thesis. The co-author statements have been made available to the assessment committee and are also available at the Faculty of Engineering and Science, Aalborg University.

Preface

The content presented in this dissertation is a summary of the main outcome from the Ph.D. project "*Synchronization Stability of Grid-Connected Converters under Grid Faults*", performed at the Department of Energy Technology, Aalborg University, Denmark. This Ph.D. project was supported by the REliable Power Electronics-based Power System (REPEPS) project. I wish to express my deepest gratitude to the Villum Foundation, who have funded this work and the REPEPS project as a whole.

I would like to express my sincere appreciation to my supervisor, Professor Frede Blaabjerg, for his excellent guidance, support, and encouragement throughout my entire study. He has exceptionally many talents and skills in addition to outstanding technical leadership; all of which I have had the pleasure to learn from and work under. Also, I wish to recognize the invaluable assistance that my co-supervisors, Prof. Xiongfei Wang, and Assoc. Prof. Pooya Davari have provided during my study. Their guidance have spared me many dead-ends and frustrating moments. You have all shown me trust and freedom with responsibility during this work, which has enabled a flexible and productive collaboration. Apart from that, you have provided me with many amazing academic possibilities and tasks beyond any of my expectations. These have all helped me to become a better researcher, a better presenter, and a better thinker.

I would like to pay my special regards to Ph.D. students Heng Wu, Shih-Feng Chou, Joachim Steinkohl, and all members of the REPEPS project for many fruitful discussions during the whole of my Ph.D.

Lastly, I wish to acknowledge the support and great love of my wife, Jacqueline; my daughter, Ea; alongside my friends and family, who have always supported and motivated me in my work. Without their inputs and encouragement, this work would not have been accomplished.

Mads Graungaard Taul
Aalborg University, May 12, 2020

Part I

Report

Chapter 1

Introduction

1.1 Background

Modern society sustainment and growth are entirely dependent on a stable and reliable supply of electrical energy that experiences no or very few disruptions for an optimal function. The primary purpose of a modern power system is to deliver the requested power in an economical way with an acceptable level of reliability [1]. Due to a global increase in electricity consumption, as well as the desire to reduce CO_2 emissions, the capacities of renewable energy sources, such as wind turbines and photovoltaic systems, have increased significantly in the past decades [2]. With a substantial increase of renewable energy resources in electrical power systems, security and stability of electricity supply, and the overall power system reliability are at risk, which may introduce fatal consequences in the future, unless intelligent technologies and solutions accompany this growth. These consequences include an increased risk of large geographic power outages, which are extremely hazardous and costly for critical loads such as hospitals, large data centers, and industrial production lines. Such problems refers to the power system reliability, which is defined as:
"The probability of a system performing its purpose adequately for the period of time intended under the operating conditions encountered" [3].

The assessment of power system reliability and risk assessment can be divided into *system adequacy* and *system security* [3], as shown in Fig. 1.1. System adequacy describes whether a system entails sufficient generation facilities to satisfy the load demand of the customers. This refers to the static levels of generation and loading [4]. Also, this describes the long-term operation, including system design and facility planning. On the other hand, short-term dynamics such as transients are characterized by the system security, which relates to the ability of a system to respond to abrupt disturbances and abnormal event in the power system [1]. A power system can very well have high system adequacy, but as a result of unforeseen random abnormal events such as faults, loss of generation, or loss of loads, the system security may be at risk.

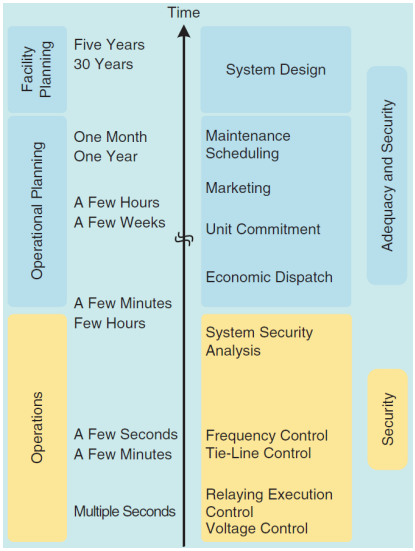

Fig. 1.1: The operation and planning of the multitime-scale power system dynamics where the focus in this thesis will be on the short-term control dynamics in the operations and security category. Source: [4].

With a low power system security, the customer loads will experience interruptions, which may imply high system interruption costs associated with the energy not being supplied. According to a 2001 study by the Electric Power Research Institute, it is estimated that the U.S. economy has an annual loss in the range of $104-164 billion as a result of power system outages [5]. In the Nordic countries, based on a 2017 report, more than 300 disturbances happen every year, which causes that energy is not being supplied to the end customer. This amounts estimated energy not supplied of 7 GWh every year [6]. According to a 2007 survey, it is estimated that the European business suffers an annual loss of €150 billion due to poor power quality as a result of interruptions, voltage sags, and harmonic pollution [7]. To that end, due to voltage sags and short interruptions, the cost of downtime may be as high as 10 % of the annual turnover of a company [8]. Due to such high customer interruption costs, an increasing focus is devoted to understanding and enhancing the power system reliability and security.

Within the European network, according to the Council of European Energy Regulators (CEER), the average expected customer interruption time per year or System Average Interruption Duration Index (SAIDI) is between 10 to more than 400 minutes [9, 10]. Countries like Germany, Denmark, and Sweden have the lowest customer interruption time, whereas countries like Portugal, Hungary, and Ireland have the highest. According to [11], the SAIDI including exceptional events is 12 minutes in Germany whereas it is 314 minutes in the U.S. Actually, more than 80% of all customer related reliability issues (faults in the network) originate from the distribution system [3, 9]. With a massive introduction of power electronic-based generation in the distribution system, the system reliability, security, and stability will be affected,

which demands robust and reliable power electronics-based converters including their control.

Besides the undesired customer interruption cost originating from the instability during large-signal disturbances, large penalties are now also given to product manufacturers and plant operators who do not comply with the agreed dynamical requirements during fault conditions. As an example, Ørsted and two other partners on the Hornsea One 1.2 GW wind farm, have agreed to pay more than £10 million for failing to remain connected during a lightning strike in England in August 2019 which caused a major blackout in the UK during rush hour [12]. This is an example of the importance, not only from the public point of view but also for the operators of such converters and power plants, to have a robust and stable operation of converter-based generation during fault conditions.

Apart from lightning strikes, it is reported in [13] that several recent wildfires in California have induced tripping of large-scale photovoltaic (PV) power plants of 1,200 MW [14] and 900 MW [15], respectively. Further investigation into the unintended disconnection showed that the synchronization unit (phase-locked loop (PLL)) employed by the converter was responsible for the interruption and that the disconnection were caused by a momentary loss of synchronization between the converter and the grid. Therefore, the impact of the integration of converter-based generation into the power system must be understood, their performance must be robust and should be controlled such that the power system reliability level will be retained or possibly improved.

1.1.1 Power Electronics-based Power System

With a rapid increase in renewables, a high share of distributed power generation compared to centralized power generation will happen in the next few decades [16]. A future power system dominated by power-electronic converters interfaced with wind farms, micro-grids, and big PV power generation plants, provide a high degree of freedom regarding grid controllability and utilization of harvested energy [17]. Yet, a power electronics-based power system dominated by decentralized power production from renewable energy sources, connected through multiple paralleled converters may introduce several problems as well.

First, the enormous buffer of energy stored as rotational energy in the synchronous generators in conventional power plants will be lost or significantly reduced since power electronic converters do not inherently provide any rotational inertia [18, 19]. Given this condition, the robustness of the power system against grid-disturbances and severe grid faults will be reduced since the system frequency is much more susceptible to disturbances.

In a power electronics-based power system, converters connecting the grid with renewable energy sources should not merely be grid-following elements, but should to a greater extent, also behave as grid-supporting elements and provide ancillary services to the power system [20, 21]. This together with fault ride-through requirements of grid-connected converters [20–23], highlights the importance and the necessity of being able to model and assess the response of grid-connected converters under grid

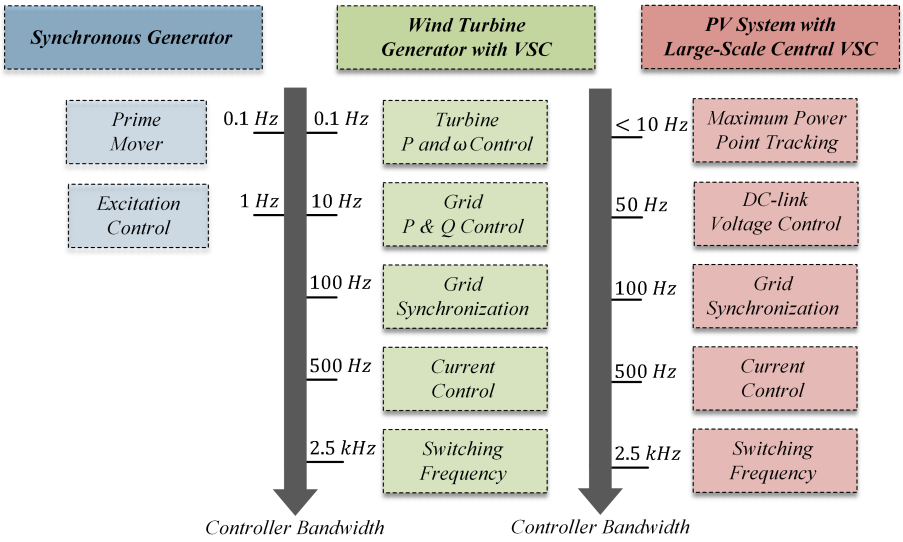

Fig. 1.2: Comparison of the control structure and controller bandwidth of a conventional synchronous generator, a large wind-turbine generator [28] and a photovoltaic (PV) system with a large-scale centralized converter.

faults. Conventional synchronous generators are during faults able to inject a large fault current into the grid, which is essential for voltage support and activation of circuit breakers within the grid. Unlike conventional generators, voltage-source converters (VSCs) are usually only able to inject a fault current of maximum 1-2 pu. This will significantly change the voltage support and relay activation during a short-circuit fault in a power electronic-based power system [21]. Furthermore, the control strategy of a grid-connected converter will affect the overall network during a fault condition [24]. Thus, to develop suitable control suggestions for paralleled converters in a future power grid, analyzing how the control of these converters influence the fault, and disclose how these converters interact during a fault must be understood and precisely modeled.

Compared to a traditional generator, modern power-electronic converters including nonlinear and wide bandwidth control dynamics, introduces high-frequency harmonics in the grid current, resulting in poor power quality and system stability degradation. The transition from synchronous generators (SGs) to VSCs is also shown to introduce oscillations in a wide range of frequencies due to the high control bandwidth of these converters [25]. Due to the switching behavior of converters and thereby small-time constants of switching components, dynamic couplings between converters and the power system network occur [26, 27]. Compared to SGs whose dynamics are located in the low-frequency sub-synchronous range, the dynamics of grid-connected converters are spread over a much broader frequency range as visualized in Fig. 1.2. This implies that the probability for exciting resonances in the power system, the converter output filters, or resonances between generators, is much higher when using power converters compared to synchronous machines (SMs). To

that end, the challenges of grid-connected converters interacting with each other via the non-ideal power grid have been widely reported [29–31].

Besides the introduction of a wide frequency range operation of VSCs, replacing SGs with VSCs also implies that the dynamical response during abnormal events can be designed and shaped as desired [32]. Previously, when the integration of renewables was low, requesting voltage and frequency support during faults was not necessary due to the inherent support provided by the SMs. Nevertheless, as the integration of converter-based generation has become significant, transmission system operators and distribution system operators demand low-voltage ride-through capability during faults to support the local grid voltage.

Based on this, the converter-based generation should not only aim to maximize the revenue of the proprietor of the renewable energy source. Additionally, they should seek to minimize the overall customer interruption cost and improve the system-level reliability, security of supply, and yearly unavailability of the system by performing low-voltage ride-through capability.

Another important issue relates to the modeling of large-scale power systems as these become more and more cumbersome due to the increasing complexity of the system. To make a successful transition from a traditional centralized system to a decentralized system, the interactions between grid-connected converters and their influence on power system stability, reliability, and resiliency must be understood and addressed while the constitution of distributed generation is still rather low. As a modeling tool, the state-space formulation is a general approach to analyzing the stability of power systems. To that end, with increased penetration of paralleled power-electronic converters, state-space models become very complicated to develop and compute [33]. Therefore, an impedance-based or component connection modeling approach has been proposed as being more feasible [31, 34]. As an assessment tool, impedance-based methods which are based on the minor loop gain, are widely used [29, 31, 35]. Common to all of these methods is that they are developed for a linearized system model, i.e. they are not applicable for transient stability assessments, which is the focus of this project. Additionally, many of the mentioned prior-art studies only describe the stability associated with the inner current loop control of VSCs, ignoring the slow outer synchronization and power loops, which due to interactions with the grid impedance, cause instability and sub-synchronous oscillations [27, 35].

To address the issues of security of supply for power electronics-based power systems, this dissertation focuses exclusively on the potential enhancements in power system security, electrical security of supply, and prevention of power outages. As this is closely related to the assessment of system stability during large-signal disturbances, the investigation towards control methods and modeling approaches for enhanced power system security as well as transient and dynamic responses are performed. Therefore, by understanding the mechanism of converter transient instability, models that can assess this on a large-scale setup can be made. Additionally, improved control strategies, which decrease the probability of transient instability of the distributed generators, and loss of electrical supply should be given. Accordingly, a focus on fault conditions and large-signal transient stability of modern and future power electronics-based power systems is preserved. With an increased level of transient stability and robustness towards grid fault conditions, the probability of cas-

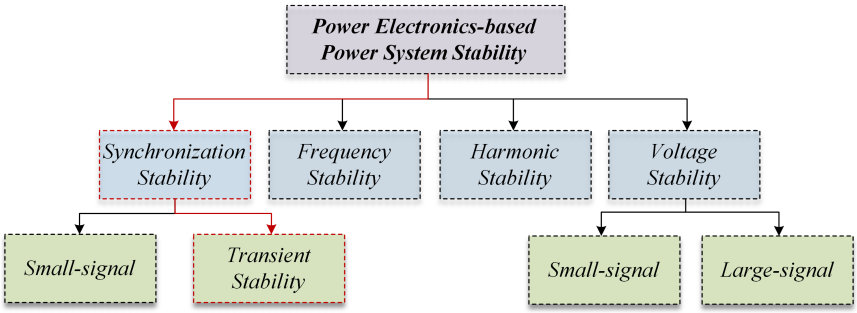

Fig. 1.3: Stability categorization in a power electronics-based power system. Blue denotes the physical parameter of interest and green describes the size of the disturbance. The transient synchronization stability, which is the focus of this dissertation, is highlighted in red.

cading outages will be reduced, which can reduce the occurrences of severe outages and system blackout, ultimately implying a reduction in the unwanted high customer interruption cost.

To identify the main project objectives of this thesis, the definition of today's power system stability is described. This includes a categorization of the stability definitions eligible for power electronic converters and how this differs from the classical power system definitions.

1.1.2 Today's Power System Stability

Stability definitions for classical power systems include rotor angle stability, frequency stability, and voltage stability, each of which can be sub-categorized into small-signal and large-signal stability [36]. However, for a power system dominated by power electronic converters, a mapping of the stability categories needs to be reformulated, e.g. as shown in Fig. 1.3.

At first, for the revised stability categorization, frequency stability is kept and is still an important metric to monitor and control when any synchronous generation is included. However, compared to the past, the issues related to frequency stability is changing. Due to the gradual retirement of SMs and fluctuating energy yield from renewable energy sources, the system inertia is decreasing and fluctuates with the stochastic energy yield from wind and solar. This implies that during disturbances in load or generation, the system frequency is easier to perturb. To capture this effect, the rate of change of frequency (RoCoF) is often more applicable to describe this sensitivity. Large RoCoF is an issue considering tripping schemes from grid codes and the mechanical rotating parts of the synchronous generations that cannot tolerate too fast acceleration or deceleration [37–39]. Therefore, one may argue that modern frequency stability may be more precisely characterized using the RoCoF index for stability evaluation. Seen from a pure power-electronic point of view, frequency is not a determining parameter, as a deviation from 50 Hz is not a problem if detected properly. Hence, frequency stability or RoCoF stability is more vital in systems with SMs and pre-designed protection equipment.

Secondly, due to the broad time-scale and frequency-coupling dynamics of grid-connected converters, harmonic instability is becoming an increasing challenge in today's power systems [40]. This has motivated the definition of harmonic stability, which assesses these wide-frequency effects and interactions [28]. Besides this, the rotor-angle stability used for SMs is replaced with synchronization stability, which is divided into small-signal stability and large-signal transient stability, see Fig. 1.3. As harmonic stability is a collection of several small-signal stability problems, it can as well describe the small-signal synchronization stability. This project focuses on the synchronization stability of grid-connected converters during grid faults, i.e., transient stability. This is highlighted with red in Fig. 1.3.

Conventionally, power system transient stability refers to the ability of SMs to remain in synchronism with the grid, following a large-signal disturbance. This area is well described for SMs but lacks understanding when replacing SMs with power-electronic converters. To that end, the synchronizing process of power-electronic converters is not related to any mechanical parts but is purely software-implemented. Accordingly, synchronization stability is included in Fig. 1.3 instead of the conventional rotor-angle stability to characterize whether a power-electronic converter can remain in synchronism with the external network following a disturbance. During abnormal events such as grid faults, the magnitude of the disturbance is too large for a linearized system model to be representable. Therefore, the nonlinear characteristics of the converter synchronization process cannot be neglected and should be assessed using transient stability evaluations. This also means that linear tools and models including impedance-based analysis, eigenvalue analysis, participation factor analysis etc. cannot be employed. Thus, nonlinear models are mandatory, and stability assessment, including getting a physical understanding of the instability phenomenon, becomes more cumbersome. To get an overview of the available models, assessment methods, and mitigation methods of synchronization stability during grid faults, a detailed description of the state-of-the-art is given in the following. This includes a description of the previous work describing grid-connected converters under grid faults, a thorough review of modeling and mitigation of transient synchronization stability, the use of grid-forming converters to enhance the transient stability, and modeling of large-scale nonlinear systems.

1.1.3 Synchronization Stability during Grid Faults

Power system faults may be caused by extreme weather conditions, malfunctioning of electrical components, relay failures, human errors etc. [41]. Considering short-circuit grid faults, these can be divided into symmetrical and asymmetrical faults, where the latter is the most frequently occurring type. The different types of short-circuit faults, the distribution of their occurrence, and the severity that each of them pose to the power system stability is depicted in Fig. 1.4. As can be noticed, even though three-phase symmetrical faults are rare, they pose the largest threat to the system stability. Consequently, both symmetrical and asymmetrical faults are important to study when characterizing the converter behavior and system stability under such abnormal events.

Most grid-connected converters in applications of PV and wind power systems

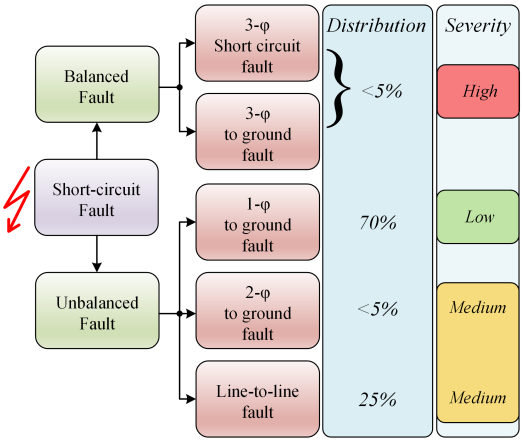

Fig. 1.4: Different types of line faults including their distribution of occurrence and severity of impact on the power system network [41].

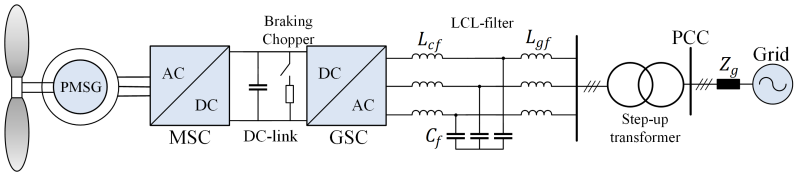

Fig. 1.5: Type IV wind turbine system with a full-scale power converter connected to the grid through an output LCL filter and step-up transformer. MSC: Machine-side converter, GSC: Grid-side converter. PMSG: Permanent magnet synchronous generator. Source: **[J2]**.

are controlled as grid-following converters that inject a set of currents that follow or are synchronized to the grid [32, 42]. An example of this is shown with a Type IV full-scale wind turbine system in Fig. 1.5 where its grid-following control structure is shown in Fig. 1.6. The basic grid-following control structure consists of a synchronization unit (often a synchronous reference frame phase-locked loop (SRF-PLL)), which provides the reference angle for the voltage at the point of common coupling (PCC), and an inner current controller to track the desired references. Even though the grid-following structure is widely used, it is shown to have destabilizing behavior during grid faults and weak-grid conditions [43, 44]. This issue is further noticed with increasing more stringent grid code requirements.

Despite the large body of literature analyzing low-voltage ride-through (LVRT) capability of grid-connected converters [45–53], the grid voltage sag is rarely considered severe, which is where the risk of loss of synchronization (LOS) or transient instability is highest. However, some articles have been published that describe the PLL instability during grid faults using different modeling approaches, analysis methods, and mitigation techniques [43, 54–70]. A time-line of the development of understanding, modeling, and mitigating LOS has been made, which is presented in Fig. 1.7. Here, the publications are grouped into contributions in terms of modeling and stability

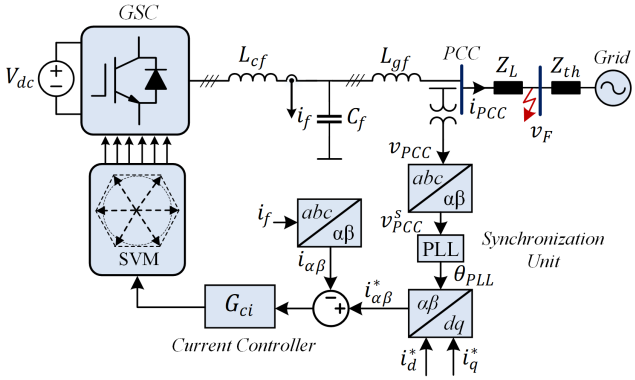

Fig. 1.6: Structure of grid-side converter control operated in grid-following mode. The red arrow indicates the location of a grid fault. Source: **[J2]**.

analysis, and into control methods and techniques for LOS mitigation. These are shown in blue and green, respectively.

Before unfolding the chronological time-line of research in transient synchronization stability, it should be mentioned that much work has been done previously on the synchronization of grid-connected converters under grid faults. This include the pioneering work about grid-synchronization of power-electronic converters during distorted and unbalanced conditions, including faults [42, 71–74]. To that end, a solution for synchronization issues during severe grid faults was briefly described in [75]. However, since these works do not specifically address the synchronization stability and associated dynamic power flow problem, these are not included in the following time-line.

The earliest found publication describing the LOS phenomenon was [54], where the authors identify the static limitation for the injected current of a converter during grid faults. Even though these static limits are very well known in the field of power systems and power transfer between an SM and the grid, it is the first to identify this limitation in regards to synchronization instability and highlight potential difficulties in meeting the grid code requirements during severe grid faults. Besides this, the authors propose to increase the active current component proportionally to the experienced voltage drop, which should help the converter not to inject currents violating the identified static network limit. Despite the insight of this formulation, the method is only valid for steady-state network conditions and do not recreate the dynamics of the converters. To address this, the authors in [55, 58] propose a quasi-static large-signal model for a PLL-synchronized grid-following converter where a destabilizing positive feedback loop, resulting from the coupling between the injected current and PCC voltage is identified. This coupling becomes significant during weak-grid and low-voltage conditions. Based on this model, several papers propose control methods, which either eliminate or decrease the negative influence of this positive feedback loop.

At first, the positive feedback loop can be reduced or entirely eliminated by in-

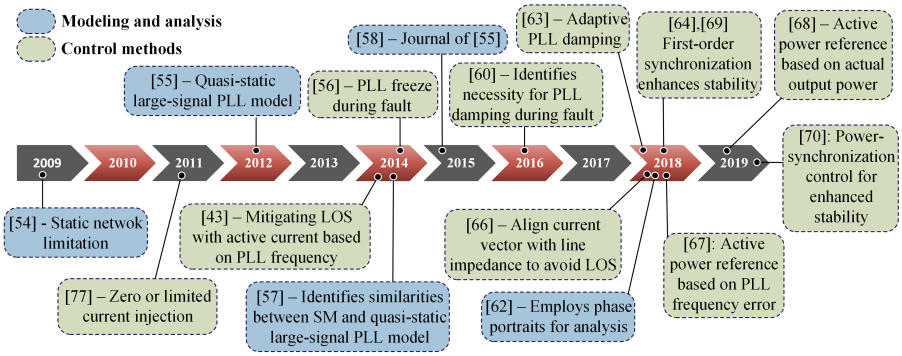

Fig. 1.7: Timeline diagram of selected state-of-the-art literature for modeling and control methods for large-signal synchronization stability of grid-connected converters.

jecting a limited or zero current magnitudes [76]. This method will not comply with the grid codes as a specific reactive current component should be injected. In [43], a control loop is added, which changes the active current reference based on the PLL frequency deviation from the anticipated nominal one. A very similar approach is presented in [67] where, instead of changing the active current reference, the active power reference is modified based on the anticipated PLL frequency error. Besides the effectiveness of these methods, an additional control loop is included, which further complicates the stability assessment of the nonlinear system. To that end, no proof of stability is given. A different but more theoretical approach is presented in [66], where the authors propose to align the injected current vector in such a way to match the impedance angle of the external grid. This effectively eliminates the positive feedback loop, and the method is proven to be globally asymptotically stable. However, this is based on the assumption that accurate estimations of the equivalent network resistance and reactance can be provided.

Research Gap 1 (Impedance estimation for current alignment)
The appealing mitigation strategy in [66], which enables grid code compliance and eliminates the destabilizing positive feedback loop of PLL-synchronized converters, is reliant on a rapid estimation of the network impedance when the fault occurs. Therefore, if such an estimate cannot be performed, this method has no practical applicability.

Regarding modeling, it is presented in [57], that the quasi-static large-signal PLL model has the equivalent form as the equations governing the mechanical motion of an SM. Accordingly, equivalent damping and inertia can be formulated for the PLL giving a more intuitive understanding of how the PLL parameters may influence the dynamic response of the converter. Along these lines, the equal area criterion (EAC), which is used for rotor-angle transient stability evaluation of SMs may also be used to describe the large-signal synchronization stability of the PLL-synchronized converter. Based on this intuition, the authors in [68] present a control method for mitigating

LOS. In this work, the active power reference can be set to the measured active power. The idea behind this is to cancel the difference between the electrical and mechanical powers of the PLL-synchronized converter modeled as an equivalent SM where if these are equal, any positive damping will provide transient stability.

One drawback of the EAC formulation is that the equivalent damping of the PLL is neglected, which results in a conservative stability assessment. To that end, the necessity of sufficient PLL damping to enhance transient stability is described in [60]. As no known analytical solution exists for the second-order quasi-static large-signal PLL model, subsequent research aimed to get an accurate stability prediction through a numerical approximation. Since the quasi-static PLL model is of second-order, its numerical solution can be presented and compared in an intuitive manner using phase plane trajectories [62]. Even though this may be used to assess the stability of a given system, it is unclear how well the nonlinear system approximates the real system alongside how the critical system damping or area of attraction can be determined.

Research Gap 2 (Lyapunov function and area of attraction estimation)
The equal-area criterion is based on the Lyapunov stability of a simplified system which is conservative. Formulating a Lyapunov function that has no assumption of the PLL damping would improve the stability assessment since its conservatism could be reduced. To that end, a numerical approach to determine the sufficient critical damping or area of attraction of the synchronization process is lacking.

Based on the understanding that synchronization instability may arise as a result of insufficient PLL damping, new methods for tuning and designing the converter synchronization unit during severe faults were developed. In [64, 69], adaptive methods for the PLL integral gain are proposed. Here it is shown that by removing the integral gain during the fault, transient stability can be enhanced since the synchronization unit will be a first-order overdamped system. Likewise, it is shown in [70], that a converter using power synchronization control will have the same enhanced transient stability since its synchronization system is of first-order. Along these lines, it is proposed much earlier in [56] to simply freeze the PLL during a severe fault to avert LOS. This may, at this time, be seen as a method to provide infinite damping to be able to ride through any severe grid fault. However, its accuracy are being questioned since its output states are frozen at the pre-fault states, which makes it blind to potential phase jumps.

Research Gap 3 (PLL freezing and phase-angle jumps)
In the state-of-the-art, it is repeatedly mentioned that the PLL freezing method cannot achieve satisfying tracking since its output is based on pre-fault conditions. Nevertheless, how the PLL freezing works during phase jumps and severe grid faults are unknown, and it remains a research gap to investigate this. Such analysis is beneficial since the PLL freezing method is a simple and efficient approach to avert LOS, and its stability can be mathematically proven.

Table 1.1: Methods to mitigate LOS based on changing the injected current vector.

Ref.	Year	Proposal
[54]	2009	Increase active current proportional to voltage drop
[76]	2011	Injection of zero or limited current magnitude
[43]	2014	Increase active current reference based on PLL frequency error
[67]	2018	Increase active power reference based on PLL frequency error
[66]	2018	Align current vector angle with line impedance angle $\left(\frac{i_q^*}{i_d^*} = -\frac{X}{R}\right)$
[68]	2019	Set $P^* = P_{meas}$ to eliminate ac/decelerating areas

Table 1.2: Methods to mitigate LOS based on modifying the synchronization loop

Ref.	Year	Proposal
[56]	2014	Freeze the PLL during the fault
[60]	2016	Decrease PLL bandwidth to enhance stability
[62]	2018	Increase damping ratio of PLL
[63]	2018	Adaptive decrease integral gain during fault
[64, 69]	2018/2019	Switch PLL to a first-order system during fault
[70]	2019	Enhance transient stability using power synchronization control (also first-order synchronization)

With this, the introduced control methods can be divided into techniques where the injected currents are modified and methods where the PLL dynamics are changed during the fault. The development of those two groups is shown chronologically in Table 1.1 and Table 1.2, respectively.

1.1.4 Utilization of Grid-Forming Technology

In addition to the need for better models for PLL-synchronized converters during grid faults, the fundamental instability issue originates from the grid-following behavior of the converter. Thus, employing a grid-forming controller may be beneficial to enhance the security of supply in future power systems [77]. It is disclosed in [78–80], that the robustness towards weak-grid conditions can be highly improved using a grid-forming controller. This is in line with the discussion on the PLL freezing method from the previous section since the grid-following converter with PLL freezing actually operates as an open-loop grid-forming converter. Despite this, limited work has been conducted to verify whether this property of grid-forming control can be extended to solve the LOS issues associated with grid-following converters during grid faults. To that end, the robust operation of the grid-forming converter is usually lost during grid faults since the converter control is switched to grid-following current control to limit the converter currents [78, 81–83].

Research Gap 4 (Grid-forming control for enhanced transient stability)
To utilize grid-forming control to enhance the large-signal synchronization stability during grid faults, the converter needs to keep its grid-forming properties during the fault, i.e., it cannot be allowed to switch to a current-limited grid-following

structure. Hence, a grid-forming controller, which can ride through faults without violating the converter current limitation, is needed to enhance the transient instability during severe faults.

1.1.5 Modeling of Large-Scale Power Electronics-based Power Systems

Besides improved models and enhanced control for single-converter transient stability studies, an even greater demand is present when assessing the stability of large-scale systems. Considering a large-scale renewable power system consisting of hundreds or perhaps thousands of interconnected converters [23, 84, 85], including all necessary control, models capable of predicting the mutual coupling behavior of such systems are still not reported. A large-signal model of such a system could be developed by averaging the differential equations of the system, neglecting the switching behavior. However, considering the number of nodes in a large-scale power system, the computational requirements for such a model will not be convenient [30]. In [86], it is reported that the only accurate method to characterize fault currents in the case of a power electronics-based power system is through dynamic time-domain simulations, which, however, when the number of units increases, becomes highly impractical. For multi-converter systems, the modeling complexity increases rapidly. Therefore, new modeling approaches need to be introduced. To analyze and describe a large-scale system during fault conditions, reduced-order modeling and aggregation techniques will be necessary.

In [87], a reduced-order modeling approach is considered for a power system consisting of voltage-controlled and current-controlled VSCs. Here the authors not just remove the fast states of the converter but also use a so-called "peel-off and add-back" approach where they restore the primary behavior of the fast states. As presented in [88], a reduced-order model for a large linear power system can be developed by approximating a discrete-time system transfer function by a Fourier expansion that identifies the important properties of the system. Nevertheless, both of these models are based on small-signal behavior. In [23], the aggregated model of the grid-connected converters is simply made by assuming the output to contain only the fundamental frequency, ignoring harmonics, switching performances, and mutual interactions between converters. A reduced-order model for a variable-speed wind farm is presented in [89]. The model is described as useful for a large power system with dispersed wind farms and does not aim to describe the interaction dynamics within the farm. Furthermore, the developed model describes the linearized dynamics of the system, eliminating the possibility of analyzing fault behavior. In [90], the importance of including power electronic converter dynamics when using aggregated models to analyze oscillations in wind farms is described. Nevertheless, only the power converter connecting the wind farm to the main grid is modeled, ignoring the effects of the hundreds of interconnected converters within the wind farm itself. In [91], a review is done to identify the present aggregation methods available for wind farms. These include fully-aggregated, semi-aggregated, and multi-machine models, which can be used depending on the uniformity of the wind speed within the

farm. Unfortunately, none of these methods consider any inner dynamics and power electronic converters are not addressed in the modeling. The paper states that almost no research has been done to identify the inner dynamics of wind farms, and the authors recognize that the influence of power electronic converters cannot be ignored when performing prediction of the equivalent behavior at the PCC. One challenging task in this regard is to identify how much the converter model can be simplified without sacrificing too much on the accuracy when analyzing transient stability.

Research Gap 5 (Reduced-order and aggregated modeling)
Reduced-order models of grid-connected converters that can accurately capture the large-signal synchronization process during grid faults are needed. This includes an identification of salient dynamic features for large-scale studies and how paralleled as well as interconnected systems may be aggregated.

1.2 Thesis Motivation and Research Tasks

As previously discussed, grid-following converters are at risk of experiencing low-frequency instability during severe grid faults. This can lead to converter disconnection despite the demand for grid-supporting functionalities, large loss of generation, and a high undesired customer interruption cost associated with local blackouts. To improve this, the root cause and fundamental instability phenomenon of large-signal synchronization stability of grid-following converters must be understood and properly described. Even though the PLL has been identified as the problem from a small-signal point of view, how to analyze and avert it in a large-signal manner, still remains a challenge. To achieve a power electronics-based power system where most or all generation and loads are interfaced with power-electronic converters, the large-signal instability problems associated with these need to be addressed. From the introduction and state-of-the-art descriptions, it is identified that three distinct issues need to be addressed to increase the future security of supply of power electronics-based power systems. These include a detailed understanding of the characteristics that excite the instability during faults taking into account the grid code requirements on LVRT capability. To that end, one needs to be able to accurately assess the transient stability of the system by other means than detailed time-domain simulations. This is especially important when dealing with large-scale multi-converter systems. Therefore, reduced-order models that capture the governing dynamics of large-signal synchronization instability and new methods to estimate the stability boundary of the non-linear system are needed. Apart from enhanced modeling and assessment tools, grid-connected converters need to actively perform countermeasures to minimize the risk of LOS during severe grid faults. Such control methods need to be effective and have a simple implementation without an increased complexity of the control structure. Besides these, all the reviewed works are limited to symmetrical faults and the classical SRF-PLL. However, this does not line up with that the vast majority of grid faults are asymmetrical and that during such conditions, more complicated synchronization units need to be employed. Accordingly, it remains to be studied how the

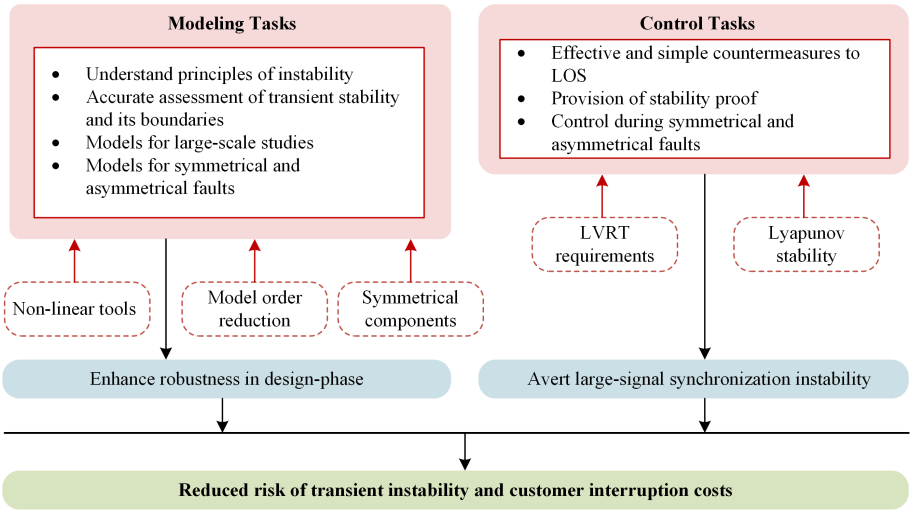

Fig. 1.8: Research tasks of this Ph.D. thesis: Synchronization Stability of Grid-Connected Converters under Grid Faults [92]. LOS: Loss of synchronization. LVRT: Low-voltage ride-through.

transient synchronization stability can be modeled during asymmetrical faults. To that end, how to avert LOS using improved control is still to be analyzed.

By developing reduced-order non-linear models, which can be used to accurately assess the transient synchronization stability during severe faults, these can be used for large-scale studies where high-order converter equivalents are of no interest. Based on these, potential contingency problems may be identified already in the design phase. To that end, by proposing efficient and simple converter countermeasures during severe faults, LOS, decreased security of supply, and an increased customer interruption costs can be averted in future power electronics-based power systems. The main motivation and project tasks of this Ph.D. project for enhancing the transient synchronization stability are outlined in Fig. 1.8.

1.2.1 Research Questions and Objectives

The main objective of this Ph.D. study is to widen the knowledge on transient synchronization stability of grid-connected converters, including how to model it and how to avert loss of synchronization. The overall objective of this Ph.D. study is condensed into the following research question:

"How can the transient synchronization stability of grid-connected converters be modeled and analyzed, and how should the power converter be controlled to avert loss of synchronization and enhance the power system stability during grid faults?"

To accommodate this, modeling of the power systems and parts of it, including complex and non-linear behaviors, have to be feasible and doable. Models capable of revealing the electromagnetic coupling as well as control interactions between grid-connected converters should be developed only including the most important effects

of the system, by introducing reduced-order models. Such models should also be able to predict the system stability and help to assess how to analyze and control multi-converters during severe grid faults. Based on the overall research question, multiple sub-objectives are formulated to help to answer the problem and more clearly address the project tasks seen from Fig. 1.8 and research gaps given in the introduction part. These are divided into questions in regards to modeling and questions in regards to enhanced control.

For the *modeling*, the following sub-questions are formulated:

- How should the synchronization instability phenomenon be understood, and what are the main excitation drivers that cause it?
- How can a simplified reduced-order nonlinear model that accurately captures the nonlinear synchronization dynamics of the converter and grid-interactive system be developed?
- How can transient synchronization stability be modeled and analyzed during symmetrical and asymmetrical grid faults, including more complicated synchronization units used for sequence-component extraction and phase tracking?
- How can nonlinear tools be adopted to estimate the area of attraction and critical damping of the system?
- How should multi-converter systems be modeled to analyze the large-signal synchronization stability under grid faults?

For the *control* during large-signal fault conditions, the following sub-questions are formulated:

- How can simple, efficient, and mathematical proven stable control methods be developed to enhance and avert the synchronization instability during grid faults?
- How can the transient stability under asymmetrical faults be enhanced using modified control, considering sophisticated synchronization units?
- How can a grid-forming converter that keeps its robust properties during grid faults be designed to enhance transient stability?

With the detailed set of sub-questions, the research objectives of this project can be defined as follows:

Understand and describe the instability phenomenon occurring during grid faults for a single-converter system
As described previously, even though several publications address the loss of synchronization of grid-following converters under severe grid faults, the fundamental instability phenomenon is not well understood. Neither are the key parameters, which causes instability, clearly highlighted. Before going into the detailed modeling and control of grid, a full analytical description of the understanding of the static instability phenomenon will be given in this Ph.D. project.

Reduced-order model of the synchronization process of a grid-following converter under grid faults
Since accurate and computationally efficient reduced-order models for transient stability evaluation is required for large-scale power electronics-based power system studies during grid faults, this will be addressed in this project. This includes a justification on how the high-order model can be reduced, a description of the model derivation, both analytically and numerically, and experimental verification of the proposed model. This is performed both for symmetrical and asymmetrical conditions. To analyze asymmetrical faults, symmetrical component theory is used.

Extension of reduced-order models to represent paralleled grid-connected power converters
With most previous work being focused on single-converter systems, the static stability limit of multi-converter systems will also be considered in this Ph.D. project. This includes different interconnection methods using real-world network parameters. The model-reduction approach from single-converter systems will be extended to multiple converters from where the transient stability assessment can be performed. The stability assessment will be based on a numerical evaluation of a presented reduced-order model which is based on reduced-order modeling and aggregation techniques.

Identify stability boundary and critical damping of the nonlinear PLL-synchronized system
Based on the reduced-order nonlinear model, nonlinear tools, including phase portraits and Lyapunov theory, will be used to determine the critical sufficient PLL damping and area of attraction. The critical damping and area of attraction will be numerically identified and verified against experimental results.

Control solutions to enhance the transient stability during severe grid faults
Besides the above research objectives, which are related to the modeling and analysis of the system, it is desired, when instability would occur, to change the control such that instability can be averted. From the state-of-the-art analysis, several methods which improve or guarantee transient stability are available. However, many of them either include additional control loops or assumptions that cannot be justified in practice. To address this, methods that are simple, robust, and can guarantee stability are of interest. Therefore, based on the previously identified research gaps, this Ph.D. project analyzes how

- the PLL freeze method can be utilized during severe faults with phase jumps to avert instability.
- the network impedance can be rapidly estimated under grid faults to correct the injected current vector to enhance transient stability.
- a control solution for complex synchronization units during asymmetrical faults can be made.
- grid-forming converters can be used to enhance the stability under grid fault conditions and how the converter should be controlled to maintain the grid-forming structure during the fault.

All of these points will be individually analyzed, and their performance will be experimentally verified.

1.2.2 Project Limitations

The following assumptions, simplifications, and limitations have been performed in this work.

- All dynamics related to energy harvesting or conversion is neglected in this project. This includes the generator-side dynamics for wind turbine systems, the maximum power-point tracking and boost stage of PV systems, and governor/turbine dynamics of conventional generation units. Only the ac-side dynamics are considered to the grid. This can be assumed since a back-to-back configuration is considered where each converter can be analyzed individually.
- The external network seen from the grid-connected converter is assumed to be represented by static line parameters and a Thevenin equivalent.
- The nonlinear effects of converter step-up transformers are neglected, and the transformer is mostly represented by its leakage inductance. Any influence associated with surge arrestors, fuses, or circuit breakers is out of the scope of this project.
- For the grid-following PLL-synchronized converter, which is mostly considered in this Ph.D. project, the outer power loops, including dc-link voltage control or active power control, and the reactive power control are neglected for this work. This is done since the current references during severe faults are directly set based on the LVRT requirements on the local voltage support and not the outer loops.

1.3 Thesis Outline

This Ph.D. thesis is divided into two parts: a ***Report*** part and a collection of ***Selected Publications*** done in the Ph.D. study period. How the selected publications are used to define the structure of the thesis is visualized in Fig. 1.9. Here, it is also evident, which publications are related to which chapter. The ***Report*** is divided into content related to the modeling tasks defined and content addressing the control tasks defined. The remainder of the Ph.D. thesis is as follows: *Chapter 2* provides a comprehensive description of the synchronization instability phenomenon for single-converter systems. This includes a thorough explanation of the static stability limit of grid-connected converters operated under grid faults. This limit serves as a reliable tool in understanding why LOS occurs and which parameters are related to stability. As will be explained, this tool only works as a necessary condition for transient stability, which is why the control dynamics of the converter need to be considered. Based on these, *Chapter 3* presents a reduced-order model to assess the large-signal synchronization stability of grid-following converters. This is offered both under symmetrical and asymmetrical fault conditions, and the proposed models are experimentally verified. Lastly, for the modeling part, the static stability limits of different multi-converter

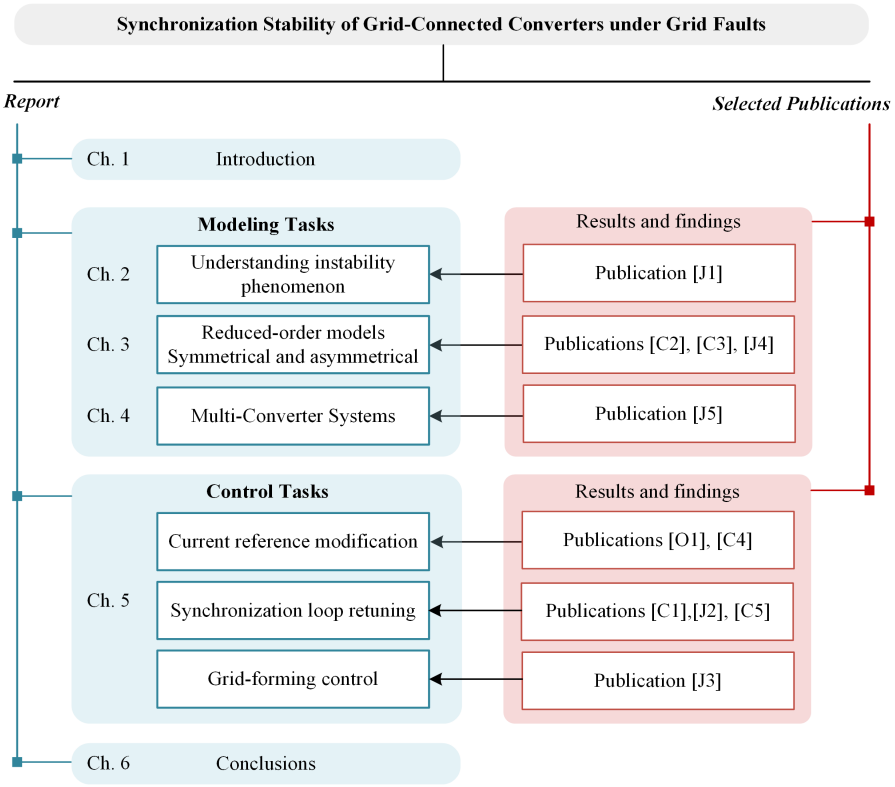

Fig. 1.9: Report structure and identification of how the selected publications in this thesis fit in regard to the defined research tasks [92].

configurations are derived and presented in *Chapter 4*. A case study with real-world network parameters are used to test the accuracy of the presented models and assess the transient stability during different fault conditions.

Chapter 5 includes the control-related content, which shows how the transient synchronization stability of grid-connected converters can be enhanced by utilizing either a simple, efficient solution for grid-following converters or by adopting a proposed realization of grid-forming converters.

Finally, the main findings and conclusions of this Ph.D. project are outlined in *Chapter 6* and relevant future research activities in regard to this project theme are highlighted.

1.4 List of Publications

The results and outcomes of this Ph.D. project have been disseminated as publications in the form of journals, conferences, and a book chapter. The main content of this thesis is based on some of these publications, as shown in Fig. 1.9, whereas a full list

of publications performed during this Ph.D. study can be found below:

Publications in Refereed Journals

[J1] **M. G. Taul**, X. Wang, P. Davari, and F. Blaabjerg, "An Overview of Assessment Methods for Synchronization Stability of Grid-Connected Converters Under Severe Symmetrical Grid Faults," in *IEEE Trans. Power Electron.*, vol. 34, no. 10, pp. 9655-9670, Oct. 2019.

[J2] **M. G. Taul**, X. Wang, P. Davari, and F. Blaabjerg, "Robust Fault Ride-Through of Converter-based Generation during Severe Faults with Phase Jumps," in *IEEE Trans. Ind. Appl*, vol. 56, no. 1, pp. 570-583, Jan.-Feb., 2020.

[J3] **M. G. Taul**, X. Wang, P. Davari, and F. Blaabjerg, "Current Limiting Control with Enhanced Dynamics of Grid-Forming Converters during Fault Conditions," in *IEEE Journal Emerg. Sel. Topics Power Electron.*, vol. 8, no.2, pp. 1062-1073, June 2020.

[J4] **M. G. Taul**, S. Golestan, X. Wang, P. Davari, and F. Blaabjerg, "Modeling of Converter Synchronization Stability under Grid Faults: The General Case," under review in *IEEE Trans. Power Electron.*, 2020.

[J5] **M. G. Taul**, X. Wang, P. Davari, and F. Blaabjerg, "Modeling of Large-Signal Synchronization Stability of Multi-Converter Systems," under review in *IEEE Journal Emerg. Sel. Topics Power Electron.*, 2020.

- **M. G. Taul**, X. Wang, P. Davari, and F. Blaabjerg, "Current Reference Generation based on Next Generation Grid Code Requirements of Grid-Tied Converters during Asymmetrical Faults," in *IEEE Journal Emerg. Sel. Topics Power Electron.*, 2019.
- **M. G. Taul**, N. Pallo, A. Stillwell, and R. Pilawa-Podgurski, "Theoretical Analysis and Experimental Validation of Flying-Capacitor Multilevel Converters under Short-Circuit Conditions," under review in *IEEE Trans. Power Electron.*, 2020.
- Y. Gui, C. C. Chung, F. Blaabjerg, and **M. G. Taul**, "Dynamic Extension Algorithm Based Tracking Control of STATCOM Via Port-Controlled Hamiltonian System," in *IEEE Trans. Ind. Informat.*, vol. 16, no. 8, pp. 50765087, Aug. 2020.
- B. Shakerighadi, E. Ebrahimzadeh, **M. G. Taul**, F. Blaabjerg, and C. L. Bak, "Modeling and Adaptive Design of the SRF-PLL: Nonlinear Time-Varying Framework," in *IEEE Access*, vol. 8, pp. 28635-28645, 2020.

Publications in Refereed Conferences

[C1] **M. G. Taul**, X. Wang, P. Davari, and F. Blaabjerg, "Grid Synchronization of Wind Turbines during Severe Symmetrical Faults with Phase Jumps," in *Proc IEEE ECCE*, Portland, OR, USA, 2018, pp. 38-45.

[C2] **M. G. Taul**, X. Wang, P. Davari, and F. Blaabjerg, "An Efficient Reduced-Order Model for Studying Synchronization Stability of Grid-Following Converters during Grid Faults," in *Proc. IEEE COMPEL*, Toronto, ON, Canada, 2019, pp. 1-7.

[C3] **M. G. Taul**, X. Wang, P. Davari, and F. Blaabjerg, "Systematic Approach for Transient Stability Evaluation of Grid-Tied Converters during Power System Faults," in *Proc. IEEE ECCE*, Baltimore, MD, USA, 2019, pp. 5191-5198.

[C4] **M. G. Taul**, R. E. Betz, and F. Blaabjerg, "Rapid Impedance Estimation Algorithm for Mitigation of Synchronization Instability of Paralleled Converters under Grid Faults," accepted for *Proc. IEEE EPE*, Lyon, France, 2020.

[C5] **M. G. Taul**, X. Wang, P. Davari, and F. Blaabjerg, "Frequency-Locked Frequency-Adaptive Loops for Enhanced Synchronization Stability of Grid-Following Converters during Grid Faults," submitted to *Proc. IEEE COMPEL*, Aalborg, Denmark, 2020.

[O1] R. E. Betz and **M. G. Taul**, "Identification of Grid Impedance During Severe Faults," in *Proc. IEEE ECCE*, Baltimore, MD, USA, 2019, pp. 1076-1082.

- J. Steinkohl, **M. G. Taul**, X. Wang, F. Blaabjerg, and J.-P. Halser, "A Synchronization Method for Grid Converters with Enhanced Small-Signal and Transient Dynamics," in *Proc. IEEE COMPEL*, Padua, Italy, 2018, pp. 1-7.

- Q. Wu, X. Wang, **M. G. Taul**, and F. Blaabjerg, "Conceptual Systematic Stability Analysis of Power Electronics based Power Systems," in *Proc. IEEE ECCE*, Baltimore, MD, USA, 2019, pp. 2232-2238.

- N. Pallo, **M. G. Taul**, A. Stillwell, and R. Pilawa-Podgurski, "Fault Ride-Through of Flying-Capacitor Multilevel Converters through Rapid Fault Detection and Idle-mode Operation," submitted to *Proc. IEEE COMPEL*, Aalborg, Denmark, 2020.

- J. B. Nørgaard, **M. K. Graungaard**, T. Dragičević, and F. Blaabjerg, "Current Control of LCL-Filtered Grid-Connected VSC Using Model Predictive Control with Inherent Damping," in *Proc. IEEE EPE*, Riga, 2018, pp. P.1-P.9.

Book Chapter

- D. Zhou and **M. G. Taul**, "Abnormal Operation of Wind Turbine Systems" in Control of Power Electronic Converters and Systems, Vol. 3, F. Blaabjerg, Ed.: Elsevier, 2020, Ch. 19.

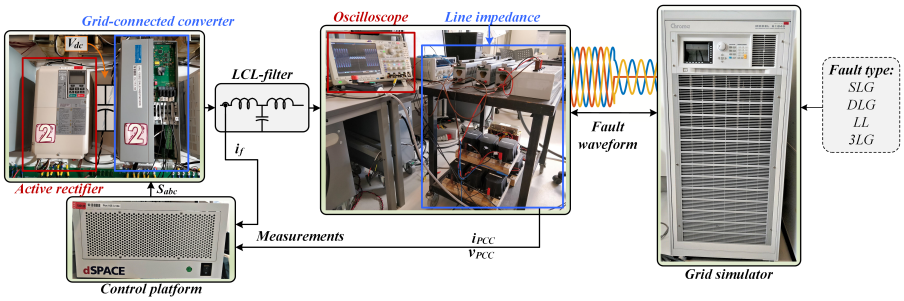

Fig. 1.10: Laboratory test setup used for experimental verification. A programmable grid simulator is used to generate the different grid faults, and a grid-connected converter is interfaced through a line impedance. Source: **[J4]**.

Table 1.3: Main parameters of the system in Fig. 1.10

Symbol	Description	Physical Value
S_b	Rated power	7.35 kVA
V_b	Nominal grid voltage	400 V
f_n	Rated frequency	50 Hz
V_{dc}	DC-link voltage	730 V
L_{cf}	Converter-side inductor	0.072 pu / 5 mH
L_{gf}	Grid-side inductor	0.0433 pu / 3 mH
C_f	Filter capacitor	0.0684 pu / 10 μF
f_{sw}	Switching frequency	10 kHz
f_s	Sampling frequency	10 kHz
Z_L	Line impedance	0.04+0.1j pu

1.5 Experimental Platform used in Ph.D. Project

The experimental results to be used in this Ph.D. thesis are all obtained using the test setup shown in Fig. 1.10 with the main system parameters listed in Table 1.3. An active rectifier supplies a steady dc-link voltage to the grid-connected converter under test. The grid-connected converter is a 15 kVA Danfoss VLT FC-302 inverter, which is interfaced with an emulated grid through an output LCL-filter and a modular line impedance. The converter-side current, grid-side current, and PCC voltage are all measured and fed back to the dSPACE expansion box responsible for the digital closed-loop control. The dSPACE expansion box includes of a DS1007 PPC processor board for code actuation, a DS2004 high-speed A/D board for current and voltage sensing, and a DS5101 digital waveform output board for PWM generation. The grid and grid faults, in particular, are emulated using a Chroma Regenerative Grid Simulator Model 61845, which can be programmed to emulate any short-circuit grid fault at the fault location by tight closed-loop control of each phase. The control parameters for the experimental verification in the following chapters will either be listed in the respective chapter where the results are presented or can be found in the related publications to that particular chapter.

Chapter 2

Static Limit for Synchronization Stability of Single-Converter Systems

2.1 Background

During any mismatch between power system generation and system loading, a transient occurs, which for the conventional power system results in swings of the machines' rotors [93]. These swings originate due to a net unbalance between accelerating and decelerating torque exerted in the rotor of the generator. For large-signal disturbances, these swings may exceed a specific value from where pole-slipping occurs and synchronization is lost, which is also known as loss of synchronization or loss of synchronism. In the case of SMs, two undesired consequences arise: pole-slipping may destroy the rotor of the machine, and the power system may become unstable, which may cause a voltage collapse and in worst case a total system blackout. As synchronous machines are being replaced with power electronics-based generators, one must assure that the transient stability of these systems are maintained during large-signal disturbances. To ensure this, two properties are required of the system: at first, if a stable operating point exists as a result of a severe fault, either during or after the disturbance, the system must be able to be attracted to this point. Secondly, if the system is unstable during the disturbance, the fault must be cleared in due time such that the system can retain the post-fault equilibrium stably. This Ph.D. project focuses exclusively on the former requirement. Based on that, this chapter is devoted to describe the fundamental principle of converter synchronization stability under severe grid faults alongside with highlighting which parameters cause LOS. This will be developed from a steady-state point of view, also known as the static stability limit, for a single-converter infinite-bus system.

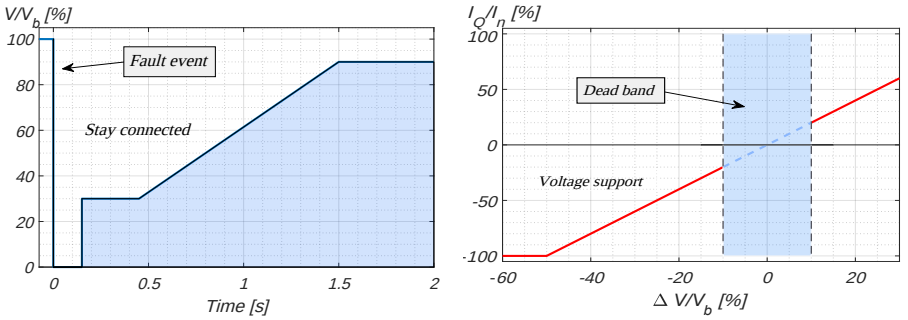

Fig. 2.1: Grid-code requirements from the German grid operator BDEW during low-voltage fault conditions [95]. (a): V is the lowest value of the three line-to-line voltages, and V_b is the nominal voltage. (b): Voltage support by injection of reactive current proportionally to voltage drop/rise. Source: **[J1]**.

As previously reported in [43, 44, 59, 66, 94], grid-tied converters operating in weak grids or during severe grid faults are susceptible to experience LOS using a voltage-based synchronization method, e.g., SRF-PLL. However, before jumping in to the dynamical details of the synchronization stability including the PLL, one should understand the fundamental operation and limitations of the grid-following converter and its interaction with the external grid. Actually, during severe grid faults, static instability may happen due to a physical barrier in the active and reactive powers that can be transferred between the converter and the grid. This is independent of whether a PLL is employed and how its dynamics are tuned. Therefore, the static network instability or necessary stability condition is to be initially understood before any additional dynamics are to be introduced.

The reader should familiarize themselves with the test system considered for this analysis. This is shown in Fig. 1.5, which include a distributed generator such as a wind turbine where a full-scale power electronic converter is used to harvest the energy from the renewable energy source and transfer it to the grid. Due to the decoupling between the machine-side and grid-side for a type IV wind turbine system, only the grid-side converter is considered. The machine-side converter, synchronous machine, and mechanical circuits of the wind turbine system are realized as a constant voltage source since the aim of this work is to investigate the synchronization issues associated with severe grid faults and not interactions between the dc and ac side. During a low-voltage situation where the converter current is sharply limited to around 1 pu, the harvested energy from the wind turbine cannot be delivered fully to the grid. This results in surplus energy being accumulated in the DC-link capacitor resulting in over-voltages during the fault. Usually, the DC-side contains a chopper circuit used to dissipate the surplus energy during a fault, which facilitates that a near constant DC-link voltage can be assumed. This is depicted in Fig. 1.6 where the control topology used for the grid-following converter is shown. During a severe grid

fault, the converter should remain connected, as seen in Fig. 2.1(a) and allocate its current capability to reactive current injection, Fig. 2.1(b) as requested by the German BDEW grid code [95].

2.2 Static Current Transfer Limit

Loss of synchronization can be well understood from the analysis of a stable operating point during the fault. This is here referred to as a the static current transfer limit and serves as a necessary condition for transient stability. For this analysis, the interaction between the PCC where the grid-connected converters is connected, and the external Thevenin equivalent grid is analyzed. This is shown in a single-line diagram in Fig. 2.2(a) where the fault resistance (R_F) is highlighted in red. Assuming the fault to be nearly solid where $R_F << Z_{th}$, the equivalent two-bus single-line diagram depicted in Fig. 2.2(b) is realized. The complex power injected by the converter at sending end bus can be written as

$$\boldsymbol{S_{PCC}} = P_{PCC} + jQ_{PCC} = \boldsymbol{v_{PCC}}\boldsymbol{i}^*_{\boldsymbol{PCC}} = \boldsymbol{v_{PCC}}\frac{\boldsymbol{v}^*_{\boldsymbol{PCC}} - \boldsymbol{v}^*_{\boldsymbol{F}}}{\boldsymbol{Z}^*_{\boldsymbol{L}}} = V_{PCC}e^{j\delta}\frac{V_{PCC}e^{-j\delta} - V_F}{Z_L e^{-j\theta_Z}} \tag{2.1}$$

Substituting the vectors with its complex variables and identifying the real and imaginary parts give the active and reactive powers as

$$P_{PCC} = \frac{V^2_{PCC}R_L}{Z^2_L} + \frac{V_{PCC}V_F X_L \sin(\delta)}{|Z_L|^2} - \frac{V_{PCC}V_F R_L \cos(\delta)}{Z^2_L} \tag{2.2}$$

$$Q_{PCC} = \frac{V^2_{PCC}R_L}{Z^2_L} - \frac{V_{PCC}V_F X_L \cos(\delta)}{|Z_L|^2} - \frac{V_{PCC}V_F R_L \sin(\delta)}{Z^2_L} \tag{2.3}$$

where $Z_L = \sqrt{R^2_L + X^2_L}$ and $\delta = \theta_{PLL} - \theta_g$ is the angle between $\boldsymbol{v_{PCC}}$ and $\boldsymbol{v_F}$. Since the grid-following converter is a current-controlled device, it is advantageous to express the sending-end equations in current components rather than power components. Dividing the obtained active and reactive power expressions from the sending-end ter-

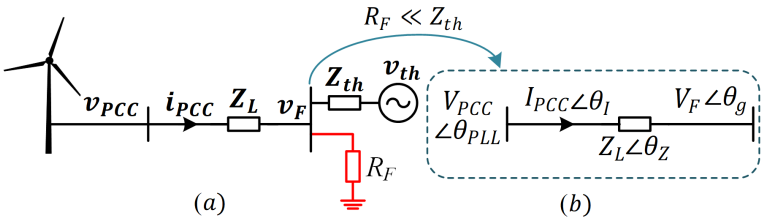

Fig. 2.2: (a): Power transfer between wind turbine connection point and fault point represented as a single line diagram. (b): When a nearly solid three-phase fault occurs, the digram can be simplified as indicated by the blue arrow. R_F is the fault resistance. Boldface symbols denote vector notation. Source: **[J1]**.

minals with its terminal voltage, the injected active and reactive currents are obtained as

$$I_a = \frac{V_{PCC}R_L}{Z_L^2} + \frac{V_F X_L \sin(\delta)}{Z_L^2} - \frac{V_F R_L \cos(\delta)}{Z_L^2}, \tag{2.4}$$

$$-I_r = \frac{V_{PCC}X_L}{Z_L^2} - \frac{V_F X_L \cos(\delta)}{Z_L^2} - \frac{V_F R_L \sin(\delta)}{Z_L^2}. \tag{2.5}$$

Considering a worst-case symmetrical fault where $V_F = 0$ then

$$I_a = \frac{V_{PCC}R_L}{Z_L^2}, \quad I_r = -\frac{V_{PCC}X_L}{Z_L^2} \tag{2.6}$$

$$\implies \frac{I_a}{I_r} = -\frac{R_L}{X_L} \quad \text{when} \quad V_F = 0. \tag{2.7}$$

From (2.7), it becomes evident that pure reactive power cannot be transferred as required by the grid code without overcurrent provision. Also, it can be observed that the active and reactive power injected by the converter when $V_F = 0$ only serves as losses in the resistance and reactance of the line impedance. To that end, the PCC voltage is entirely determined by the line impedance and the injected currents, which means that a grid-following converter has no voltage to follow, i.e., instability occurs. As can be seen from (2.7), the grid code requirements on pure reactive current injection cannot be satisfied and will result in static instability if attempted.

Considering the voltage at the faulted bus not to be zero, but to have a very small value, it can be concluded that for a given injection of reactive current, some positive active power must be injected due to the presence of the line resistance. Hence, if the voltage V_F drops below some critical value, which is dependent on the network parameters, pure reactive power injection is not possible, and an unstable non-physically realizable operating point is attempted.

According to [41], power system faults are highly resistive, and as shown in [96], the voltage waveform at the fault location during reactive current injection can be considered decoupled from the converter current. Based on this, it can be assumed that the voltage magnitude at the fault location remains constant during the fault, independent on the converter current injections. With this, the blue-dotted lines shown in Fig. 2.3 are used to obtain the static stability limit of the system.

Fig. 2.3(a) shows an arbitrarily injected current vector that causes a voltage drop on the line impedance, $\boldsymbol{Z_L}$, which forms the shown vector diagram. When the magnitude of the injected current is increased, the angle between the PCC voltage and the voltage at the fault location is increased. Fig. 2.3(b) shows a limit case from where the magnitude of the injected current cannot be further increased without instability. If this is attempted, $\boldsymbol{v_F}$ cannot be located at the circle with a constant magnitude, which implies, that a non-existing operating point is attempted. The limit case, shown in Fig. 2.3(b), can mathematically be expressed as

$$V_F \leq Z_L I_{lim} \sin(-\theta_I - \theta_Z) \quad \implies \quad I_{lim} \leq \frac{V_F}{Z_L \sin(-\theta_I - \theta_Z)}. \tag{2.8}$$

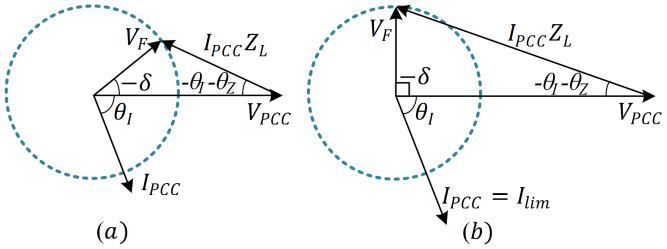

Fig. 2.3: Phasor diagram of current injection during a fault where the dotted blue circles represent a fault voltage with constant magnitude and arbitrary angle. (a): a stable case, (b): a limit case where the angle between sending end and receiving end voltage is 90° [43]. Source: **[J1]**.

Generally, the limit of the current magnitude given any θ_I can be written as

$$I_{lim} \leq \frac{V_F}{Z_L|\sin(\theta_I + \theta_Z)|} \quad \forall \quad \theta_I, \theta_Z \in \Re. \tag{2.9}$$

(2.9) represents the critical limit or necessary condition for attaining synchronization stability. This means that no matter the synchronization method used, instability will occur if this constraint is not fulfilled. During purely overexcited operation where $\theta_I = -90°$ as requested by most grid codes under severe grid faults (Fig. 2.1(b)), this reduces to

$$I_{lim} \leq \frac{V_F}{Z_L \cos(\theta_Z)} = \frac{V_F}{R_L}, \tag{2.10}$$

which is only depending on the fault voltage magnitude and the line resistance. This means that the line reactance does not influence the theoretical static limit for the injected current magnitude. To that end, if the line is purely inductive, the limitation on the injected capacitive reactive current extends to infinity, and no instability will occur. This is intuitive as the converter may inject any reactive current to an inductive line. Besides the current limit presented, it can be seen from (2.9), that for any current and impedance angle, the maximum allowed converter current magnitude will be

$$I_{lim} = \frac{V_F}{Z_L}. \tag{2.11}$$

Therefore, if the nominal current injection is considered (1 pu), then if $V_F > Z_L$, a stable operating point will always exist, and the current transfer can be accomplished.

To better exemplify this, the stable area for the injected current vector is depicted in Fig. 2.4 for three fault conditions with increasing severity. As previously mentioned, if the magnitude of the injected current vector is below V_F/Z_L, then it will always be located within the green stable operating area. However, considering the converter to inject purely capacitive reactive current during the fault, then as depicted in Fig. 2.4(c), $I_{lim} < 1$ pu, which implies that the attempt to satisfy the grid code requirements will result in a non-realizable static operating point and immediate system instability.

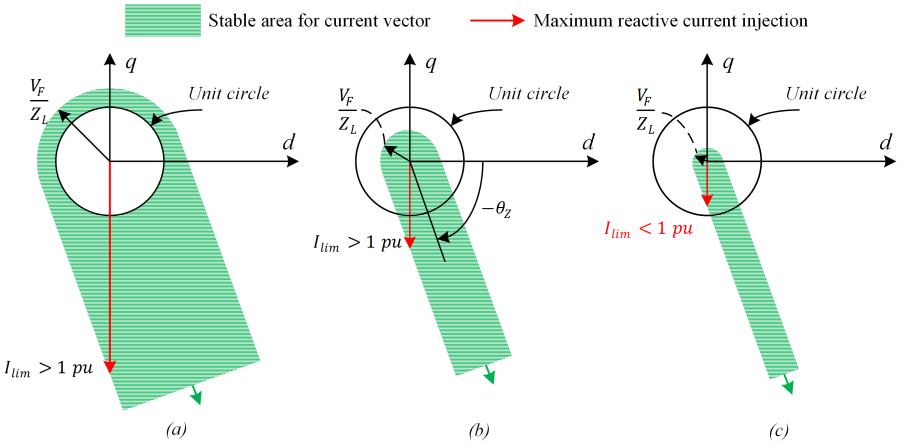

Fig. 2.4: Depiction of the stable area of injected current vector during grid faults. (a) : a grid fault where $V_F/Z_L > 1$ pu, (b) : a more severe grid fault where still $V_F/Z_L > 1$ pu but margins are reduced, and (c) : an extremely severe grid fault where $V_F/Z_L < 1$ pu and nominal capacitive reactive current cannot be injected as requested by the grid code [43]. All cases are shown for $X/R = 2.5$.

Remark 2.2.1 (Current Alignment for Ensured Stability)
It can be seen from (2.9), that when the angle of the current vector is aligned with the negative of the impedance angle ($\theta_I = -\theta_Z$), the injected current has no limit and theoretically an infinite amount of current can be injected. This is the foundation for the LOS mitigation method in [66], which will be further discussed in *Chapter 5*.

2.2.1 Stability Assessment using Static Limit

A full-order simulation model of the grid-following structure shown in Fig. 1.6 is developed to test the validity of the static stability limit in (2.9). Two test cases are conducted where the first is designed to be a stable case, and the second is designed to be an unstable case considering the stability constraint in (2.9). This is presented in Fig. 2.5 for two designs of the PLL, where the damping ratio of PLL 2 is larger than that of PLL 1. As can be seen, the static stability does not alone provide a sufficient condition for transient stability. The dynamics of the PLL have an impact as well. From Fig. 2.5(a), one can notice that the PLL needs a certain damping to attain a stable response. With that being said, the static stability limit is, as can be expected, accurate when (2.9) is not being satisfied, i.e., it is a necessary condition for stability. Nevertheless, it can be disclosed that the dynamics of the PLL needs to be accounted for if an accurate transient stability assessment is to be attained.

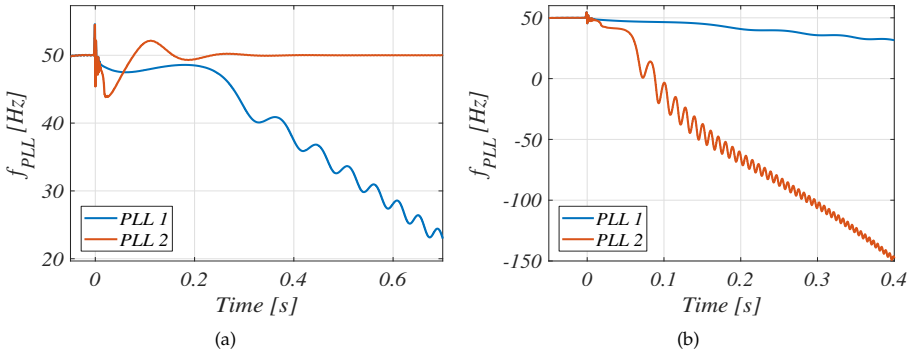

Fig. 2.5: Stability analysis of PLL used to validate current transfer limits presented in (2.9) during a fault at 0 seconds. Two PLL dynamics are tested where PLL 2 has a higher bandwidth than PLL 1. Capacitive reactive current is injected and $R_L = 0.04$ pu. (a): Voltage at fault locations drops to 0.05 pu (stable from static limit). (b): Voltage at fault location drops to 0.03 pu (unstable from static limit).

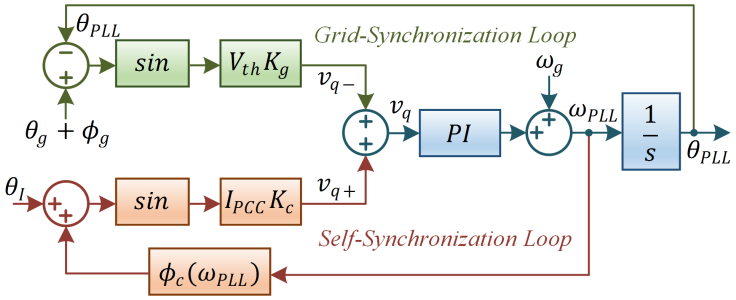

Fig. 2.6: Quasi-static large-signal model of the converter, grid network, and SRF-PLL [58]. The grid-synchronization loop (green part) represents the usually seen synchronization model of an SRF-PLL, whereas the self-synchronization loop (red part) represents the interaction between the converter operation and the voltage at the PCC. Source: **[J1]**.

2.3 Quasi-Static Large-Signal Model

In the previous subsection, it was shown that the static stability limit is indeed descriptive and accurate when no stable operating point exists. However, to be able to assess the transient stability in more details, the PLL dynamics need to be considered. This type of model is referred to as quasi-static, as only the outer PLL dynamics are included, whereas the internal current control and voltage feed-forward are neglected and assumed ideal. The justification for this assumption will be given in the next chapter. In the following, using the formulation around the quasi-static large-signal model as initially presented in [58, 66, 97], more physical interpretation and understanding of LOS can be disclosed. Using the network model from Fig. 2.2 and following the derivation in **[J1]**, the q-axis component of the PCC voltage can be expressed and visualized as the block diagram shown in Fig. 2.6. This consists

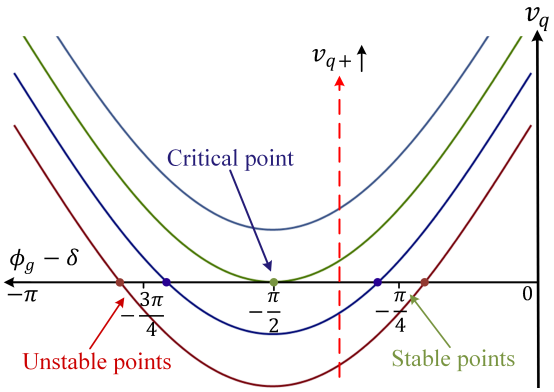

Fig. 2.7: Operating points for $v_q = 0$ for increasing self-synchronization term during injection of capacitive reactive current [66]. δ is the angle difference between the PCC voltage and grid voltage. Source: **[J1]**.

of a grid-synchronization loop, usually included for small-signal PLL analysis and a self-synchronization loop, originating since the injected converter currents themselves create a voltage drop on the line impedance, which is observed in the PCC voltages that the converter attempts to synchronize to. Hence, the self-synchronization loop is a destabilizing term since the converter will aim to synchronize to a voltage which may constitute a significant part created by the converter itself. Here, the power transfer problem, as described in the previous subsection, is visualized as a positive feedback system which is depending on the injected current vector (I_{PCC}) and the network impedance (K_C). The fundamental principle of the SRF-PLL is to regulate $v_q = 0$. However, as it is depicted in Fig. 2.7, for an increasing v_{q+} (or decreasing v_{q-}/grid faults), the nonlinear curve for v_q as function of δ may not have a solution to $v_q = 0$. To that end, as shown in Fig. 2.7, only the solution where $\delta > -\pi/2$ represents a stable operating point. The model formulation in Fig. 2.6, even though it has the same static limitation as in (2.9) **[J1]**, gives an intuitive visualization of why LOS occurs and which parameters influence it. To that end, it stipulates many ideas and attempts to decrease or eliminate the positive feedback loop (v_{q+}) as this is the main instability excitation driver. Accordingly, the static instability originates as a result of low grid voltages (low grid-synchronization term, v_{q-}) and high injected currents and network impedances (high self-synchronization term, v_{q+}).

2.3.1 Analogy between PLL and a Synchronous Machine

As mentioned above, the quasi-static model from Fig. 2.6 reveals the same analytical stability assessment as for the static network model in (2.9). However, as it was seen in Fig. 2.5, the dynamics of the PLL need to be considered for an accurate assessment. Due to the desire for an analytical expression for the stability, then by considering the dynamics of the PLL, a second-order nonlinear model can be obtained. For an inductive line impedance, it is shown in **[J1]** that this equation may be put on an

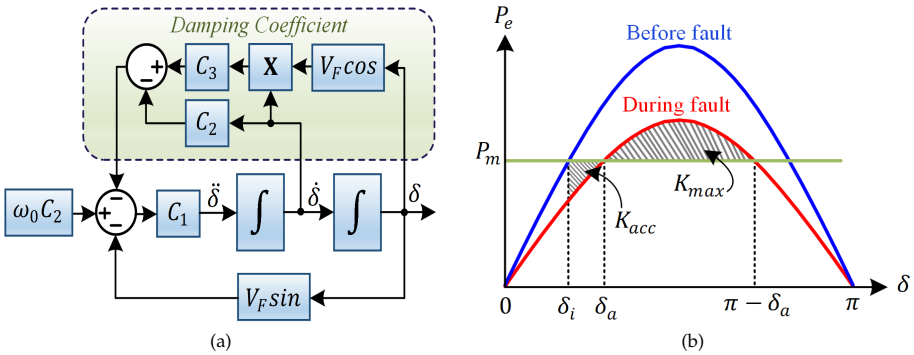

Fig. 2.8: Quasi-static model is analogous to synchronous machine equations. (a): Block diagram of the synchronization model based on the second-order non-linear equation in (2.12) derived for an inductive grid [57]. The equivalent damping term can be identified. (b): P_e and P_m versus δ from (2.12) are shown for the pre-fault condition and during the fault. The accelerating area (K_{acc}) and maximum decelerating area (K_{max}) used in the EAC to assess the transient synchronization stability are visualized. Source: **[J1]**.

equivalent synchronous machine model form as

$$\underbrace{\frac{1}{C_1}}_{M_v}\ddot{\delta} = \underbrace{\omega_0 C_2 - V_F \sin(\delta)}_{P_m - P_e} - \dot{\delta}\underbrace{(C_3 V_F \cos(\delta) - C_2)}_{\text{Damping Coefficient}}, \tag{2.12}$$

where

$$C_1 = \frac{K_i}{1 - K_p C_2}, \quad C_2 = L_L I_{PCC} \cos(\theta_I), \quad C_3 = \frac{K_p}{K_i}.$$

Here, the equivalent damping coefficient is identified and highlighted in Fig. 2.8(a). It is evident that the damping coefficient is a nonlinear function of δ, which is depending on the PLL controller gains, the injected currents, and the line impedance. The analogy of this model to the synchronous machine has initiated the idea of assessing the transient stability using the equal-area criterion as commonly applied for simple SM configurations. Doing this, an analytical expression for the accelerating area (K_{acc}) and the critical deceleration area (K_{max}) can be obtained, which are visualized in Fig. 2.8(b). Then if $K_{acc} > K_{max}$, the system is predicted to be unstable. This approach neglects the nonlinear damping term and, therefore, provides a conservative stability assessment. Therefore, to attain a more accurate stability prediction capability, two approaches will be pursued in the following chapter: (i): based on the nonlinear second-order model, can an analytical expression for the transient stability including the damping term be derived? And (ii) can a numerical approach be used to estimate the transient stability, including the nonlinear damping coefficient, for a reduced-order model that does not assume the grid to be purely inductive?

2.4 Summary

In this chapter, the fundamental instability LOS phenomenon is described and physically explained. Initially, a static stability limit for the injected current magnitude is presented. This serves as a strong tool in understanding the synchronization issue, which is related to the power transfer between two or more buses. To that end, this static limit is a necessary condition for stability. To attain an accurate transient stability evaluation it is shown that the dynamics of the PLL must be included. A quasi-static PLL model was presented, which provides an intuitive understanding of the instability phenomenon and identifies a positive feedback loop, originating due to the currents injected by the converter itself. Based on a purely inductive grid, a second-order model with an equivalent form as for a synchronous machine can be developed. This enabled the identification of equivalent system damping, which is shown to have a significant impact on the transient stability. Accordingly, the entire PLL dynamics must be included for accurate transient stability assessment.

Related Publication

[J1] **M. G. Taul**, X. Wang, P. Davari and F. Blaabjerg, "An Overview of Assessment Methods for Synchronization Stability of Grid-Connected Converters Under Severe Symmetrical Grid Faults," in *IEEE Trans. Power Electron.*, vol. 34, no. 10, pp. 9655-9670, Oct. 2019.

Main contribution:
An overview of available methods for evaluating the large-signal synchronization stability is presented. This includes a comprehensive comparison of the different models, which is experimentally verified, alongside a discussion of the future trends and remaining challenges within this topic.

Chapter 3

Reduced-Order Modeling of Converter Synchronization Stability

3.1 Background

Based on the previous chapter, a quasi-static model of the PLL-synchronized converter was presented. By comparing the quasi-static large-signal model to a full-order switching and averaged model, it can be seen in Fig. 3.1 that this simplified representation yields a close approximation of the full-order model in the case of a severe grid fault. In addition to this, from the questions formulated at the end of *Chapter 2*, it is desired to attain an analytical expression or applicable numerical approach to predict the system stability, both of which cannot be accomplished using the quasi-static large-signal model from *Chapter 2*. Furthermore, the quasi-static large-signal model from *Chapter 2* assumes the external network to be purely inductive or resistive. However, the static stability limit is depending on the fault voltage magnitude and the line resistance when the converter allocates its current injection capability to reactive current. Therefore, the line resistance cannot be neglected in the model.

This chapter aims to address these issues by developing a reduced-order model for the grid-following converter that is valid for a line impedance being both resistive and inductive. To that end, a computationally efficient numerical approach is proposed to estimate the critical damping ratio and area of attraction of the nonlinear system. Lastly, it will be shown why a numerical approach may be more suitable for systems governed by nonlinear trigonometric function when the Lyapunov stability theory is adopted on the proposed model. For the above, this is conducted for symmetrical grid faults. However, as most grid faults are actually asymmetrical, the reduced-order modeling approach is extended to asymmetrical faults using symmetrical component

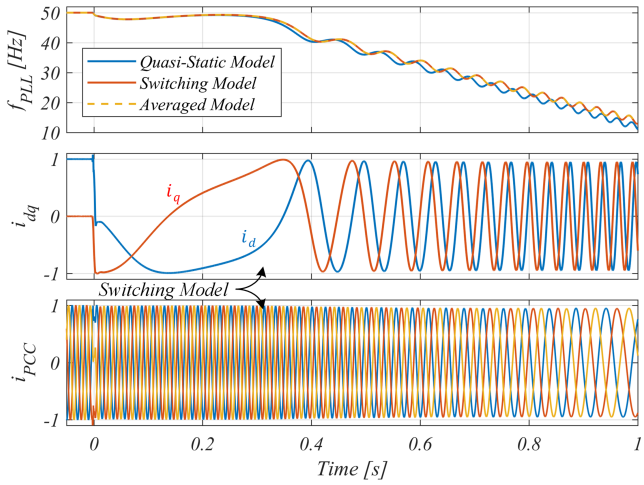

Fig. 3.1: PLL frequency response for the quasi-static model, averaged model, and a detailed switching model where a severe three-phase fault ($V_F = 0.05$ pu) appears at 0 s. Subplot 2 and 3 contain the per-unit dq-axes and three-phase injected currents obtained from the switching model. The simulations are performed on the system shown in Fig. 1.6. Source: **[J1]**.

theory and a more sophisticated synchronization structure.

3.2 Symmetrical Faults

The new reduced-order nonlinear model is developed from the considered grid-following converter shown in Fig. 3.2. The converter is connected to a line impedance and a Thevenin equivalent grid where a symmetrical fault ($\mathbf{Z_f}$) is considered to occur in between. As seen, the full converter control is represented as an ideal current source, oriented by the dynamics of the SRF-PLL. Such a representation can be assumed for two reasons. First, the dominating dynamics of loss of synchronization lies in the low-frequency range. Secondly, the bandwidth of the inner current regulator is usually placed much higher than that of the PLL, which facilitates that they can be analyzed individually [58, 61, 67]. With that being said, instabilities associated with the current controller and control delays interacting with the passive filter resonances are beyond the predictability of this model. Accordingly, this model should only be used to analyze issues with slow modes, originating from the imbalance in active power injection, as this is the focus here. As previously justified, the fault voltage magnitude is considered decoupled from the converter current injection. Using this, the q-axis component of the PCC voltage can be written as

$$v_q = Z_L I_{PCC} \sin(\theta_I + \phi_c) - V_F \sin(\delta) \tag{3.1}$$

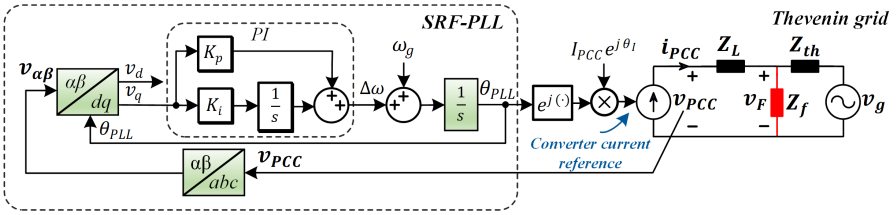

Fig. 3.2: Simplified model of a grid-tied converter during a power system fault where the fault location is denoted as v_f. A simplified grid-following control structure consisting of an SRF-PLL and an ideal current controller is used for the analysis. Z_L: Line impedance, Z_{th}: Thevenin grid impedance, Z_f: Fault impedance. Source: **[C2]**

where $\delta = \theta_{PLL} - \theta_g$. From the SRF-PLL in Fig. 3.2, the estimated phase angle can be expressed as

$$\theta_{PLL} = \int \left(K_p v_q + K_i \int v_q \, \mathrm{dt} + \omega_g \right) \, \mathrm{dt}. \tag{3.2}$$

Using that $\int \omega_g \mathrm{dt} = \theta_g$, subtracting this to the left-hand side to achieve δ, the second-order nonlinear model for the PLL-synchronized converter can be obtained as

$$0 = \ddot{\delta} + D(\delta)\dot{\delta} + F(\delta), \tag{3.3}$$

where

$$D(\delta) = \frac{K_p V_F \cos(\delta)}{1 - K_p I_{PCC} L_L \cos(\theta_I)}, \tag{3.4}$$

$$F(\delta, \dot{\delta}) = \frac{K_i \left(V_F \sin(\delta) - Z_L(\dot{\delta}) I_{PCC} \sin(\theta_I + \phi_c(\dot{\delta})) \right)}{1 - K_p I_{PCC} L_L \cos(\theta_I)}. \tag{3.5}$$

The mathematical derivation of this is carefully explained in **[C2]**. This model contains the information of both the line resistance and reactance, contrary to the formulations presented in (2.12) in the previous chapter. Since the second-order nonlinear equation in (3.3) has no known analytical solution, numerical methods must be applied to compute the solution. Also, since the system is of second order, phase-plane analysis can be used to visualize the trajectories of the state variables instead of solving the time-consuming full-order simulation model [98]. Using phase-plane analysis, one can graphically view the state trajectory in the $(\boldsymbol{x}, \dot{\boldsymbol{x}})$ phase-plane, which has a unique solution given initial conditions and that $F(\delta, \dot{\delta})$ and $D(\delta)$ are continuously differentiable [99]. To visualize the solution in the phase-plane, the second-order nonlinear system must be expressed as a set of coupled first-order equations on the form

$$\dot{\boldsymbol{x}} = \boldsymbol{f}(\boldsymbol{x}) \tag{3.6}$$

where $\boldsymbol{x} = (x_1, x_2)$ and $\boldsymbol{f}(\boldsymbol{x}) = (f(x_1, x_2), f(x_1, x_2))$. Using the variable transformation as $(x_1 = \delta, x_2 = \dot{\delta})$, the second-order system may be expressed as

$$\begin{bmatrix} \dot{x_1} \\ \dot{x_2} \end{bmatrix} = \begin{bmatrix} f_1(x_1, x_2) \\ f_2(x_1, x_2) \end{bmatrix} = \begin{bmatrix} x_2 \\ -F(x_1, x_2) - D(x_1)x_2 \end{bmatrix}. \tag{3.7}$$

Table 3.1: Main parameters of the detailed simulation model and experimental test setup

Symbol	S_b	V_b	V_{dc}	f_0	f_{sw}	f_s	L_{cf}	L_{gf}	C_f	K_{pc}	K_{ic}
Value	7.35 kVA	400 V	650 V	50 Hz	10 kHz	10 kHz	0.07 pu	0.04 pu	0.07 pu	12	1000

How to set up and solve the mathematical problem for transient stability assessment is summarized in Fig. 3.3. Details on deriving the initial conditions for the state variables can be found in **[C2]**. To assess the accuracy and efficiency of the developed reduced-order model, the transient stability predictions for different cases are compared between the proposed model, a detailed simulation model, and experimental tests from a laboratory setup. The detailed model and experimental results include the converter switching behavior, output LCL-filter, and an inner current controller with PCC voltage feed-forward. The parameters used for the different test cases are listed in Table 3.1, and the modeled, simulated, and experimentally measured results are shown in Fig. 3.4. The phase-plane trajectories of three different damping ratios are shown in Fig. 3.4(a) where $\zeta = 3.35$ represents the critical damping, sufficient for transient stability when the fault voltage drops to $V_F = 0.045$ pu. These results are shown as a function of time in Fig. 3.4(b), which are compared to the results of the detailed simulation model in Fig. 3.4(c). As can be seen, the reduced-order representation of the PLL-synchronized converter has a nearly exact match with the detailed model when studying the large-signal synchronization stability and estimated frequency. The damping ratio is a function of the control parameters of the PLL as $\zeta = \frac{K_p}{2}\sqrt{V_{PCC}/K_i}$.

From the experimental results in Fig. 3.4(d)-(f), it is clear that the simplified model serves as a strong tool in accurately capturing the dominant characteristics of the system during severe symmetrical grid faults. Even though the discrepancy between the reduced-order model and the experimental results is small, the observed error may very well be caused by the passive component values not precisely matching the modeled ones from Table 3.1.

3.2.1 Nonlinear PLL Damping

With the reduced-order model being a clear representative of the detailed full-order system, it is desired to analyze whether an analytical expression for a sufficient condition can be obtained. Using (3.3), it is possible to set up the equivalence between the reduced-order model and the second-order swing equation of a synchronous machine. By dividing (3.3) with K_i, the equivalent system inertia and damping can be derived as

$$J_{eq} = \frac{1}{K_i}, \quad D_{eq}(\delta) = \frac{K_p}{K_i}\frac{V_F\cos(\delta)}{1 - K_p I_{PCC} L_L \cos(\theta_I)}. \tag{3.8}$$

It is evident that the equivalent system damping is proportional to K_p and inversely proportional to K_i. Hence, this gives a relationship between the PLL controller parameters and their influence on the damping coefficient. It can be seen that there exist three possibilities to achieve infinite damping: $Kp = \infty$, $K_p = 1/(I_{PCC}\cos(\theta_I))$, or $K_i = 0$. The first possibility is clearly not an option since one cannot assign an infinite

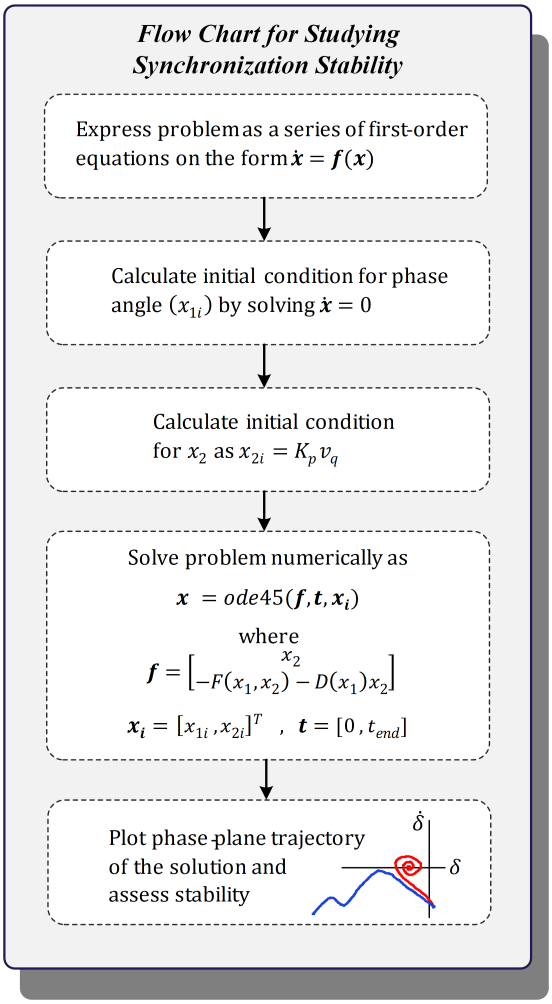

Fig. 3.3: Flow chart describing how to assess the converter synchronization stability, including how to set up the nonlinear problem, how to calculate the initial conditions, and how to compute the solution. ode45: Ordinary differential equation solver based on a variable step size Runge-Kutta method for numerical integration. Source: **[C2]**

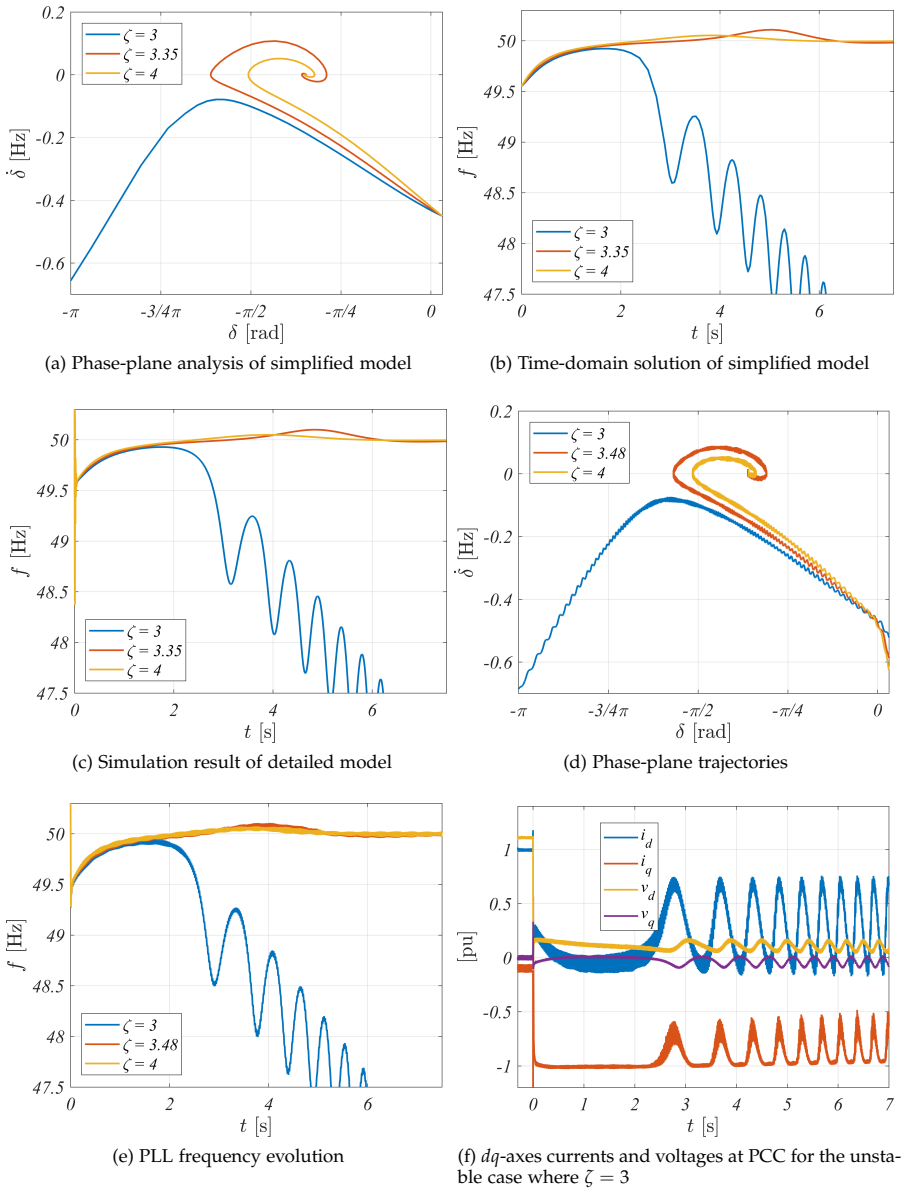

(a) Phase-plane analysis of simplified model

(b) Time-domain solution of simplified model

(c) Simulation result of detailed model

(d) Phase-plane trajectories

(e) PLL frequency evolution

(f) dq-axes currents and voltages at PCC for the unstable case where $\zeta = 3$

Fig. 3.4: Simulation results (a)-(c) and experimental results (d)-(f), showing the influence of PLL damping ($\zeta = \frac{K_p}{2}\sqrt{V_{PCC}/K_i}$) on the converter synchronization stability during a severe symmetrical grid fault. $V_F = 0.045$ pu and $K_p = 0.1948$ for all results. Source: **[C2]**.

number to a control parameter. The second approach only works when $\theta_I \neq \pm\pi/2$ since this will automatically result in the first approach. Also, during severe faults, θ_I is $-\pi/2$ or close to it. The last option removes the integral action from the SRF-PLL, making it a first-order synchronization loop as previously proposed in [69]. However, besides the selection of the PLL controller gains, it can be observed that the sign of the damping coefficient depends on $\cos(\delta)$. Thus, as negative-feedback regulation is used, a positive system damping is needed to ensure stability. If $\pi/2 < \delta < -\pi/2$, the damping will be negative, and the overall regulation will act as a positive-feedback system, leading to instability. Considering an operating point to exist during the fault, then if e.g., $K_i = 0$, δ will never overshoot to cause a negative damping, i.e., the system is globally stable. This approach will be further discussed in *Chapter 5*. Since setting $K_i = 0$ makes the synchronization unit blind to frequency deviations, it may instead be desirable to know how large or how small to set K_p or K_i, respectively, to guarantee transient stability. The Lyapunov stability theory is used to analyze this.

3.2.2 Stability Assessment using Lyapunov Function

The trajectory of the nonlinear dynamics of the synchronization process is similar to the study of a nonlinear mass-spring-damper system. Suppose that a mass in a system is dragged to a non-relaxed position of the spring and suddenly released. What will be the characteristics of the system, and will the trajectory of the system be stable? In the case of a linearized system, the linear approximation will no longer be valid for this large disturbance. This is similar to the synchronization process of a grid-connected converter during a severe grid fault. Thus, to assess whether the system will be able to remain stable after the mass is dragged (the voltage is dropped) depend on the nonlinear dynamics of the system. One way to analyze this analytically, is to investigate whether the total energy of the system will decrease during the fault. Using (3.3) with $\theta_I = -\pi/2$, the system may be written as

$$0 = \frac{1}{K_i}\ddot{\delta} + \frac{K_p}{K_i}V_F\cos(\delta)\dot{\delta} + V_F\sin(\delta) - R_L I_{PCC}. \tag{3.9}$$

The total energy of the system can be used as a candidate for a Lyapunov function, which is

$$\begin{aligned} V(\delta,\dot{\delta}) &= \frac{1}{2K_i}\dot{\delta}^2 + \int_0^{\delta} V_F\sin(\sigma) - R_L I_{PCC}\mathrm{d}\sigma \\ &= \frac{1}{2K_i}\dot{\delta}^2 + V_F(1-\cos(\delta)) - \delta R_L I_{PCC}. \end{aligned} \tag{3.10}$$

For the function to be a Lyapunov function it must be a scalar positive definite satisfying that $V(0,0) = 0$ and $V(\delta,\dot{\delta}) > 0\ \forall\ \delta,\dot{\delta} \neq 0$. Furthermore, its time-derivative of any state trajectory must be negative semi-definite meaning that $\dot{V}(\delta,\dot{\delta}) \leq 0$. Since the system is autonomous (the system dynamics are independent on time, i.e., time-invariant equations), then by the chain rule we obtain

$$\dot{V}(\boldsymbol{x}) = \frac{d}{dt}V(\boldsymbol{x}) = \frac{\partial V(\boldsymbol{x})}{\partial \boldsymbol{x}}\frac{d\boldsymbol{x}}{dt} = \frac{\partial V(\boldsymbol{x})}{\partial \boldsymbol{x}}\dot{\boldsymbol{x}} = \frac{\partial V(\boldsymbol{x})}{\partial \boldsymbol{x}}f(\boldsymbol{x}). \tag{3.11}$$

By using that

$$\frac{1}{K_i}\ddot{\delta} = -\left(\frac{K_p}{K_i}V_F\cos(\delta)\dot{\delta} + V_F\sin(\delta) - R_L I_{PCC}\right), \tag{3.12}$$

the time-derivative of (3.10) is

$$\dot{V}(\delta,\dot{\delta}) = -\frac{K_p\dot{\delta}V_F\cos(\delta)}{K_i}. \tag{3.13}$$

One might also intuitively come up with this expression since the change in the total energy equals the power dissipated by the nonlinear damping term in (3.8). However, as can be seen from (3.13), one cannot generally determine the sign of the nonlinear damping term. Considering the PLL controller gains to be positive values, and if the sign of $\dot{\delta}$ and $\cos(\delta)$ are the same, then the equilibrium point will be globally stable. However, since one cannot guarantee that it will actually converge to this equilibrium point, it cannot be categorized as asymptotically stable. Accordingly, to assess the stability, another Lyapunov candidate must be pursued, the trigonometric functions in (3.9) must be approximated, or a numerical approach must be attempted. In the following, a numerical approach is proposed to estimate the stability boundary, critical damping, and area of attraction.

3.2.3 Numerical Approach to Determine Critical Damping and Area of Attraction

From the previous subsection, it is seen that due to the nonlinearity being a trigonometric function, it is difficult to assess whether the time-derivative of the Lyapunov function is negative semi-definite or not. One attempt to analytically deal with this could be to use an approximation of an infinite series expansion, e.g., Taylor approximation of the trigonometric functions in (3.9). Due to the low model order of the developed model, a numerical approach is preferred instead to assess the sufficient stability condition for the proceeding of this work. Compared to the detailed nonlinear simulation model, the proposed reduced-order representation can be rapidly computed for a large number of initial conditions. Using phase-portraits, the solution for each trajectory can be used to graphically visualize the area of attraction and associated critical damping for the nonlinear system. The time needed to reach a conclusion on the transient stability using the reduced-order model is on average more than 4,000 times shorter compared to the detailed switching simulation model (See **[C2]** for details on computational power and software specifications). This implies that performing a parameter sweep and plotting the phase-portrait of the system can be accomplished within seconds. As found from (3.8), the equivalent damping can be increased by increasing the proportional gain. This is done for different fault voltage magnitudes in Fig. 3.5 from where it is evident that for increased severity of the grid fault (lower V_F), the proportional gain of the PLL, needs to be increased accordingly to provide the sufficient critical damping. The damping ratio highlighted in Fig. 3.5 is computed from the linearized PLL model as

$$\zeta = \frac{K_p}{2}\sqrt{\frac{V_{PCC}}{K_i}}, \tag{3.14}$$

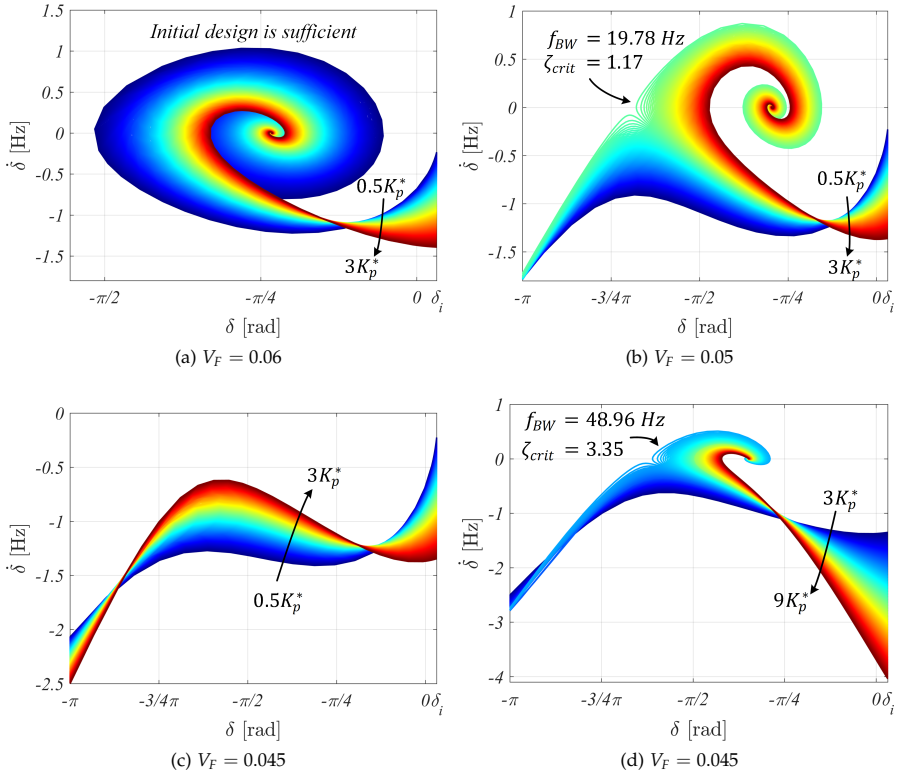

(a) $V_F = 0.06$ (b) $V_F = 0.05$

(c) $V_F = 0.045$ (d) $V_F = 0.045$

Fig. 3.5: Phase portraits for a varying PLL proportional gain, K_p of the system in Fig. 3.2. K_p^* denotes the initial PLL design for normal operating conditions. The color code goes from blue to red, where the damping increases towards the red graphs. Each sub-figure is shown for 200 different initial conditions. Source: **[C3]**.

where V_{PCC} is the nominal PCC voltage. As evident from Fig. 3.5, an increasing K_p also implies an increased controller bandwidth of the PLL. Too high bandwidth for the PLL is undesired since this will interfere with the inner current controller. Therefore, instead of increasing the proportional gain, one can decrease the integral gain of the PLL which has practically no effect of the bandwidth. Results of this is contained in **[C2]**. The area of attraction and critical PLL damping of the system when

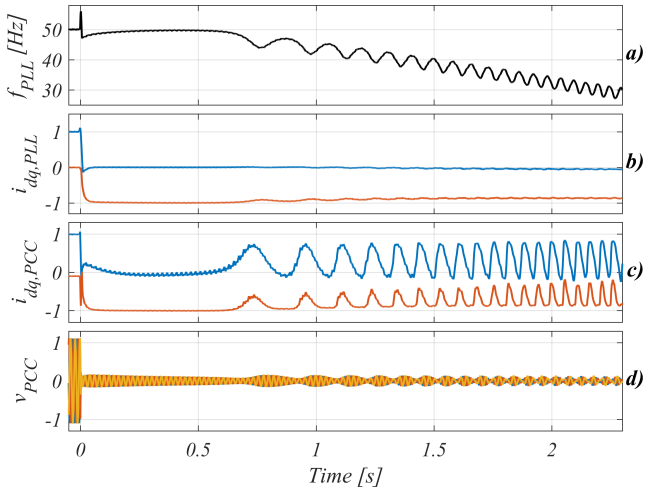

(a)

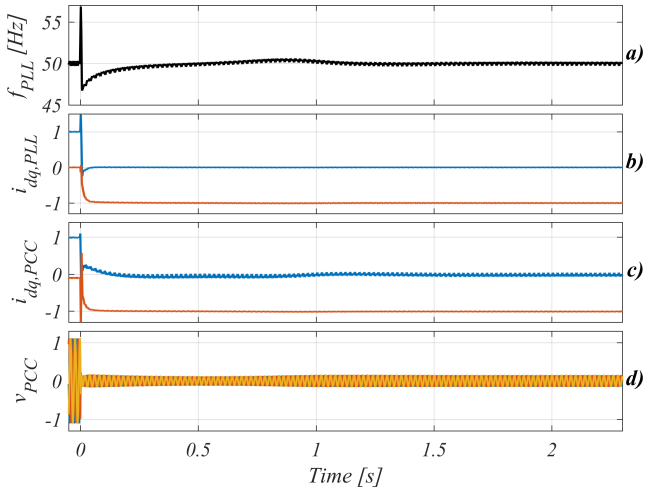

(b)

Fig. 3.6: Experimental results testing the critical damping obtained from the reduced-order model in Fig. 3.5(d). At 0 s the voltage at the fault location drops to 0.045 pu. (a): PLL damping ratio of 2.9, which is an unstable case. (b): PLL damping ratio of 3.27, which is a stable case (critically at the tipping point). Source: **[C3]**.

$V_F = 0.045\,\text{pu}$ is experimentally verified, as shown in Fig. 3.6. The sub-figures of Fig. 3.6 contain a): the estimated PLL frequency, b): the dq-axes current referenced to the PLL angle, c): the dq-axes currents references to the actual PCC voltage angle, and d): the three-phase PCC voltages. The difference in critical damping obtained using the reduced-order model, and the experimental setup is only 2.4 %. This strongly supports the applicability of the reduced-order model being used for transient stability assessment, and its computationally efficient properties make it possible to rapidly estimate the area of attraction and associated critical PLL damping.

3.3 Asymmetrical Faults

From the previous section, it was shown that a reduced-order model with the SRF-PLL dynamics can be used accurately asses the transient stability during symmetrical faults. However, as described in [41], more than 95% of all grid faults are asymmetrical. This means that the modeling framework presented in the previous section only represents a small subcategory of the framework needed for all grid faults. To that end, during asymmetrical grid faults, converters cannot only use a simple SRF-PLL for synchronization to the asymmetrical grid voltages. Under such conditions, notch-filtering is needed to extract the fundamental frequency positive- and negative-sequence voltage components. In this analysis, a dual reduced-order generalized integrator frequency-locked loop (DROGI-FLL) is used for synchronization [100]. This section presents a generalized modeling framework that puts focus on the reduced-order modeling and transient stability assessment of grid-following converters under any short-circuit fault type. Also, to take into account the present [101, 102] and future LVRT requirements on potential dual-sequence current injection during asymmetrical faults, the modeling framework considers converter current injections in both fundamental sequence frames. The grid-following converter under study is shown in Fig. 3.7(a) where a detailed view on the grid-following control for dual-sequence operation is shown in Fig. 3.7(b), and the structure of the DROGI-FLL can be seen in Fig. 3.7(c).

Deriving the q-axis component for the PCC voltage, as shown in (3.1), for both sequences

$$v_q^+ = V_F^+ \sin(\theta_F^+ - \theta^+) + Z_{LT} I^+ \sin(\phi_{LT}^+ + \theta_I^+) \tag{3.15}$$

$$v_q^- = V_F^- \sin(\theta_F^- - \theta^-) + Z_{LT} I^- \sin(\phi_{LT}^- + \theta_I^-), \tag{3.16}$$

one will find that the necessary stability conditions during asymmetrical faults are

$$I^+ \leq \frac{V_F^+}{|Z_{LT} \sin(\phi_{LT}^+ + \theta_I^+)|}, \quad I^- \leq \frac{V_F^-}{|Z_{LT} \sin(\phi_{LT}^- + \theta_I^-)|}. \tag{3.17}$$

Logically, the necessary conditions for transient stability are the same for both sequences. Also, during pure reactive current injection, the condition is only depending on the fault voltage magnitude and the line resistance. An example of this is shown in Fig. 3.8, where a double line-to-ground (DLG) fault is simulated. In Fig. 3.8(a), the line resistance is chosen in order to provide a stable operating point during the fault,

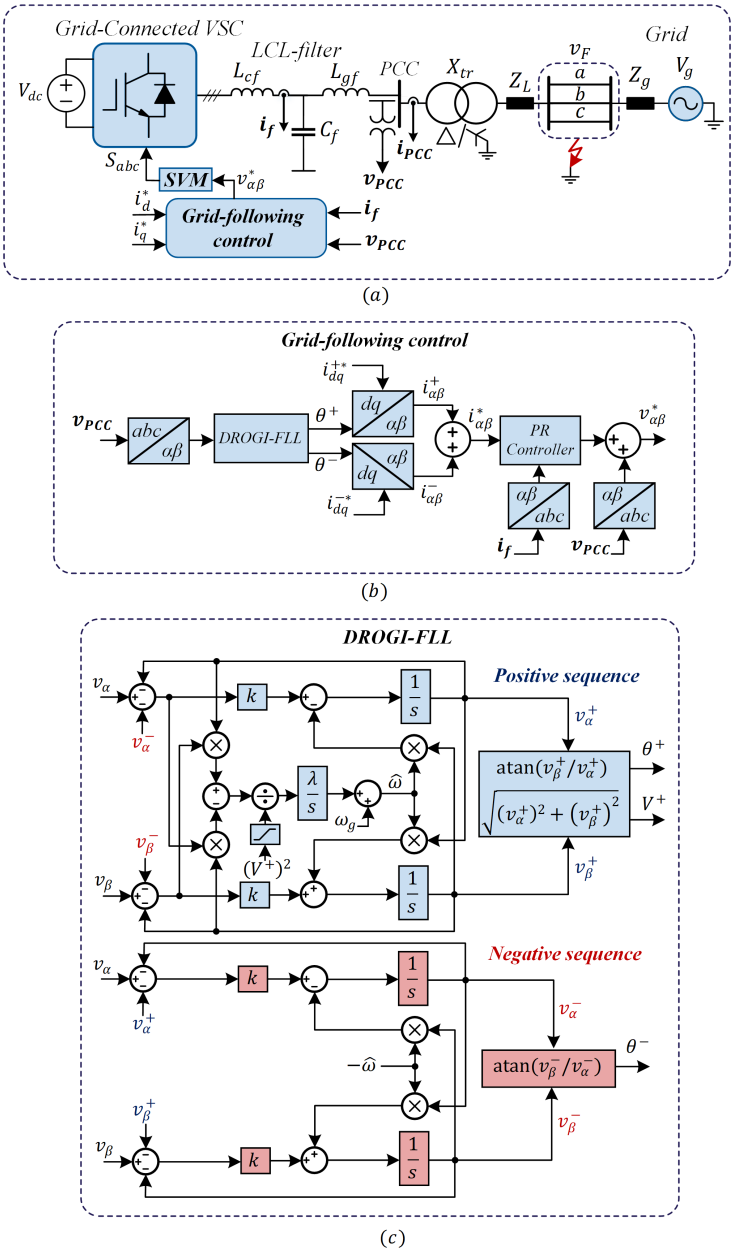

Fig. 3.7: Considered system under study for asymmetrical faults. (a): Structure of grid-tied converter with grid-following control connected to the grid where an asymmetrical grid fault is considered to occur at v_F. SVM: Space Vector Modulation. (b): Complete outlook of the grid-following control. (c): Detailed view of the DROGI-FLL used for sequence extraction and synchronization. Source: **[J4]**

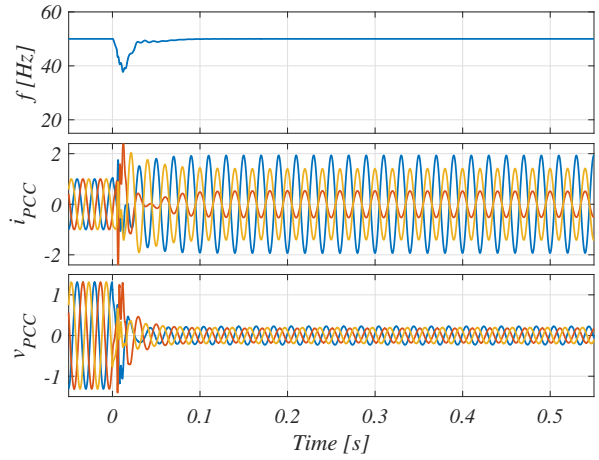

(a)

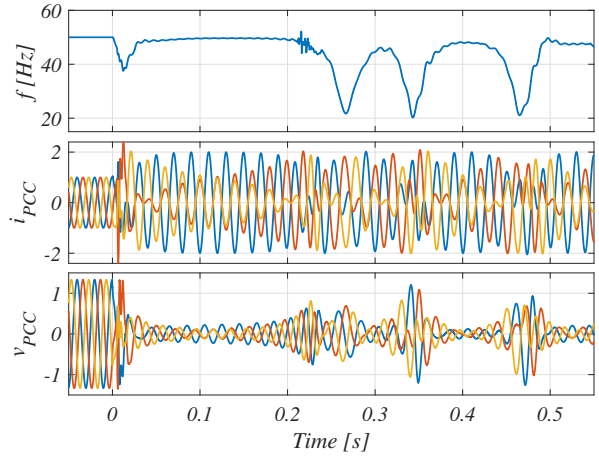

(b)

Fig. 3.8: Detailed simulation of system in Fig. 3.7 for a double line-to-ground (DLG) fault ($V_F^{\pm} = 1/3\,\text{pu}$) where 1 pu of current in both sequences are injected with $\theta_I^+ = -\pi/2$ and $\theta_I^- = \pi/2$. (a): The static limitations from (3.17) are met with $R_L = 0.32$, (b): The static limitations from (3.17) are violated with $R_L = 0.34$. Source: **[J4]**.

Table 3.2: Expressions for calculating symmetrical components at fault location for different fault types. SLG: Single line-to-ground. DLG: Double line-to-ground. LL: Line-to-line. Sym. Comp.: Symmetrical components.

Sym. Comp.	SLG	DLG	LL	3LG
V_F^+	$V_{th}^+ - \frac{Z_{th}^+(V_{th}^+ + V_{th}^-)}{Z_{th}^+ Z_{th}^- + Z_{th}^0 + 3Z_F}$	$\frac{(V_{th}^+ Z_{th}^- + V_{th}^- Z_{th}^+)(Z_{th}^0 + 3Z_F)}{Z_{th}^+ Z_{th}^- + Z_{th}^+ Z_{th}^0 + Z_{th}^- Z_{th}^0 + 3Z_F(Z_{th}^+ + Z_{th}^-)}$	$V_{th}^+ - \frac{Z_{th}^+(V_{th}^+ - V_{th}^-)}{Z_{th}^+ + Z_{th}^- + Z_F}$	$\frac{V_{th}^+ Z_F}{Z_{th}^+ + Z_F}$
V_F^-	$V_{th}^- - \frac{Z_{th}^-(V_{th}^+ + V_{th}^-)}{Z_{th}^+ Z_{th}^- + Z_{th}^0 + 3Z_F}$	$\frac{(V_{th}^+ Z_{th}^- + V_{th}^- Z_{th}^+)(Z_{th}^0 + 3Z_F)}{Z_{th}^+ Z_{th}^- + Z_{th}^+ Z_{th}^0 + Z_{th}^- Z_{th}^0 + 3Z_F(Z_{th}^+ + Z_{th}^-)}$	$V_{th}^- - \frac{Z_{th}^-(V_{th}^+ - V_{th}^-)}{Z_{th}^+ + Z_{th}^- + Z_F}$	0
V_F^0	$\frac{Z_{th}^0(V_{th}^+ + V_{th}^-)}{Z_{th}^+ Z_{th}^- + Z_{th}^0 + 3Z_F}$	$V_F^+ \frac{Z_{th}^0}{Z_{th}^0 + 3Z_F}$	0	0

whereas in Fig. 3.8(b), the resistance is increased to violate the necessary stability conditions. As can be observed, the necessary conditions can accurately be used to assess whether a fault scenario will result in instability. However, as discussed in the previous section with the damping ratio of the synchronization unit, it cannot determine whether a system will remain stable when the necessary conditions are not violated. Therefore, the dynamics of the DROGI-FLL need to be accounted for. To that end, for the simulation study shown in Fig. 3.8, the voltage sequence components were directly controlled at the fault location with a controllable voltage source. Under a real condition, the voltage magnitudes of the sequence components at the fault location depend on the short-circuit impedance and the injected currents by both the converter and the external grid. Therefore, before including the dynamics of the DROGI-FLL to assess the transient stability during asymmetrical faults, the $V_F^{\pm}$ components in the q-axis equations, (3.15) and (3.16), need to be updated to account for the coupling between the grounded short-circuit fault, the converter, and the external grid.

3.3.1 Equivalent Sequence-Domain Modeling of VSC

To determine $V_F^{\pm}$ during different grid faults, the phase-domain representation of the system is transformed into a positive-sequence network, a negative-sequence network, and a zero-sequence network. Based on these networks, Thevenin equivalents are derived to preserve the sequence voltages at the fault location. The approach of this, and how to transition from the phase-domain representation to sequence equivalents is visualized in Fig. 3.9. Details on how to derive the parameters for the sequence equivalents based on the converter operation is detailed in **[J4]**. The sequence equivalents obtained, as shown in Fig. 3.9 are decoupled. However, during asymmetrical faults, the sequence equivalents are coupled at the fault location, interconnected depending on the short-circuit type. In this work, single line-to-ground (SLG), DLG, and line-to-line faults are considered. The phase configurations of these at the fault locations are shown in Fig. 3.10. Based on the constraints from each fault type in Fig. 3.10, e.g., $i_{Fb} = i_{Fc} = 0$ for an SLG fault, it can be mathematically determined how the sequence equivalents from Fig. 3.9 should be interconnected during a particular fault type. Based on the constraints from Fig. 3.10, the interconnection of the sequence equivalents for the three fault types can be seen in Fig. 3.11. From these, the actual positive-sequence, negative-sequence, and zero-sequence voltage components at the fault location can be calculated. For each fault type, including symmetrical

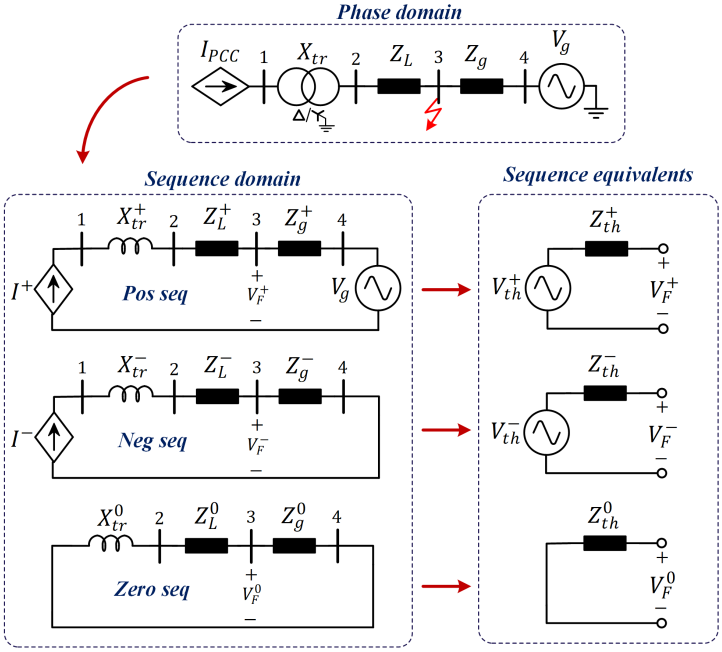

Fig. 3.9: Considered system represented in the phase domain, used to define the sequence domain networks from where the Thevenin sequence equivalents can be derived. The fault location is on bus 3, and the PCC is on bus 1. Source: **[J4]**.

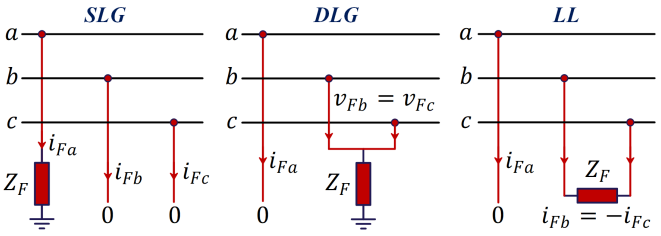

Fig. 3.10: Phase configurations at fault location for a single line-to-ground (SLG), a double line-to-ground (DLG), and a line-to-line (LL) fault. Source: **[J4]**.

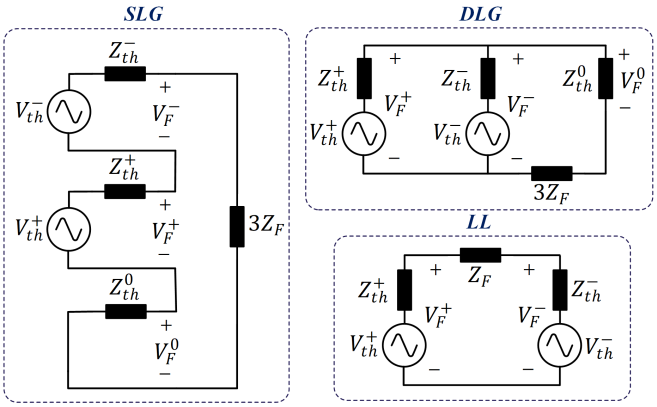

Fig. 3.11: Interconnection of equivalent sequence domain models for an single line-to-ground (SLG), a double line-to-ground (DLG), and a line-to-line (LL) fault. Source: **[J4]**.

faults, these are derived, and the expressions for the sequence components are listed in Table 3.2.

3.3.2 Reduced-order Large-Signal Model and Verification

To assess the large-signal synchronization stability dynamically, the expressions for V_F^+ and V_F^- (Table 3.2), depending on the fault type, are used in the expressions for the q-axis PCC voltage component from (3.15)-(3.16) and the dynamical model of the DROGI-FLL. This forms the reduced-order large-signal model shown in Fig. 3.12. As can be seen, the PCC voltage is estimated using the equivalent sequence networks, which is then fed to the DROGI-FLL. Depending on the electrical frequency estimated by the DROGI-FLL, the frequency-dependent network impedance is updated. In this way, any other synchronization unit different from the DROGI-FLL may be used, since the main model proposal lies in the simplified formulation of the PCC voltage fed to the synchronization unit. The reduced-order large-signal model is compared to a detailed simulation model and the results obtained from an experimental test setup. Details on the parameters and experimental setup can be found in **[J4]**. Different fault conditions are tested where the injected currents and the fault type are modified. To compare the model's applicability to identify the critical damping ratio of the synchronization unit, the control parameters of the DROGI-FLL are swept. The two control parameters, k, λ, of the DROGI-FLL are designed as

$$k = \frac{2\omega_N}{\sqrt{2}}, \quad \lambda = \omega_N^2. \tag{3.18}$$

Regarding the damping ratio, it can be shown that $\zeta \propto \frac{1}{\omega_N^2}$. Hence, the damping ratio can be increased by decreasing ω_N. In this way, the stability boundary can be estimated by sweeping ω_N during the different test cases. The results for the different fault types, both with and without negative-sequence current injection, are shown

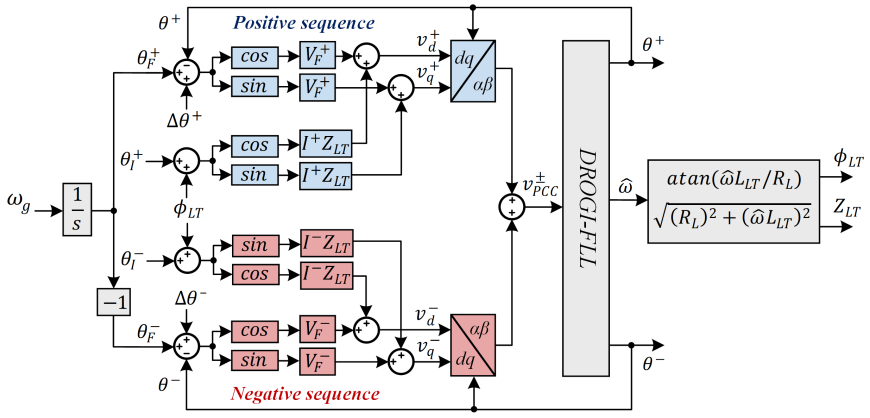

Fig. 3.12: The proposed simplified large-signal model for grid-synchronization stability evaluation during asymmetrical fault conditions for the system in Fig. 3.7. V_F^+ and V_F^- are obtained from Table 3.2 based on the fault type and converter operating mode. Source: **[J4]**.

Table 3.3: Boundary of synchronization stability of the proposed model, detailed simulation model, and experimental setup by varying ω_N in the DROGI-FLL, which is directly related to the damping ratio of the synchronization dynamics as in (3.18). Source: **[J4]**.

Fault Type	Stable?	Proposed Model	Simulation	Experimental
SLG	✔	$\omega_N = 34$	$\omega_N = 39$	$\omega_N = 41$
$I^+, I^- = 1,1$	✘	$\omega_N = 35$	$\omega_N = 40$	$\omega_N = 42$
DLG	✔	$\omega_N = 23$	$\omega_N = 23$	$\omega_N = 29$
$I^+, I^- = 1,0$	✘	$\omega_N = 24$	$\omega_N = 24$	$\omega_N = 30$
DLG	✔	$\omega_N = 19$	$\omega_N = 19$	$\omega_N = 28$
$I^+, I^- = 1,1$	✘	$\omega_N = 20$	$\omega_N = 20$	$\omega_N = 29$
LL	✔	$\omega_N = 30$	$\omega_N = 29$	$\omega_N = 38$
$I^+, I^- = 1,0$	✘	$\omega_N = 31$	$\omega_N = 30$	$\omega_N = 39$
LL	✔	$\omega_N = 25$	$\omega_N = 25$	$\omega_N = 33$
$I^+, I^- = 1,1$	✘	$\omega_N = 26$	$\omega_N = 26$	$\omega_N = 34$
3LG	✔	$\omega_N = 21$	$\omega_N = 22$	$\omega_N = 26$
$I^+, I^- = 1,0$	✘	$\omega_N = 22$	$\omega_N = 23$	$\omega_N = 27$

with simulations and the experimental test setup in Table 3.3.

It is observed that the proposed model matches the detailed simulation model with some conservatism towards ω_N. To that end, it can be seen that the experimental test setup possesses some unmodeled robustness during all test conditions. This is likely caused by a non-zero fault detection time in the experimental system, which is assumed zero in the simulation and proposed model. The increase in ω_N to estimate the stability boundary is also observed to occur in the simulation model when the fault detection time is non-zero. Hence, the presented reduced-order large-signal model for transient stability assessment during asymmetrical faults is rather accurate in its prediction with some conservatism, which leaves some headroom for model uncertainty and unmodeled dynamics.

3.4 Summary

In this chapter, reduced-order large-signal models are presented for both symmetrical and asymmetrical grid faults, which do not assume the line impedance to be purely resistive or inductive. For the case of symmetrical faults, it is shown that the damping ratio of the synchronization dynamics is nonlinear with respect to the estimated phase angle. As a result of this, a sufficient stability condition for transient stability using the total energy of the system as a Lyapunov candidate function could not be attained. Instead, a numerical approach was presented where a large number of test cases can be rapidly computed to estimate the critical damping ratio of the PLL and the system's area of attraction. The critical damping ratio obtained from the reduced-order model, visualized as phase portraits, were observed to be highly accurate when compared to experimental tests. To assess the transient stability during asymmetrical faults, this chapter also presented an extensive sequence-domain modeling framework of a grid-following converter with dual-sequence current injection. Here, necessary conditions for stability have been derived for both sequence frames where the voltage magnitude at the fault location is estimated using an equivalent sequence-domain modeling approach. This approach was merged with the dynamics of the operating synchronization unit to form a reduced-order large-signal model for large-signal synchronization stability evaluation during asymmetrical grid faults. Simulation and experiments verified the accuracy of the presented model.

Related Publications

[C2] **M. G. Taul**, X. Wang, P. Davari and F. Blaabjerg, "An Efficient Reduced-Order Model for Studying Synchronization Stability of Grid-Following Converters during Grid Faults," in *Proc. IEEE COMPEL*, Toronto, ON, Canada, 2019, pp. 1-7.

Main contribution:
A reduced-order large-signal model with no assumption on the line impedance structure is derived and expressed as a second-order nonlinear equation. This reduced-order model can be used for rapid transient stability assessment with a low computational burden and high modeling accuracy.

[C3] **M. G. Taul**, X. Wang, P. Davari and F. Blaabjerg, "Systematic Approach for Transient Stability Evaluation of Grid-Tied Converters during Power System Faults," in *Proc. IEEE ECCE*, Baltimore, MD, USA, 2019, pp. 5191-5198.

Main contribution:
To circumvent the need to use time-consuming time-domain simulation models to assess the transient stability of grid-following converters, this paper presents a systematic approach to perform the assessment. This approach is based on a fast numerical solution strategy of a reduced-order structure, which is visualized using phase-plane trajectories. Based on the systematic approach, a guideline on how to set the PLL controller gains and protection relays to ensure transient stability is given.

[J4] **M. G. Taul**, S. Golestan, X. Wang, P. Davari and F. Blaabjerg, "Modeling of Converter Synchronization Stability under Grid Faults: The General Case," submitted to *IEEE Trans. Power Electron.*, 2020.

Main contribution:
Necessary stability conditions for transient stability during asymmetrical grid faults are presented, which show that the positive- and negative-sequence frames can be analyzed individually, at least from a static point of view. A generalized model framework, which represents the grid interactions and converter control as equivalent sequence networks are presented. This can, together with the dynamics of any synchronization unit, be used to establish the proposed reduced-order large-signal model for transient stability assessment during any short-circuit fault type.

Chapter 4

Synchronization Stability of Multi-Converter Systems

4.1 Background

As previously described, grid-following PLL-synchronized converters are at risk of losing synchronism with the external network during severe grid faults while complying with LVRT requirements on dynamical voltage support. This issue has been addressed in the previous chapters, describing the root cause of instability and how to model and assess the stability. Yet, all of these analyses and previous work are developed for a single-converter-infinite-bus system. Consequently, the presented methods for modeling large-signal synchronization stability are no longer valid when studying paralleled converter operation and multi-converter systems.

The authors in [103–108] have addressed the synchronization stability of multi-converter systems, whereas only [107, 108] consider the large-signal dynamics. Yet, from previous literature, limitations in the presented models exist. In [107], only converters that share the same point of synchronization (POS) and point of connection (POC) are considered, which only represents one possible configuration of paralleled converter systems. In [108], no such assumptions are made. However, the modeling approach is only developed for two paralleled converters, whereas the dynamical coupling between them becomes impractical to model when considering large-scale multi-converter systems where model-order reduction and a small computational burden are required.

Addressing these limitations, this chapter develops the necessary conditions for large-signal synchronization stability of three different system configurations which serve to cover a large part of all multi-converter systems. These necessary conditions are used to establish reduced-order models for each configuration, which can be used for the transient stability assessment. Finally, to avert modeling the dynamical couplings between converters in multi-converter systems, an aggregated model is

proposed, which preserves the frequency dynamics of an entire wind farm collector string.

4.2 Necessary Conditions for Transient Stability

The paralleled converter configurations are shown in Fig. 4.1 For the configuration in Fig. 4.1(a), the voltage at the PCC is

$$\boldsymbol{v_{PCC}} = K_g(\omega_g)V_{th}e^{j(\theta_g+\phi_g)} + \sum_{i=1}^{n} K_c(\omega_i)I_i e^{j(\theta_{Ci}+\phi_{ci})}, \tag{4.1}$$

with

$$K_g(\omega_g) = \left|\frac{\boldsymbol{Z_{fe}}(\omega_g)}{\boldsymbol{Z_{fe}}(\omega_g)+\boldsymbol{Z_{th}}(\omega_g)}\right|, \quad K_c(\omega_i) = \left|\boldsymbol{Z_L}(\omega_i) + \frac{\boldsymbol{Z_{fe}}(\omega_i)\boldsymbol{Z_{th}}(\omega_i)}{\boldsymbol{Z_{fe}}(\omega_i)+\boldsymbol{Z_{th}}(\omega_i)}\right|, \tag{4.2}$$

$$\phi_g(\omega_g) = \angle\left(\frac{\boldsymbol{Z_{fe}}(\omega_g)}{\boldsymbol{Z_{fe}}(\omega_g)+\boldsymbol{Z_{th}}(\omega_g)}\right), \quad \phi_c(\omega_i) = \angle\left(\boldsymbol{Z_L}(\omega_i) + \frac{\boldsymbol{Z_{fe}}(\omega_i)\boldsymbol{Z_{th}}(\omega_i)}{\boldsymbol{Z_{fe}}(\omega_i)+\boldsymbol{Z_{th}}(\omega_i)}\right), \tag{4.3}$$

where θ_g is the angle of V_{th}, $\theta_{Ci} = \theta_i + \theta_I$ is the angle of the injected current vector of the i^{th} converter, θ_I is the reference current angle relative to the estimated PLL angle of the converter control, and ω_i is the estimated frequency by the i^{th} converter. The necessary stability condition or static current limitation can be derived by solving for I_C in $v_q = 0$. The q-axis component of the PCC voltage can be written as

$$v_{PCC,q} = \underbrace{K_g(\omega_g)V_{th}\sin(\theta_g+\phi_g-\theta_{PLL})}_{\text{Grid-Synchronization Term, } v_{q-}} + \underbrace{nK_c(\omega_{PLL})I_C\sin(\theta_I+\phi_c(\omega_{PLL}))}_{\text{Self- and Cross-Synchronization Terms, } v_{q+}}. \tag{4.4}$$

For the case where the paralleled converters share the same POS and POC, the necessary static stability condition for the maximum current magnitude that can be injected is

$$I_C \leq \frac{V_{th}K_g(\omega_g)}{nK_c(\omega_{PLL})|\sin(\theta_I+\phi_c(\omega_{PLL}))|}. \tag{4.5}$$

From (4.5), it is seen compared to (2.9), that LOS is n times more likely to occur considering the same fault voltage magnitude when n paralleled converters are operated in parallel. Following the same procedure for the system configurations in Fig. 4.1(b) and (c), the following q-axes voltage components and necessary stability conditions can be formulated:

$$\begin{aligned} v_{POS,q} = {} & \underbrace{K_g(\omega_g)V_{th}\sin(\theta_g+\phi_g-\theta_{PLL})}_{\text{Grid-Synchronization Term, } v_{q-}} + \underbrace{I_C nK_c(\omega_{PLL})\sin(\theta_I+\phi_c(\omega_{PLL}))}_{\text{Self- and Cross-Synchronization Term, } v_{q+1}} \\ & + \underbrace{I_C Z_{tl}(\omega_{PLL})\sin(\theta_I+\phi_{tl}(\omega_{PLL}))}_{\text{Additional Self-Synchronization Term, } v_{q+2}} \end{aligned} \tag{4.6}$$

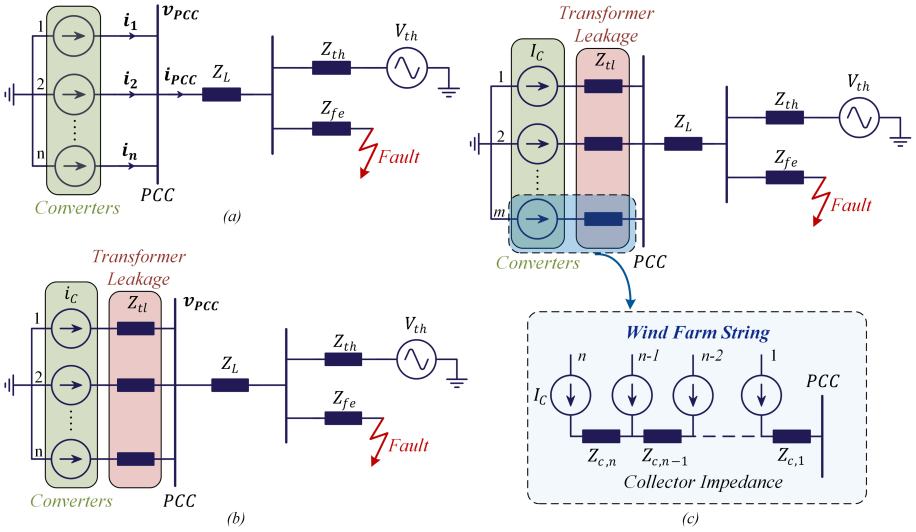

Fig. 4.1: Simplified single-line diagram of paralleled converters with (a): common points of synchronization and point of connection, (b): different points of synchronization but a common point of connection, (c): with different points of synchronization and point of connections. Each converter is interconnected in a daisy-chain configuration through collector impedances represented as $Z_{c,i}$. Source: **[J5]**.

and

$$I_C \leq \frac{V_{th}K_g(\omega_g)}{|nK_c(\omega_{PLL})\sin(\theta_I+\phi_c(\omega_{PLL}))+X_{lt}(\omega_{PLL})\cos(\theta_I)|}, \tag{4.7}$$

for the configuration in Fig. 4.1(b), neglecting transformer resistance. For the system configuration in Fig. 4.1(c), these are

$$v_{POC,q,n} = \underbrace{K_g V_{th}\sin(\theta_g+\phi_g-\theta_{PLL,n})}_{\text{Grid-Synchronization Term, } v_{q-}} + \underbrace{mK_cI_s\sin(\theta_{Cs}+\phi_c-\theta_{PLL,n})}_{\text{Mutual-String Interaction Term, } v_{q+1}}$$
$$+ \underbrace{I_CZ_c\sin(\theta_C+\phi_{col}-\theta_{PLL,n})\frac{(n+n^2)}{2}}_{\text{Self-String Interaction Term, } v_{q+2}}. \tag{4.8}$$

and

$$I_C \leq \frac{V_{th}K_g}{|nmK_c\sin(\theta_I+\phi_c)+\frac{Z_c(n+n^2)}{2}\sin(\theta_I+\phi_{col})|}, \tag{4.9}$$

where n is the weakest link in the daisy-chain system, which violates the necessary stability condition the first. For (4.9), all collector impedances are considered equal. If this is not the case, the necessary stability condition can be expressed as

$$I_C \leq \frac{V_{th}K_g}{|nmK_c\sin(\theta_I+\phi_c)+\sum(n-i)Z_{c,i+1}\sin(\theta_I+\phi_{col,i+1})|}, \tag{4.10}$$

where i is evaluated from 0 to $n-1$. As evident from the necessary stability conditions in (4.7) and (4.9), the constraint for the injected current magnitude becomes more and more restricted. These necessary conditions can be used to compute whether an equilibrium point exists during the fault, and lay the foundations for the reduced-order models presented in the following section.

4.3 Reduced-Order and Aggregated Models

The necessary conditions developed in the previous section can only guarantee when a system is unstable, i.e., when the necessary conditions are violated. When the necessary conditions are met, the damping ratio associated with the PLL will determine whether this equilibrium point will be reached or not. To be able to assess the transient stability of paralleled converters in a computationally efficient manner, reduced-order models are developed for each of the system configurations shown in Fig. 4.1. These models are developed by merging the expressions for the q-axis voltage components with the second-order dynamics of the PLL. These are shown for the first two system configurations in Fig. 4.2(a). For the multi-converter system shown in Fig. 4.1(c), the frequency response of the collector system is a nearly global variable among the n paralleled converters. Therefore, instead of modeling each and every converter and its coupling to all other converters, an aggregated reduced-order approach is proposed instead, as shown in Fig. 4.2(b). Here, the q-axis component (v_{q+2}), represents the equivalent voltage drop caused by the entire string. In this way, the n interconnected converters in the collector system can be approximated by a single frequency estimation.

The equivalent impedance is based on a weighted sum between an aggregation method that preserves the total apparent power ($Z_{eq,S}$) [109–111], and an aggregation method based on the average voltage drop along the string [112, p. 177]. With this, the equivalent impedance is calculated as **[J5]**

$$Z_{eq} = kZ_{eq,S} + (1-k)Z_{eq,\Delta V} \quad k \in [0,\, 1]. \tag{4.11}$$

where

$$Z_{eq,S} = \frac{1}{n^2}\sum_{i=0}^{n-1}(n-i)^2 Z_{c,i+1}, \quad Z_{eq,\Delta V} = \frac{1}{n}\sum_{i=0}^{n-1}(n-i)Z_{c,i+1}. \tag{4.12}$$

In this work $k = 0.75$ has been selected based on the accuracy from numerous simulation studies. This value is, however, application-dependent and may be fine-tuned if necessary. With this, the three system configurations have been analyzed, and aggregated reduced-order models have been proposed to asses the large-signal synchronization stability for each of them.

4.4 Verification and Wind Farm Case Study

The presented necessary stability conditions and reduced-order models are compared against detailed full-order representations of paralleled converters by performing sim-

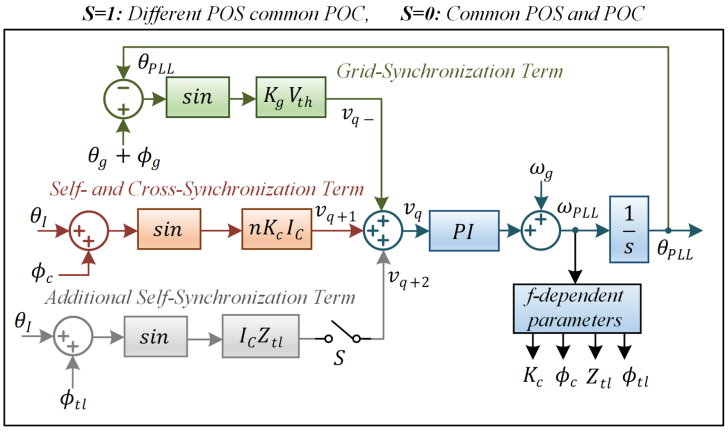

(a)

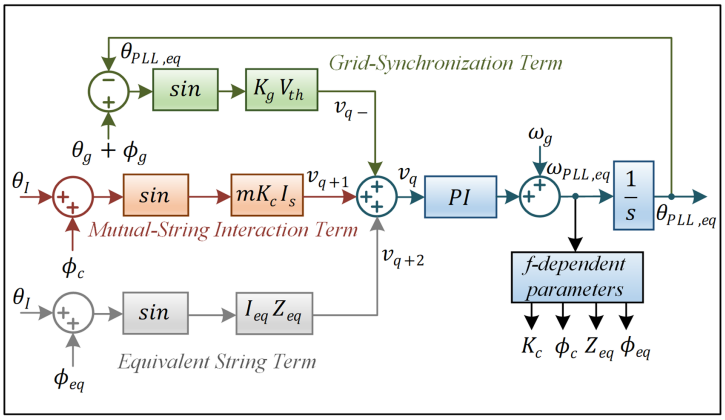

(b)

Fig. 4.2: Reduced-order quasi-static large-signal models for (a): parallel converters with common POS and POC as shown in Fig. 4.1(a) ($S = 0$ and additional self-synchronization term is zero), and paralleled converters with different POS but common POC, as depicted in Fig. 4.1(b) ($S = 1$ and additional self-synchronization term is included in the model). (b): An aggregated reduced-order quasi-static large-signal model for parallel converters with different POS and POC from Fig. 4.1(c). This represents the equivalent aggregated frequency estimation at the PCC. Source: **[J5]**.

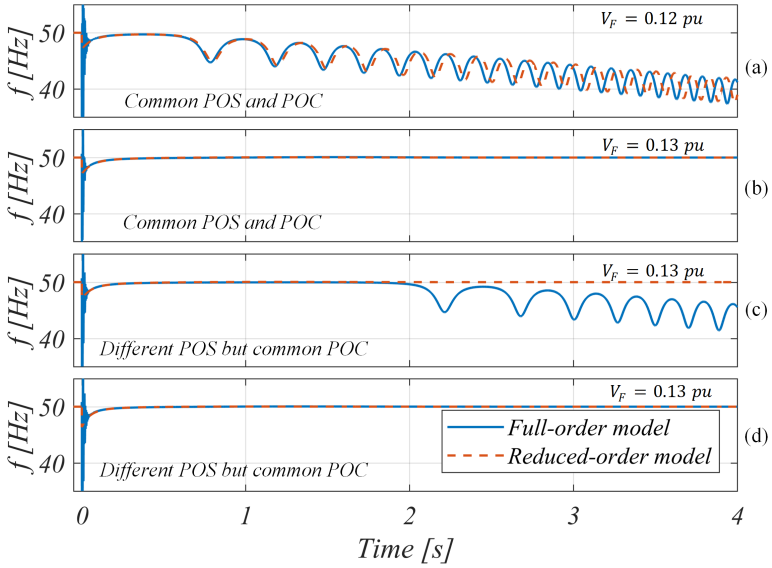

Fig. 4.3: Frequency response of the full-order simulation model and reduced-order large-signal models for different cases and system configurations. The static stability limit or critical V_F is 0.123 pu for all cases. Three paralleled converters, as shown in Fig. 4.1(a) during a grid fault with $V_F = 0.13$ pu and $V_F = 0.12$ pu are shown in (a) and (b), respectively. (c): Three paralleled converters as shown in Fig. 4.1(b) during a grid fault with $V_F = 0.13$ pu. (d) Same as (c) but with an increased damping ratio of the PLL dynamics ($K_p = 1.2K_p^*$). Source: **[J5]**.

ulations. For all simulations, the fault voltage magnitude is directly controlled at the right-side bus of Z_L. Controller and network parameters can be found in **[J5]**. Fig. 4.3 include the verifications for the configurations in Fig. 4.1(a)-(b). For both cases, the critical fault voltage magnitude during the fault is $V_F = 0.123$ pu, which means that if the voltage magnitude at the fault location drops below this value, the necessary condition for stability will be violated. In all cases, the converters are injecting pure reactive current, i.e., $\theta_I = -\pi/2$. As can be seen from Fig. 4.3(a)-(b), the necessary stability condition is indeed accurate in representing the detailed dynamic system. To that end, the reduced-order model for the configuration with common POS and POC shows an accurate reproduction of the system frequency dynamics. Fig. 4.3(c)-(d) include the results for the configuration in Fig. 4.1(b). As seen from (4.7), the necessary stability condition includes a destabilizing term from the transformer leakage reactance. However, since the necessary conditions are based on steady-state operations, it is considered that $\theta_I = -\pi/2$, which makes the destabilizing term zero. The same is true for the reduced-order model, which assumes the converter to change its operations mode to $\theta_I = -\pi/2$, instantly. Due to this, even though V_F is not violating the necessary stability condition in (4.7), it is evident from Fig. 4.3(c) that the transient impact of the transformer leakage reactance makes the full-order representation unstable since it adds a destabilizing contribution at the fault instant. However, since the necessary stability conditions are not violated in steady-state, stability can be achieved by increasing the PLL damping ratio. This is shown in Fig. 4.3(d) where the stability is

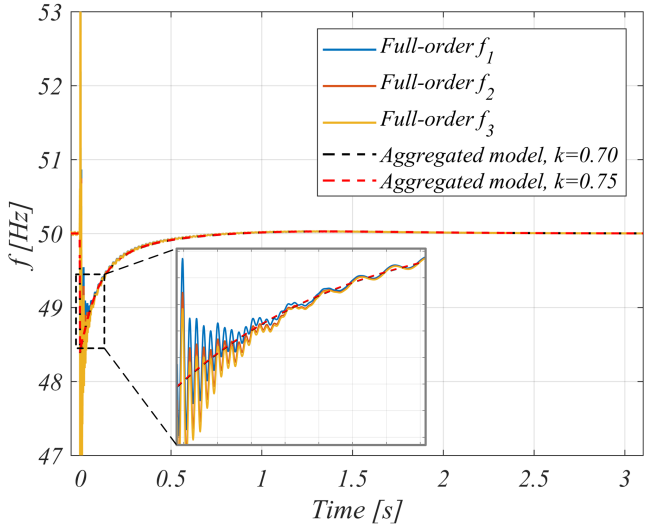

(a)

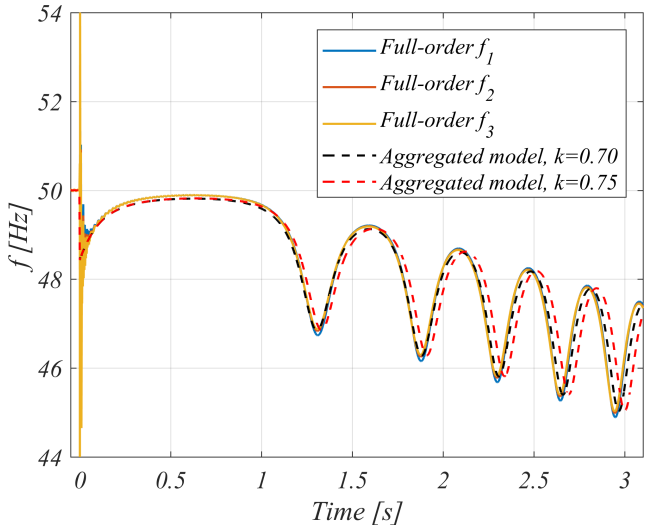

(b)

Fig. 4.4: Aggregated model accuracy shown with the frequency response of three paralleled full-order string converter models during (a): Stable operating point with $V_F = 0.08\,\text{pu}$. (b): Unstable operating point with $V_F = 0.07\,\text{pu}$. Varying k has a minor impact on the stability prediction. Source: **[J5]**.

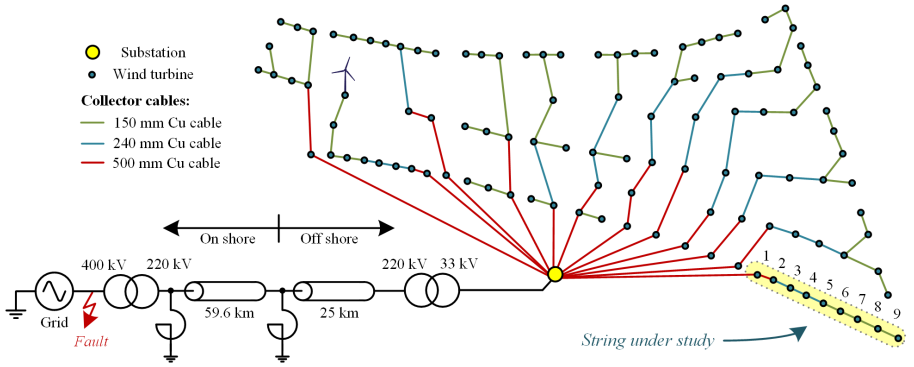

Fig. 4.5: Physical layout of Anholt 400 MW offshore wind power plant with the electrical export system and connections [40, 113]. One wind farm string with nine wind-turbine converters is under study for this work, as highlighted, where the string converter numbers are denoted. Source: **[J5]**.

again retained by increasing the proportional gain of the PLL. Also, the reduced-order model closely resembles the detailed full-order response.

Fig. 4.4 contains the comparative results for the aggregated reduced-order model for the configuration in Fig. 4.1(c) for three paralleled converters. Here, the critical fault voltage magnitude is $V_F = 0.078\,\text{pu}$. As it is evident, both the necessary condition and the aggregated model show a great match in the observed stability assessments and dynamical responses.

To further verify the aggregated reduced-order model for the system configuration in Fig. 4.1(c), the operating Anholt 400 MW wind farm is considered as a case study. The physical layout of the Anholt wind farm is shown in Fig. 4.5, which contains 111 3.6 MW wind turbines connected to the high-voltage transmission grid through a 59.6 km onshore cable and a 25 km offshore submarine cable. Detailed informations on the cable parameters and the wind farm are described in **[J5]**.

For the analysis, one wind farm string is studied, which contains nine paralleled interconnected converters separated by different collector impedances. Based on these collector impedances and the injected converter currents, the critical fault voltage magnitude, which violates (4.10) for $I_C = 1\,\text{pu}$, $\theta_I = -\pi/2$ is $V_F = 0.0788\,\text{pu}$. Due to this, two test cases are selected. A case where an equilibrium point exists with $V_F = 0.08\,\text{pu}$, and an unstable case where the necessary stability condition in (4.10) is violated with $V_F = 0.07\,\text{pu}$. These two tests are shown in Fig. 4.6.

Even for this realistic test system with non-constant collector impedances, both the necessary stability condition and aggregated reduced-order model, despite their simplicity, preserve the dominant dynamics of the entire wind farm string. Also, as seen from the zoomed transient response for both cases, the aggregated model accurately reproduces the averaged frequency consensus in the wind farm string.

To assess the computational achievements obtained by using this aggregated reduced-order model, the time needed to solve 1 s of a fault response using a full-order switching model (2 kHz), a full-order model with an averaged representation of the switch-

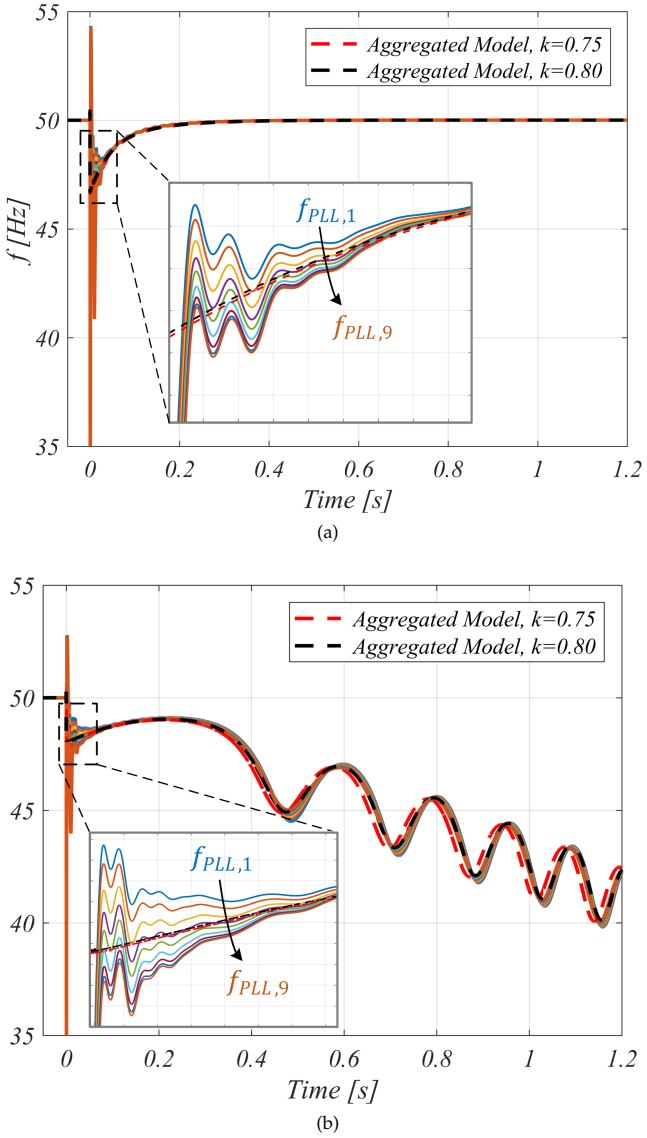

Fig. 4.6: Estimated PLL frequencies during a severe fault condition for full-order models and the proposed aggregated model. (a): Stable operating point with $V_F = 0.08\,\text{pu}$. (b): Unstable operating point with $V_F = 0.07\,\text{pu}$. Varying k has a minor impact on the stability prediction. Source: **[J5]**.

Table 4.1: Comparison of computational time for solving 1 s simulation time of Anholt Wind Farm String using different models.

Switching Model	Average Model (full-order)	Aggregated Model
642 s	34.8 s	306 ms

ing actions, and the proposed reduced-order aggregated model are compared for the highlighted Anholt wind farm string, and it is summarized in Table 4.1. Details on the computational power and used software are contained in **[J5]**. It can be noticed from Table 4.1, that in addition to accurate reproduction of the frequency estimation dynamics of the entire wind farm string, the computational burden compared with the full-order averaged representation can be reduced with a factor of 100. This highlights the benefit of using this reduced-order representation, which may be accurately employed to assess the transient stability of large-scale multi-converter systems.

4.5 Summary

In this chapter, the modeling of large-signal synchronization stability of multi-converter systems is addressed. Three different system configurations, which cover most multi-converter systems are analyzed, and necessary stability conditions are derived for each of them. Building on these conditions, reduced-order models are developed for each configuration, which includes the dynamical properties of the synchronization unit. For the system configuration representing a daisy-chain system where a non-negligible impedance separates each paralleled converter, an aggregated reduced-order model has been presented to capture the equivalent frequency response of an entire wind farm string. All presented necessary stability conditions and reduced-order models have been tested against detailed full-order simulation models, verifying their accurate preservation of the system dynamics. To that end, the operating Anholt wind power plant is considered as a case study where a wind farm string with nine interconnected converters is used to further verify the aggregated model. Again, an accurate representation of the system is attained, with a reduction in computational requirements of more than a factor of 100, and enabling even larger scale system analysis.

Related Publication

[J5] **M. G. Taul**, X. Wang, P. Davari and F. Blaabjerg, "Modeling of Large-Signal Synchronization Stability of Multiple Paralleled Converters," under review in *IEEE Journal Emerg. Sel. Topics Power Electron.*, 2020.

Main contribution:
Necessary conditions for transient stability for three descriptive multi-converter system configurations are presented. Based on these, dynamical reduced-order models are developed. For systems represented by a daisy-chain system where each converter is separated by a non-negligible impedance, an aggregated reduced-order model is proposed based on an equivalent impedance of the wind farm string together with

the dynamics of the PLL. The presented models are verified through detailed full-order simulation models, and the Anholt wind farm is included as a case study to verify the aggregated model further. High model accuracy is obtained, and the computational burden is reduced with a factor of a 100.

Chapter 5

Enhanced Synchronization Stability through Control

5.1 Background

The previous chapters have dealt with the modeling and analysis of large-signal synchronization stability for single-converter systems and multi-converter systems under symmetrical as well as asymmetrical grid faults. This is useful when evaluating the transient stability of a given system at hand. Nevertheless, during severe faults, as also captured by the developed models, instability may occur as a result of insufficient damping of the synchronization unit or due to the non-existence of a stable operating point during the fault. In the first case, it may be troublesome to estimate the sufficient damping ratio for an anticipated worst-case condition. Hence, a control method that provides a sufficient damping ratio for any conditions where the necessary stability condition is met is needed. For the latter case where no equilibrium point exists, no damping ratio can provide transient stability. Under this fallout, the converter operation needs to be altered to allow for a stable operating point during the fault. Consequently, this chapter aims to demonstrate that controller strategies can be applied to ensure large-signal synchronization stability considering these two distinct cases. Common to the control strategies introduced is that simplicity should be prioritized, in order to avoid any additional control loops with its own associated stability issues. Four control methods are presented in this chapter. A simple and robust method to provide stability irrespective of whether a stable operating point exists or not is shown for the SRF-PLL. This method can also comply with zero-voltage ride-through requirements as requested by some grid codes. To that end, a method that provides sufficient damping for transient stability when a stable operating point exists, is proposed for the family of frequency-locked loops (FLLs), which is often used under asymmetrical conditions. To that end, an improved current-reference injection method with rapid impedance estimation is developed to provide an equi-

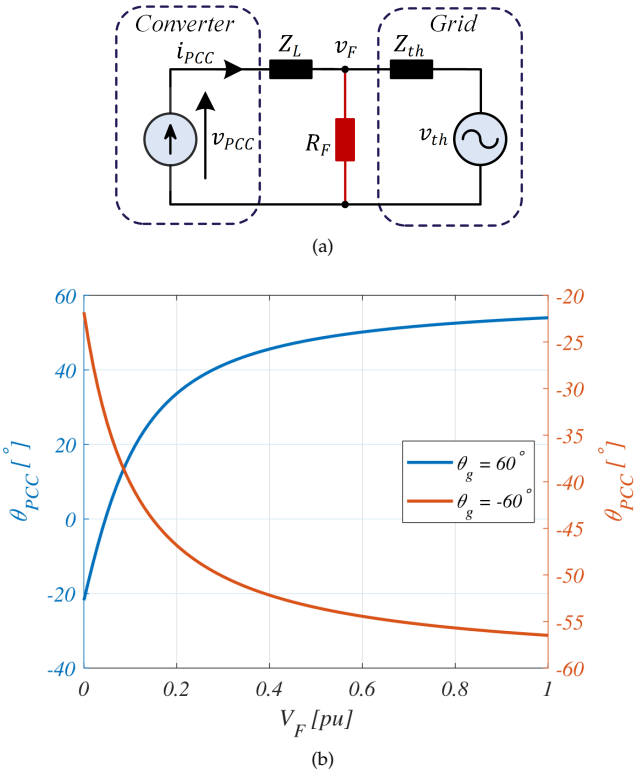

Fig. 5.1: System diagram and phase-angle jump at PCC. (a): Simplified circuit diagram of the grid-following converter during a symmetrical fault. (b): Phase jump at the PCC as a function of the fault voltage magnitude and the sign of the phase jump happening at the fault location. The line impedance considered is $Z_L = R_L + jX_L$, and the converter is considered to inject nominal capacitive reactive current. Source: **[J2]**.

librium point, and a stable response during the fault is obtained. Lastly, grid-forming control is utilized to enhance the transient stability.

5.2 Phase-Locked Loop Freeze

To achieve zero-voltage ride-through and to enhance the large-signal synchronization stability of grid-following converters, it is proposed in [56, 75] and patented in [114] to simply freeze the state variables of the PLL during the fault to its pre-fault estimates. In this way, as described in [115], this method may not satisfy the grid-code requirements since phase-angle jumps will occur at the fault instant [116]. In the following, it will be shown how PLL-synchronized converters can accurately employ the PLL freezing method, also during phase jumps.

A simplified circuit diagram of the grid-following converter, represented as a controllable current source is shown in Fig. 5.1(a). Using this diagram, a phase jump

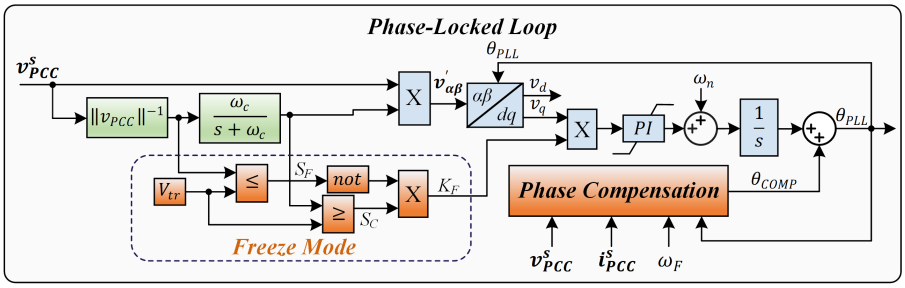

Fig. 5.2: PLL structure with adaptive normalization of the input voltage and PLL freeze mode with phase compensation. ω_F is the frozen PLL angular frequency. Source: **[C1]**.

occurring at the fault location (v_F) can be transferred to the PCC based on the converter operation. In Fig. 5.1(b), the phase jump experienced at the PCC is shown as a function of the voltage magnitude at the fault location. This is shown for a positive and negative 60° phase jump. As can be seen in Fig. 5.1, the phase-jump which propagates to the PCC is strongly dependent on V_F. To that end, when V_F approaches zero, the phase angle at the PCC is solely determined by $\theta_I + \theta_Z$. This implies that when V_F is nearly zero, the converter has to supply the resistive losses in the line, and hence the PLL cannot be aligned with the PCC and satisfy that $\theta_I = -\pi/2$. Based on this, despite the PLL is unaware of a phase jump when frozen, it may not have a significant negative effect on the converter operation, as previously anticipated. The structure of the PLL used to verify this is shown in Fig. 5.2. Here, the input voltage is adaptively normalized with the low-pass filtered magnitude of the PCC voltage, which makes the design of the PLL independent on the PCC voltage magnitude. To that end, when the voltage magnitude drops below a certain threshold value V_{tr}, then K_F is set to zero, which nullifies the PLL error. In this way, the PLL keeps operating at the frequency estimated before the fault. Accordingly, it functions as an open-loop structure which eliminates the positive feedback loop identified in *Chapter 2*. To verify the performance of the frozen PLL, its response is compared to a frozen PLL where the estimated phase angle is corrected to the actual PCC angle using phase compensation. Details on the phase compensation techniques and robustness analysis of the frozen PLL can be found in **[C1], [J2]**. Experimental tests are performed without and with phase compensation of the frozen PLL to verify this observation, as shown in Fig. 5.3.

Even though the injected current (i_d and i_q) can be improved using phase compensation, i.e., approach their references ($I^*_d = 0$, $I^*_q = -1$), it can be appreciated that the extra support observed in the PCC voltage when using phase compensation is small. Therefore, the PLL freeze method without phase compensation may successfully be used to avert synchronization instability while providing an acceptable level of reactive current injection. One advantageous feature of the frozen PLL, is that it relocates itself to avoid instability, i.e., automatically guarantees a stable operating point during any grid fault severity. Since this control structure works as an open-loop structure without its grid-following properties, it actually operates as a grid-forming structure and can, therefore, also operate under zero-voltage conditions. This underlines the

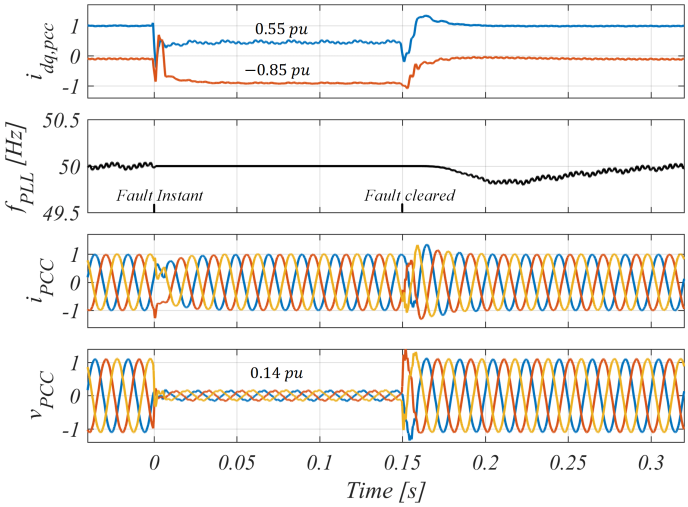

(a)

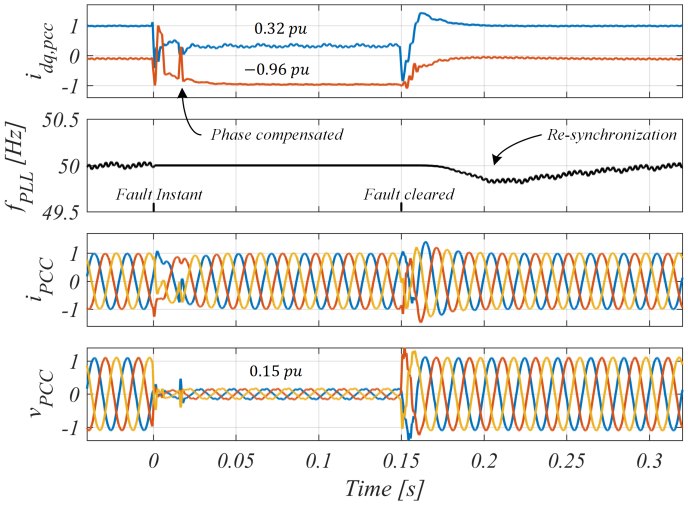

(b)

Fig. 5.3: Experimental results of performance for a $-60°$ phase jump during a fault voltage of 0.03 pu. (a): Fault response of PLL freeze without phase compensation. (b): PLL freeze with phase compensation. Source: **[J2]**.

robustness that can be enhanced by using a grid-forming structure, which will be further detailed in a later section of this chapter.

5.3 Frequency-Locked Frequency-Adaptive Loops

As mentioned in Chapter 3, the SRF-PLL cannot be used to deal with asymmetrical conditions. Therefore, in practice, a pre-filtering approach is often used to extract the fundamental positive and perhaps negative-sequence components of the PCC voltage. In this case, a LOS mitigation strategy which works for such synchronization units is needed. In this work, as considered in *Chapter 3*, a DROGI-FLL is used for the voltage sequence extraction. However, as it will be shown, the particular structure of the FLL or PLL is subordinate both in regards to the modeling and mitigation strategy. The structure of the considered grid-following control under asymmetrical conditions and the employed DROGI-FLL can be seen in Fig. 5.4(a)-(b). To that end, the equivalent *dq*-reference frame representation of the stationary-reference frame DROGI-FLL is shown in Fig. 5.4(c). For details on the derivation of this equivalent *dq*-frame structure, please refer to **[C5]**. This structure is useful to visualize the similarity between the stationary-reference frame FLLs and the SRF-PLL. In this way, any controller and modeling approaches taken for the synchronous-reference frame structures may be reflected to be valid, also, for the stationary-reference frame ones, and vice versa.

For the FLL, it is proposed to perform a frequency-lock in the frequency-adaptive loop (FAL) of FLLs to enhance the large-signal synchronization stability during asymmetrical and symmetrical grid faults. Practically, this means setting $\lambda = 0$ during severe grid faults. In addition to this, a mathematical proof for global asymptotic stability of the proposed method is provided using the Lyapunov theory.

During severe grid faults where an equilibrium point exists, transient stability can be attained, given a sufficient damping ratio associated with the synchronization unit. Since it may be difficult to analytically identify a worst-case condition of a real system and then identify the sufficient critical damping as done in Section 3.2.3, the approach proposed here, is to ensure sufficient damping in any condition where the necessary stability condition is not violated. As described previously for the DROGI-FLL, $\zeta \propto \frac{1}{\omega_N^2}$ and $\lambda = \omega_N^2$. Therefore, by setting $\lambda = 0$, an infinite damping ratio is obtained, which ensures transient stability.

Proof of Stability

Using the developed equivalent *dq*-reference frame representation of the DROGI-FLL as shown in Fig. 5.4(c) **[C5]**, the positive-sequence estimated phase angle can be written as

$$\theta^+ = \int \omega_g + k\left(Z_{LT} I^+ \sin(\phi_{LT} + \theta_I^+) - V_F^+ \sin(\delta^+)\right) dt \tag{5.1}$$

assuming a negligible influence from the cross-coupling terms. Using that $\theta_F^+ = \int \omega_g dt$ and defining $\delta = \theta^+ - \theta_F^+$, the following expression can be derived

$$0 = \dot{\delta} - k\left(Z_{LT} I^+ \sin(\phi_{LT} + \theta_I^+) - V_F^+ \sin(\delta^+)\right). \tag{5.2}$$

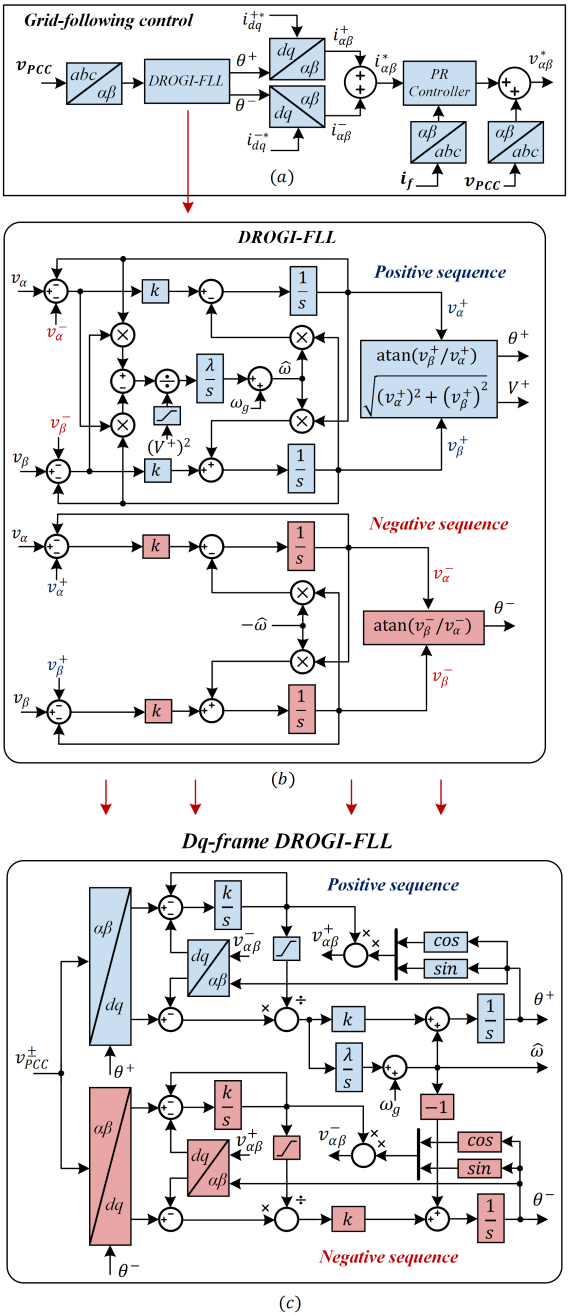

Fig. 5.4: Employed control for grid-following converter during asymmetrical faults. (a): Complete outlook of the grid-following control system shown in Fig. 3.7(a). (b): Detailed view of the DROGI-FLL used for sequence extraction and synchronization. (c): Equivalent dq-frame representation of DROGI-FLL. Source: **[C5]**.

By defining the positive definite Lyapunov candidate $V(\delta) = \delta^2$, which satisfies $V(0) = 0$ and $V(\delta) > 0 \; \forall \; \delta \neq 0$, it can be shown that this function is negative definite provided that an equilibrium point exists during the fault **[C5]**.

From this, if the static stability condition is met during the fault, the proposed control method is globally asymptotically stable, assuming the cross-coupling terms have a small influence on the system stability. This analysis is here shown for the positive-sequence control but it is equally valid for the negative-sequence one.

Experimental Verification

Two short-circuit grid faults are performed experimentally without and with performing the frequency-lock in the FAL. This is done for a symmetrical three-phase fault where the fault voltage magnitude drops to 0.3 pu and a solid DLG fault as shown in Fig. 5.5, and Fig. 5.6, respectively. It can be seen that the system is able to successfully ride through the symmetrical and asymmetrical faults when enabling the frequency-lock ($\lambda = 0$) in the FAL during the fault. Additionally, due to the equivalence between the stationary-reference frame FLLs and the many synchronous-reference frame synchronization methods, this method works identically by setting the integral gain to zero during the fault. Therefore, this serves as a holistic approach to provide stability for any synchronization unit. Yet, it has a few drawbacks which must be accounted for. At first, since the synchronization unit, as also proposed and explained for the SRF-PLL in [69], is being reduced to a first-order system, it loses its phase-tracking capabilities during external frequency deviations. To that end, an equilibrium point must exist during the fault, which may be violated under more severe conditions. In that case, the PLL freezing method may be employed as an additional action to prevent transient instability.

5.4 Improved Current-reference Injection Method

As described in the introduction, the authors in [66] proposed to align the injected current vector to match the impedance angle of the external grid. This method fully eliminates the positive feedback self-synchronization loop from Fig. 2.6. In this way, an equilibrium can always be guaranteed to exist. However, this appealing method relies on a rapid estimation of the grid impedance when the fault occurs. This has so far not been presented, which limits the practical use of this appealing method. This section aims to address this issue by presenting a rapid impedance estimation method to align the injected fault currents to ensure transient stability.

Control Method and its Stability

The basic principle behind this method can be understood from the necessary conditions for the injected current vector from e.g., n paralleled converters in (4.5), repeated here for convenience

$$I_C \leq \frac{V_{th} K_g(\omega_g)}{n K_c(\omega_{PLL}) |\sin(\theta_I + \phi_c(\omega_{PLL}))|}. \tag{5.3}$$

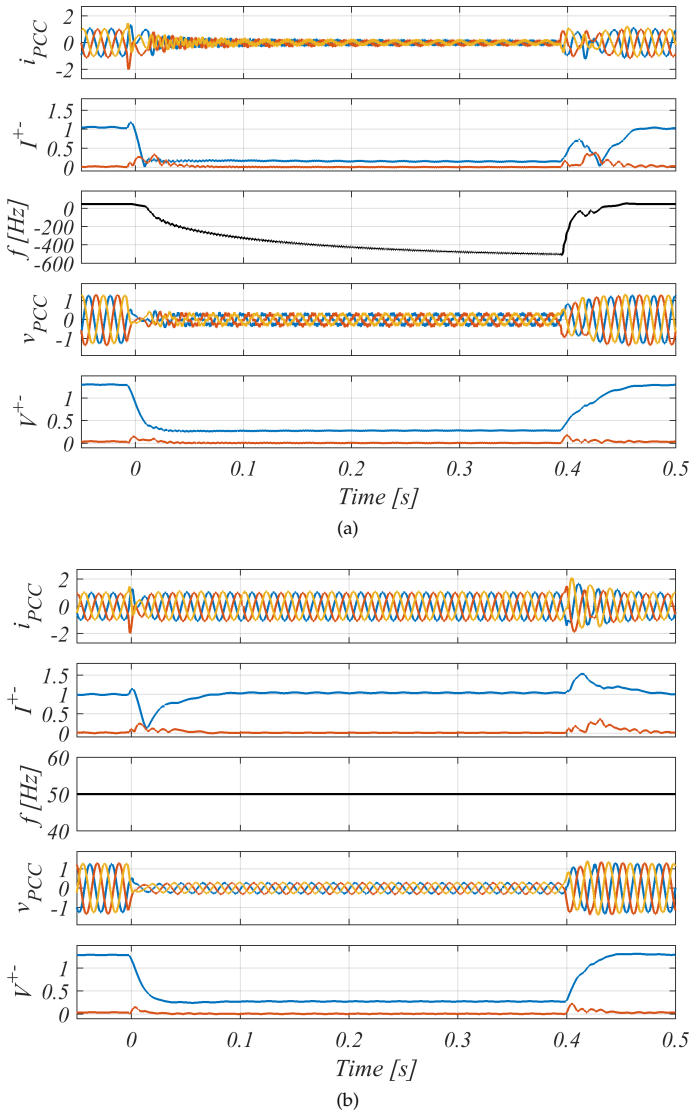

Fig. 5.5: Experimental results for a three-phase symmetrical fault ($V_F^+ = 0.3\,\text{pu}$) with nominal positive-sequence current injection during a fault. (a): Unstable response without frequency-lock in FAL. (b): Stable response with proposed frequency-lock in the FAL of the DROGI-FLL. Source: **[C5]**.

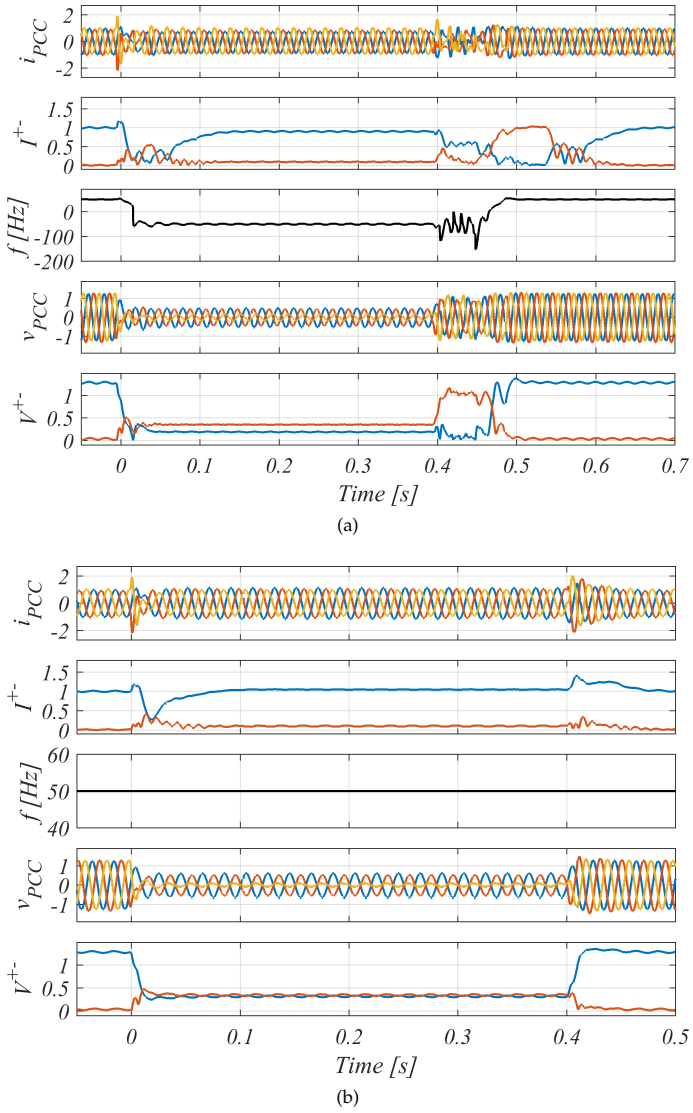

Fig. 5.6: Experimental results for a DLG fault with nominal positive-sequence current injection during a fault. (a): Unstable response without frequency-lock in FAL. (b): Stable response with proposed frequency-lock in the FAL of the DROGI-FLL. Source: **[C5]**.

It can be observed that if $\theta_I = -\phi_c(\omega_{PLL})$, then the limit magnitude for the injected current vector extends to infinity, which is independent of the severity of the fault and fault voltage magnitude. Hence, if the injected converter currents are aligned with the negative of the impedance angle, the existence of an equilibrium point during the fault can always be guaranteed. Assuming that the impedance between the converter and the fault can be represented as an RL passive impedance, then

$$\phi_c(\omega_{PLL}) = \tan^{-1}\left(\frac{\omega_{PLL}L_L}{R_L}\right), \tag{5.4}$$

which implies that the dq-frame converter currents should be selected as

$$\frac{I_q}{I_d} = -\frac{\omega_{PLL}L_L}{R_L}. \tag{5.5}$$

Doing this, while respecting a maximum limit in the converter current, $I_{lim} = \sqrt{(I_d^*)^2 + (I_q^*)^2}$, the dq-frame current references should be set as

$$I_d^* = R_L I_{lim}\sqrt{\frac{1}{R_L^2 + (\omega_{PLL}L_L)^2}}, \quad I_q^* = -\omega_{PLL}L_L I_{lim}\sqrt{\frac{1}{R_L^2 + (\omega_{PLL}L_L)^2}}. \tag{5.6}$$

This method, provided that R_L and L_L can be estimated, is globally asymptotically stable, as proven in **[C4]**. This proof can also be intuitively explained. By applying the references in (5.6) and evaluating the q-axis component of the PCC voltage in (4.4), it can be noticed that the destabilizing self- and cross-synchronization term is fully nullified and, hence, the PLL will always be able to control the grid-synchronization term to zero.

Rapid Impedance Estimation Algorithm

The impedance estimation method for rapid detection is based on the two-point method as

$$\vec{Z} = \frac{\vec{v}_{PCC,1} - \vec{v}_{PCC,2}}{\vec{i}_{PCC,1} - \vec{i}_{PCC,2}}, \tag{5.7}$$

where the sample numbers are denoted with subscripts. One issue with this two-point estimation method is that a significant difference between the two samples need to be present to get a reliable estimate of $\vec{Z}$ and avoid division with zero or a very small number. The main contribution of this impedance estimation method is to use the grid fault impulse as an excitation pulse to perform the estimate **[O1]**. In this manner, the system does not have to inject a user-defined test pulse to perform the estimation but uses the inherently large disturbance of the converter response to the grid fault. Using the derivation and explanations from **[O1]**, the grid resistance and inductance can be estimated as

$$L = \frac{\Delta v_{qr}\Delta i_{dr} - \Delta v_{dr}\Delta i_{qr}}{A - B} \quad \text{and} \quad R = \frac{\Delta v_{dr} - L(\omega_{c,2}i_{qr,2} - \omega_{c,1}i_{qr,1})}{\Delta i_{dr}} \tag{5.8}$$

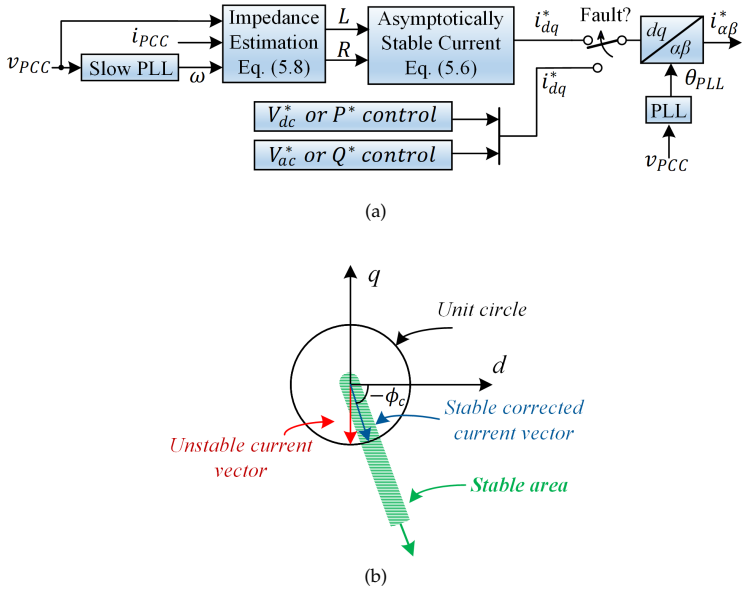

Fig. 5.7: Actuation and understanding of the proposed control, which relocates the injected current vector into a stable operating area. (a): Block diagram of proposed control structure, which is enabled when a fault is detected. (b): Graphical visualization of how the control method relocates the current vector into the stable operating area during the fault. Source: **[C4]**.

where

$$\Delta v_{dr} = v_{dr,1} - v_{dr,2}, \quad \Delta v_{qr} = v_{qr,1} - v_{qr,2}, \quad \Delta i_{dr} = i_{dr,1} - i_{dr,2}, \quad \Delta i_{qr} = i_{qr,1} - i_{qr,2},$$
$$A = \omega_{c,1}(i_{dr,1}\Delta i_{dr} + i_{qr,1}\Delta i_{qr}), \quad B = \omega_{c,2}(i_{dr,2}\Delta i_{dr} + i_{qr,2}\Delta i_{qr}). \tag{5.9}$$

Verification of Method

Three grid-following paralleled converters are simulated under a symmetrical grid fault with $V_F = 0.1$ pu without and with the current alignment control, as shown in Fig. 5.8. The control structure employed is visualized in Fig. 5.7(a) whereas the actual current alignment in the stable operating area is depicted in Fig. 5.7(b). As seen in Fig. 5.8, the paralleled system remains stable during the fault when using the proposed control. Compared to the unstable case where the d-axis current reference is zero, the d-axis reference is increased to around 0.4 pu for the three converters to relocate the current vector into the stable operating area. It should be noted that the placement of the two samples used for the impedance estimation strongly influence the estimation accuracy. However, as seen from these cases, the errors in the estimations were around 20 %, whereas the error in the X/R ratio, which is the critical metric for the proposed method, is actually below 5 %. Also, it should be mentioned that an exact estimation is only necessary when $V_F = 0$. When the fault voltage mag-

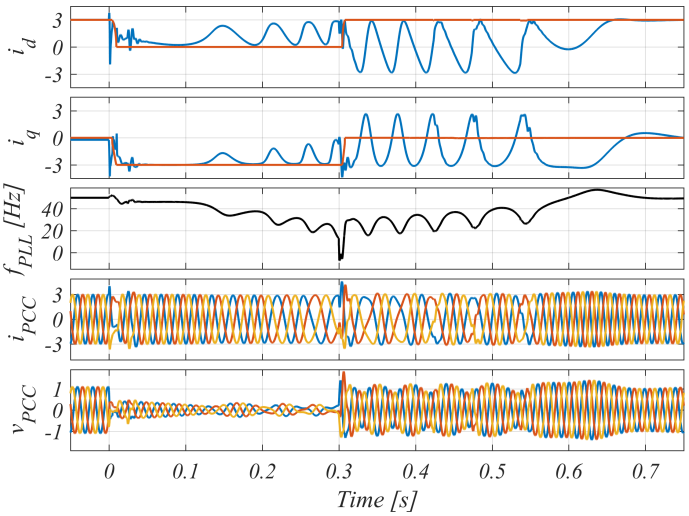

(a) Without proposed control.

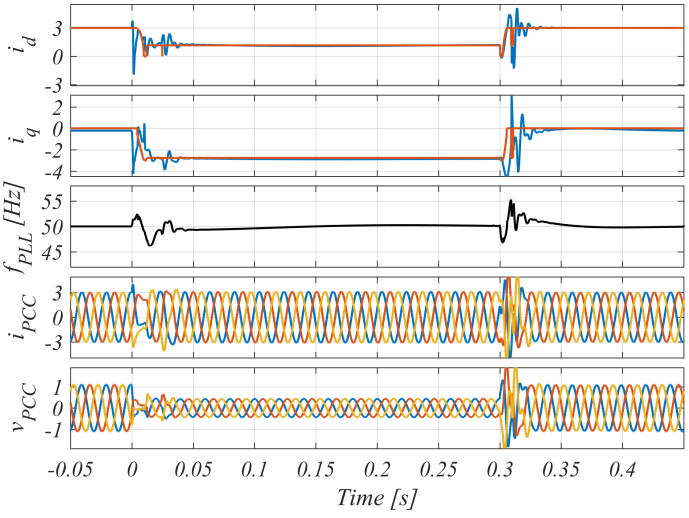

(b) With proposed control.

Fig. 5.8: The simulated response of three paralleled converters to a symmetrical grid fault $V_F = 0.1\,\text{pu}$ for 0.3 s. Subfigures contain the following variables: combined d-axis reference (red) and actual (blue), combined q-axis reference (red) and actual (blue), estimated PLL frequency, three-phase PCC currents, three-phase PCC voltages. Source: **[C4]**.

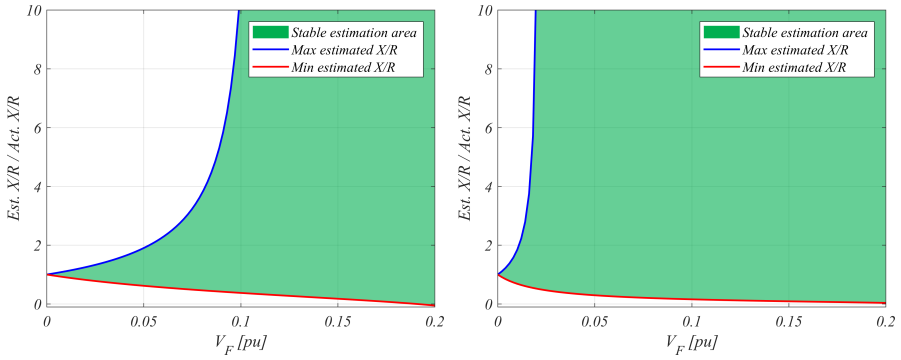

(a) Actual $X/R = 1.73$ (b) Actual $X/R = 10$

Fig. 5.9: Ratio between allowed estimated X/R ratio and the actual system X/R ratio for providing a stable operating point during the fault for varying fault voltage magnitudes. Source: **[C4]**.

nitude increases, so does the allowed estimation error. This is exemplified in Fig. 5.9 for $X/R = 1.73$ and $X/R = 10$, where it is evident that a large estimation error can be tolerated, even when the fault voltage magnitude is very low. E.g. for Fig. 5.9(b), any practical overestimated guess of the X/R ratio will result in a stable operating point during the fault. Accordingly, the presented method can be regarded as robust towards estimation errors in the impedance ratio.

With this, it has been shown that a rapid impedance estimation algorithm can be used to allow for the current alignment method to be useful. To that end, the injected currents during the fault do not follow the grid-code requirements full reactive current provision. However, when resistance is present in the line, optimal voltage support will not be for pure reactive current but as a fraction between active and reactive current as performed here. Last, the presented method allows for a significant error in the impedance estimation without affecting its performance in providing a stable operating point during the fault.

5.5 Grid-Forming Control under Grid Faults

As discussed for the PLL freezing method, this operates as an open-loop grid-forming converter to avert large-signal synchronization instability. Also, it was shown that phase jumps during the fault did not have a significant impact on the converter response when the fault is severe. However, it still relies on a frequency estimation, which is identical to the pre-fault condition, which may not be satisfied under low-inertia grids. Also, as grid-forming technology is being more and more used to deal with weak-grid conditions, this observation may imply that grid-forming strategies can be advantageous in terms of transient stability. However, during grid faults where the network voltage drops, a grid-forming strategy will respond with large current injections in an attempt to keep the voltages around nominal. This will for power-

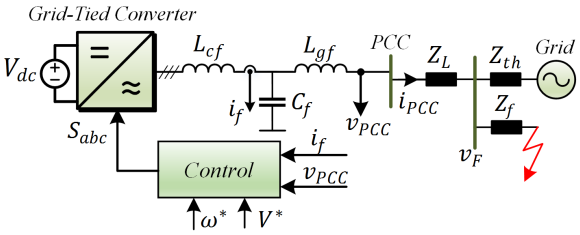

Fig. 5.10: The overall system of a grid-forming grid-tied Voltage-Source Converter (VSC) connected to an external Thevenin modeled grid with a symmetrical fault occurring close to the v_F bus. Source: **[J3]**.

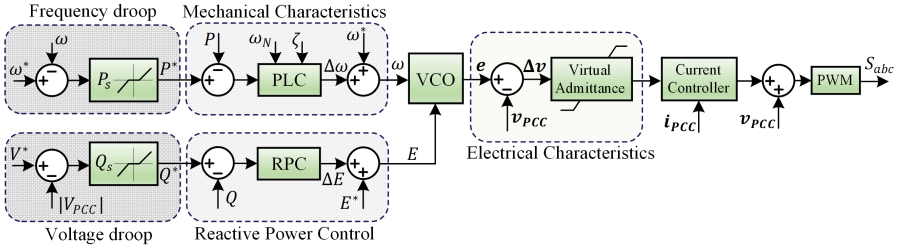

Fig. 5.11: Control block diagram of Synchronous Power Control (SPC). The Power Loop Controller (PLC) adjusts the frequency, dependent on the active power change from the droop controller with a defined natural oscillating frequency and damping coefficient. Source: **[J3]**.

electronic converters result in a fast violation of the maximum allowed current. Thus, current limitation is mandatory for such operations. Among previous research on grid-forming converters, these are often switched to grid-following structures during the fault to perform the current limitation [78, 81–83]. Such an approach needs a back-up PLL, which means that all the robustness offered by the grid-forming structure is immediately lost. Also, performing a direct current limitation during the fault of the grid-forming strategy will quickly saturate the outer power loops, which leads to instability [117]. Therefore, in this section, a method to modify the references for the outer power loops of a grid-forming converter during the fault is proposed, which allows the grid-forming converter to keep its voltage-mode robustness during the fault while performing current limitation.

The grid-forming structure used for this analysis is shown in Fig. 5.10 and is based on the synchronous power control, as shown in details in Fig. 5.11 **[J3]**.

Proposed Grid-Forming Strategy

To achieve current limitation while keeping the grid-forming structure during the fault, two fundamental actions are proposed. First, the current limitation is performed in the inner control for fast actuation. Here, a circular current limiter is used, which

limits the stationary-reference frame current as

$$\vec{i^*_{\alpha\beta}} = \begin{cases} \vec{i_{\alpha\beta}} \frac{I_{lim}}{\sqrt{i_\alpha^2 + i_\beta^2}} & \text{if} \quad \sqrt{i_\alpha^2 + i_\beta^2} > I_{lim}, \\ \vec{i_{\alpha\beta}} & \text{otherwise}, \end{cases} \tag{5.10}$$

Secondly, during the fault, the power references obtained from the droop control are modified to reflect the fact that a minimal amount of power can be transferred when considering the current limitation of the converter. Hence, the admissible power is updated during the fault based on the nominal power and the present per-unit voltage at the converter terminals as

$$S_{new} = V_{pu} S_n. \tag{5.11}$$

With the updated admissible power, the reactive power reference is set to comply with the grid-code requirements as

$$Q^* = \begin{cases} \text{Voltage Droop} & \text{if } V_{pu} > 0.9, \\ 2S_{new}(1 - V_{pu}) & \text{if } 0.5 < V_{pu} < 0.9, \\ S_{new} & \text{otherwise.} \end{cases} \tag{5.12}$$

Then, based on the updated admissible power and the calculated reactive power reference, any remaining capacity in the converter current capability is allocated to active power as

$$P^* = \sqrt{S_{new}^2 - Q^{*2}}. \tag{5.13}$$

The proposed fault-mode control of the grid-forming converter is shown in Fig. 5.12, where the outer power references are switched based on a logical control signal F_M. When a fault occurs, F_M directly switches the outer power references when the stationary-reference frame voltages are recorded to drop below 0.9 pu. However, when the voltage recovers, the outer power references are switched back to droop control when the difference between the fault-mode power references and the power references from the droop control are below some predefined threshold per-unit value, P_{diff}. This is done to avoid a large disturbance in the operation if the power references are switched when the difference is too high. For this work, P_{diff} is set to 5 % of the nominal power.

Verification of Method

The proposed strategy for the grid-forming converter is compared under a symmetrical grid fault with the grid-forming converter from [83], which is switched to a grid-following PLL-synchronized converter during the fault. This is shown in Fig. 5.13, where it is evident that the proposed grid-forming control can successfully limit the converter currents while providing a robust voltage-mode operation during the fault. For the grid-forming converter, which switches to a grid-following structure during the fault, it is observed that the currents are not adequately limited, and severe distorted overvoltages are observed at the PCC. Also, the fault-mode operation of the proposed method is labeled, which shows that the power references are seamlessly switched back to droop control approximately 180 ms after the fault recovery.

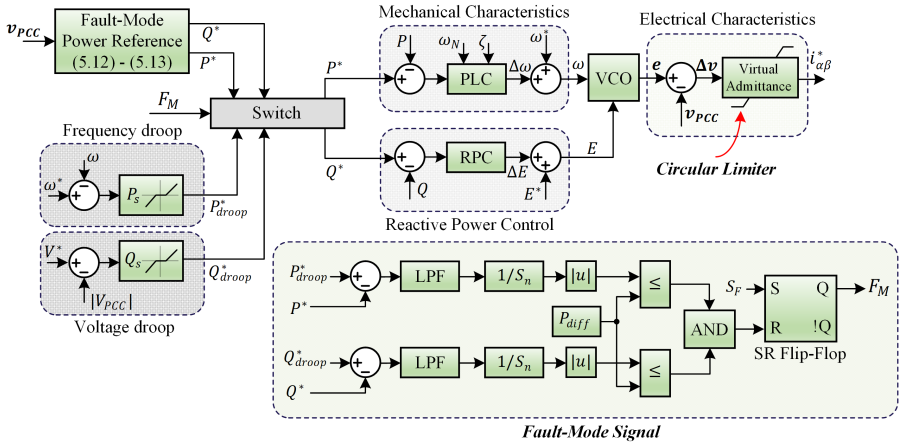

Fig. 5.12: Proposed fault-mode control structure of SPC where F_M selects between droop control and power reference control based on grid code requirements and a circular limiter is used to constrain the current reference. $F_M = 0$: Droop control. $F_M = 1$: Proposed fault-mode control. Source: **[J3]**.

5.6 Summary

In this chapter, different control strategies to avert loss of synchronization have been presented. At first, the PLL freeze method was presented, which freezes its state variables (frequency and phase) to the pre-fault values when a severe fault occurs. Despite this method being blind to phase-angle jumps, it was shown that only a negligible improvement could be achieved by correcting the phase-angle jump. Hence, this method works as a simple and very robust solution to deal with transient instability since an intra-fault operation point is always provided. Secondly, for more complex synchronization units for asymmetrical conditions, a frequency-lock was proposed for FLLs. This was shown to provide a globally asymptotically stable solution provided that an equilibrium point exists during the fault. Also, due to the equivalence between PLLs and FLLs, this method can be generalized for any synchronization structure to provide an infinite damping. After this, an improved current-reference injection method was proposed. This was based on a previously proposed method from the available literature, but with a proposed method for rapid impedance estimation, this method can now be applied in actual applications. This method is also proven globally asymptotically stable, and it always provides an equilibrium point during the fault, provided that the impedance estimation has a certain accuracy. Lastly, a grid-forming fault-mode control method was proposed to provide the robustness associated with the grid-forming structure with proper current limitation during grid faults. This method was compared to an existing solution where the grid-forming converter is switched to a grid-following structure during the fault, which clearly demonstrated the advantageous operation of the proposed grid-forming controller.

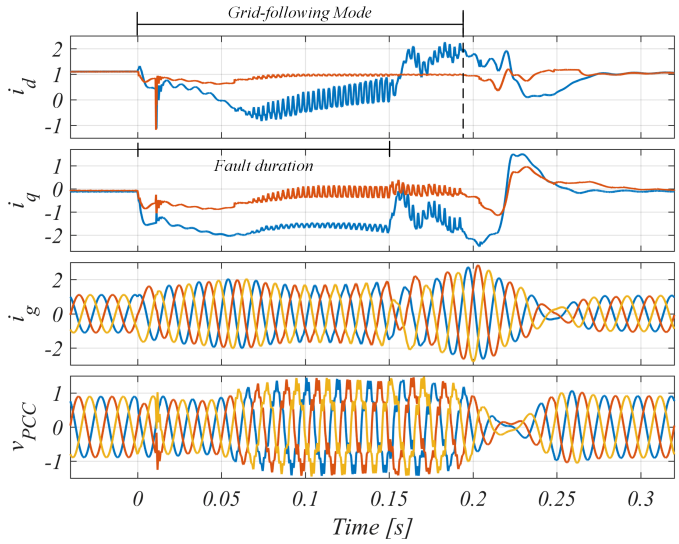

(a) Grid-following during fault [83].

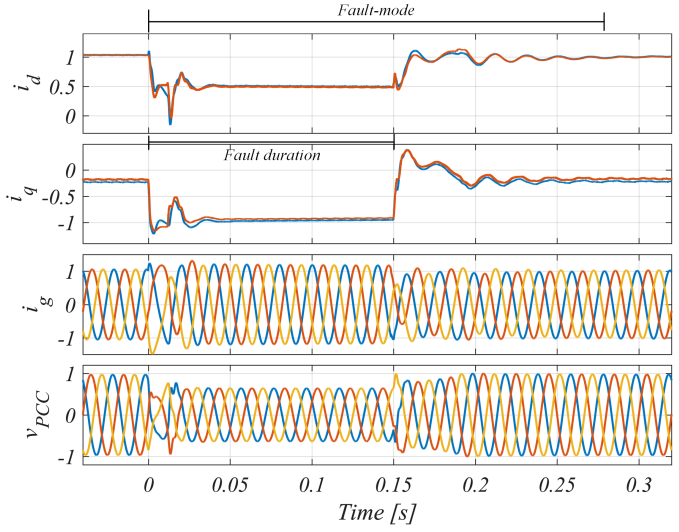

(b) Proposed grid-forming control.

Fig. 5.13: Simulated fault response during a symmetrical fault with a voltage magnitude of 0.3 pu with $SCR = 2$. For the dq-axes currents, the actual (blue) and the reference values (red) are visualized. Source: **[J3]**.

Related Publications

[C1] **M. G. Taul**, X. Wang, P. Davari and F. Blaabjerg, "Grid Synchronization of Wind Turbines during Severe Symmetrical Faults with Phase Jumps," in *Proc IEEE ECCE*, Portland, OR, USA, 2018, pp. 38-45.

Main contribution:
The performance of the frozen PLL structure under severe symmetrical faults is analyzed. A comprehensive simulation study is performed to disclose the performance of the frozen PLL compared to a structure where phase jumps are compensated. A mapping of when the frozen PLL can be applied for accurate instability prevention is given.

[J2] **M. G. Taul**, X. Wang, P. Davari and F. Blaabjerg, "Robust Fault Ride-Through of Converter-based Generation during Severe Faults with Phase Jumps," in *IEEE Trans. Ind. Appl*, vol. 56, no. 1, pp. 570-583, Jan.-Feb. 2020.

Main contribution:
An extension of **[C1]** is provided in this work. This includes analytical analysis of how phase-angle jumps during the fault influence the converter synchronization point. To that end, a robustness analysis of the PLL freeze method under grid faults with phase-angle jumps is performed, which concludes that the PLL freeze method is a simple and straight-forward strategy to cope with loss of synchronization.

[C5] **M. G. Taul**, X. Wang, P. Davari and F. Blaabjerg, "Frequency-Locked Frequency-Adaptive Loops for Enhanced Synchronization Stability of Grid-Following Converters during Grid Faults," submitted to *Proc. IEEE COMPEL*, Aalborg, Denmark, 2020, pp. x-x.

Main contribution:
As a practical implementation of a converter synchronization unit involves its ability to work under asymmetrical conditions, this paper proposes a control method that provides sufficient damping for any FLL-based synchronization structure provided that a stable operating point exists during the fault. To that end, the equivalence between the stationary-reference frame FLL and the SRF-PLL is given, which shows that the proposed method can be generalized to any synchronization method based on these principles.

[O1] R. E. Betz and **M. G. Taul**, "Identification of Grid Impedance During Severe Faults," in *Proc. IEEE ECCE*, Baltimore, MD, USA, 2019, pp. 1076-1082.

Main contribution:
By using the grid fault as a test impulse, a method for rapid impedance estimation is proposed and verified through simulation as well as experimentally. This method can be used for many different purposes and applications involving power-electronic converters in power systems.

[C4] **M. G. Taul**, R. E. Betz and F. Blaabjerg, "Rapid Impedance Estimation Algorithm for Mitigation of Synchronization Instability of Paralleled Converters under Grid Faults," submitted to *Proc. IEEE EPE*, Lyon, France, 2020, pp. x-x.

Main contribution:
By using the rapid impedance estimation algorithm proposed in **[O1]**, a previously proposed method that aligns the injected current vector based on the grid impedance is revisited. Now, with the impedance estimation algorithm, this globally asymptotically stable control method can be used for solving practical problems, since the strong assumption of the grid impedance to be known can now be removed. To that end, the proposed combined strategy is experimentally verified and it is identified that the method is robust towards estimation errors.

[J3] **M. G. Taul**, X. Wang, P. Davari and F. Blaabjerg, "Current Limiting Control with Enhanced Dynamics of Grid-Forming Converters during Fault Conditions," in *IEEE Journal Emerg. Sel. Topics Power Electron.*, 2019.

Main contribution:
Grid-forming converters are usually switched to grid-following structures during grid fault to perform a controllable limitation in the converter currents. However, such an approach makes the grid-forming converter losing its advantageous voltage-mode properties during the fault. This paper proposes an improved fault-mode grid-forming controller, which safely limits the converter current during the fault while keeping the robust performance associated with the grid-forming control.

Chapter 6

Conclusion

This chapter outlines the main findings and conclusions of this Ph.D. project. Additionally, the main contributions presented are highlighted, and further research perspectives are discussed.

6.1 Summary

This Ph.D. project seeks to perform research that can reduce the overall risk of transient instability and associated customer interruption cost of grid-connected converters operating under grid faults. This is done by focusing on how to model and assess the transient stability of power electronics-based converters to enhance the understanding of the instability phenomenon and improve the system robustness already in the design-phase. To that end, control methods with a practical and straight-forward countermeasure to transient instability have been proposed and revisited. A summary of each of the thesis' chapters is given in the following:

In *Chapter 1*, research gaps in the modeling and control of grid-connected converters and transient stability have been identified. These were used to formulate the motivation and research tasks of this Ph.D. project. The research tasks were divided into two subgroups. One for the tasks related to modeling and one with the tasks related to control. From this, the research questions and project objectives were identified, which were individually addressed in the following chapters. *Chapter 2* provided a complete and intuitive understanding of the instability phenomenon. Using a two-bus single-line diagram to represent the converter-to-grid system, a static current transfer limit (necessary stability condition) is identified, which clearly describes how and why the loss of synchronization occurs. This is based on steady-state conditions and, therefore, cannot capture the stability assessment related to the dynamical structure of the system. For that purpose, the PLL dynamics must be included as done for the quasi-static large-signal model. For this model, a destabilizing positive feedback loop is identified, caused by the voltage disturbance as a result of the currents injected by the converter itself.

The quasi-static large-signal model from *Chapter 2* assumed an either fully resistive or purely inductive grid. To remove this assumption, a reduced-order large-signal model that considers both the resistive and the inductive elements of the line impedances was proposed in *Chapter 3*. This includes a computationally efficient numerical formulation of the nonlinear problem, which can be rapidly solved hundreds of times to identify the stability boundary of the system and identify the sufficient critical damping. This model was developed for symmetrical fault conditions. However, as the vast majority of grid faults are asymmetrical, an extension of the reduced-order model was performed to be able to work under asymmetrical grid faults. This was done by developing a model in each sequence frame, which is coupled at the fault location, depending on the fault type of interest. Both the reduced-order model for the symmetrical and the asymmetrical cases are verified using an experimental test setup, revealing their accurate system representation.

Till this point, all the models and analyses presented consider a single-converter system. To improve this, the transient stability modeling of multi-converter systems was addressed in *Chapter 4*. Necessary stability conditions were derived for three distinct system configurations that serve to cover most multi-converter applications. Combining these conditions with the dynamics of the synchronization unit, a reduced-order large-signal model is proposed for each configuration. For a daisy-chain-configured system, where a non-negligible impedance exists between each converter, an aggregated reduced-order model is proposed to assess the large-signal synchronization stability of, e.g., a wind farm string. The Anholt wind farm was considered to verify the high accuracy of the transient stability assessment capability of the proposed aggregated model. To that end, the computational burden was reduced with a factor of 100 using the aggregated model, enabling even larger-scale system analysis.

From the presented models, it may be identified that either an equilibrium point does not exist during the fault or the system possess an insufficient amount of damping. In either cases, the system will experience transient instability if not properly controlled. Different controller strategies to prevent loss of synchronization was presented in *Chapter 5*. Common to all the revisited and proposed methods is that they should be competent in the instability prevention and simple in implementation. First, a PLL freezing strategy was presented. It was shown that this method, despite its unawareness to phase-angle jumps, resulted in a robust solution that always guarantees a stable operating point during the fault with an acceptable injection of currents cf. the LVRT requirements. Secondly, a frequency-lock was performed in the frequency-adaptive loop of FLLs to provide infinite system damping. This method was proven globally asymptotically stable, given the existence of an equilibrium point during the fault. In addition to changing the parameters of the PLL, a method which, based on the estimated grid impedance, aligns the injected current vector with the stable operating area was proposed. Compared to previous studies, this method has been made applicable for actual use since a rapid impedance estimation algorithm was proposed to perform the impedance estimation needed for the method to be functional. Also, this method is proven to be globally asymptotically stable, robust towards estimation errors, and it inherently provides a stable operating point for the faulted system. Lastly, the robust performance of grid-forming technology was used to enhance the

transient stability of grid-connected converters. A fault-mode grid-forming structure was proposed to ride through the fault while keeping its voltage-mode properties and providing an effective current limitation. Its effectiveness was verified and compared to a grid-forming structure that was switched to a PLL-synchronized converter during the fault. In summary, different strategies may be used to enhance the transient stability. Which one is better depends on the particular application at hand and the knowledge of the system.

6.2 Main Contributions of Thesis

The contributions are structured based on the list of research objectives from *Chapter 1*. The main contributions of this Ph.D. project are as follows:

Providing an in-depth understanding and description of the instability phenomenon occurring during grid faults for a single-converter system
An in-depth analysis and a physical understanding of the loss of synchronization phenomenon are given in *Chapter 2*. This lays the foundation for all the models and control methods presented and proposed in this Ph.D. project.

Development of reduced-order models of the synchronization process of a grid-following converter under symmetrical and asymmetrical grid faults
Accurate and computationally efficient reduced-order models for transient stability evaluation og single-converter systems are proposed in this Ph.D. project. This is done both under symmetrical and asymmetrical conditions. For analysis of asymmetrical grid faults, a generalized sequence-domain modeling framework is presented, which develops a reduced-order large-signal model that takes into account the sequence coupling at the fault location and dual-sequence converter current injection. Such reduced-order models can provide an efficient and accurate representation of the system dynamics, which may be conveniently applied for large-scale power electronics-based power system studies during grid faults.

A numerical approach for identification of stability boundary and critical damping of nonlinear PLL-synchronized systems
Based on the proposed reduced-order large-signal nonlinear model for single-converter systems, an efficient computation of phase portraits has been used to determine the critical sufficient PLL damping and area of attraction of the faulted system. A high accuracy in the estimated area of attraction is observed, which is verified against experimental results.

Development of aggregated reduced-order models for multi-converter systems
The proposed model-order reduction approach for single-converter systems is extended to multi-converter systems. This include derivations of necessary stability conditions for three descriptive system configurations. Reduced-order models are developed for each system configuration and verified through simulations. For a daisy-chain configured system used in e.g., in a wind farm collector system, an aggregated reduced-order model is proposed and compared to a string of the operating

Anholt wind farm. The computational burden is reduced with a factor of 100 using the proposed model, which facilitates larger-scale system analysis.

Enhanced and revisited control methods for transient stability improvement during severe grid faults
Several control methods, which provide an effective countermeasure to LOS while avoiding to introduce additional control loops, are proposed and revisited. These include:

- Showing that a PLL freezing method is indeed a robust and effective control method to avert LOS, also under phase-angle jumps.
- Proposing a frequency-lock for FLL-based synchronization units that provide infinite damping and guarantees system stability provided that an equilibrium point exists during the fault.
- Developing a rapid impedance estimation algorithm under grid faults to perform the estimates for aligning the converter current vector in order to ensure transient stability and a stable operating point during the fault.
- Proposing a grid-forming fault-mode controller, which keeps the robust voltage-mode properties during the fault while successfully limiting the converter currents. Using this, the grid-forming technology can be employed to enhance the power system transient stability.

6.3 Research Perspectives and Future Work

In addition to the research gaps addressed in this Ph.D. project, many other research perspectives can be chosen for future studies to improve the presented work and make it more general towards large interconnected systems with large deviations in employed control methods and parameters. Some of these perspectives and future work are summarized below.

1. Under severe grid faults, converters are obliged to inject nominal reactive current to support the local voltages. Due to this, it is assumed in this work that the outer power loops can be neglected during the fault since the current references are directly set according to the LVRT requirements. However, there may be scenarios where the outer power loops cannot be neglected or conditions where LOS may occur when the fault voltage magnitude is not extremely low. Therefore, including the impact and dynamics of the outer power loops and dc-link voltage controller is an important topic for future research.

2. In this Ph.D. project, it was encountered that when dealing with nonlinear trigonometric functions, that stability analysis through Lyapunov theory is difficult. Using the total system energy as a Lyapunov function candidate, it was not possible to determine whether this energy would dissipate to zero or not. Hence, developing better tools for building the Lyapunov function to perform stability assessment of nonlinear systems would be beneficial for this topic. To that end, approximations of the trigonometric functions using Taylor series

expansions or infinite series may be employed to provide an approximate analytical solution to the second-order nonlinear problem.

3. For the aggregated reduced-order modeling presented in this work, a homogeneous converter control and filter were assumed for the analysis. However, in a real operating condition, tolerances and uncertainties in passive components and the selection of different controller parameters may imply that this assumption is violated. Hence, the models for transient stability assessment should also allow for differences in control parameters and passive components.

4. In regards to the modeling and analysis of large-signal synchronization stability, it was described that the synchronization dynamics could be expressed in the same form as a synchronous machine. For large interconnected meshed networks, model-order reduction and system simplification are vital. For transient stability evaluation, the study of coupled nonlinear oscillators, system attraction boundaries, and the synchronization consensus in power systems has been widely performed. As shown in [118–123], the similarity between a Kuramoto oscillator model and the synchronization problem encountered in power system transient stability studies is impressive. Consequently, the Kuramoto model may be used to study the loss of synchronization of power system studies, including power-electronic grid-following converters. To that end, the damping and inertia parameters of the converter are no longer physical properties as for the synchronous machines. Therefore, these may be selected in a way that enhances the applicability of the Kuramoto oscillator approach for transient stability assessment.

5. The analysis and experimental verification presented in this Ph.D. project is performed on a small-scale low-power converter. Any influence and affections on the models and control methods when considering a realistic high-power system with different values for passive components and controller parameters should be analyzed. To that end, large-scale system analysis and validation could be performed on a hardware-in-the-loop test platform.
6. For the grid fault analyses performed in this work, the impact of the system protection including circuit breakers, have not been considered. It would be interesting to investigate how the protection influences the presented models and controller strategies.

7. The motivation for the models and control methods presented in this Ph.D. project is to enhance the overall security of supply of future power electronics-based power systems. Therefore, evaluating relevant system security indexes should be performed to identify to what extent the proposed models and control methods can improve the power system reliability.

References

[1] W. Li, *Risk Assessment Of Power Systems: Models, Methods, and Applications*, 1st ed. IEEE Press on Power Engineering, 2005, ISBN: 0-471-63168-X.

[2] E. Ebrahimzadeh, F. Blaabjerg, X. Wang, and C. L. Bak, "Dynamic resonance sensitivity analysis in wind farms," in *Proc. IEEE PEDG*, April 2017, pp. 1–5.

[3] R. Billinton and R. N. Allan, *Reliability Evaluation of Power Systems*, 2nd ed. Springer, 1996, ISBN: 978-1-4899-1862-8.

[4] S. Peyghami, P. Davari, M. Fotuhi-Firuzabad, and F. Blaabjerg, "Standard test systems for modern power system analysis: An overview," *IEEE Industrial Electronics Magazine*, vol. 13, no. 4, pp. 86–105, Dec 2019.

[5] A. Lucent, "Improving distribution grid reliability - leveraging communication networks to reduce caidi, saifi and saidi," *White Paper*, 2015.

[6] E. R. G. Nordic, "Nordic and baltic grid disturbance statictics 2017," 2017.

[7] L. Energy, "Poor power quality costs european business more than 150 billion a year," *European Power Quality Survey*, 2008.

[8] S. C. Vegunta and J. V. Milanovic, "Estimation of cost of downtime of industrial process due to voltage sags," *IEEE Trans. Power Del.*, vol. 26, no. 2, pp. 576–587, April 2011.

[9] W. Friedl, R. Vailati, M. Bollen, R. Görlich, R. Castel, D. Batic, O. Radovic, and A. Candela, "A european benchmarking of continuity of supply regulation," in *22nd International Conference and Exhibition on Electricity Distribution (CIRED 2013)*, 2013, pp. 1–4.

[10] A. Bahmanyar, S. Jamali, A. Estebsari, and E. Bompard, "A comparison framework for distribution system outage and fault location methods," *Electric Power Systems Research*, vol. 145, pp. 19–34, 2017.

[11] Set-up and challenges of germany's power grid. [Online]. Available: https://www.cleanenergywire.org/factsheets/set-and-challenges-germanys-power-grid

[12] T. Guardian. (2020) Three energy firms to pay 10.5m for failings over august blackout. [Online]. Available: https://www.theguardian.com/business/2020/jan/03/three-energy-firms-to-pay-for-failings-over-august-blackout

[13] H. N. V. Pico and B. B. Johnson, "Transient stability assessment of multi-machine multi-converter power systems," *IEEE Transactions on Power Systems*, vol. 34, no. 5, pp. 3504–3514, 2019.

[14] N. A. E. R. C. (NERC), "1,200 mw fault induced solar photovoltaic resource interruption disturbance report."

[15] ——, "900 mw fault induced solar photovoltaic resource interruption disturbance report."

[16] Q. C. Zhong, "Virtual synchronous machines: A unified interface for grid integration," *IEEE Power Electron. Mag.*, vol. 3, no. 4, pp. 18–27, Dec 2016.

[17] J. L. Agorreta, M. Borrega, J. López, and L. Marroyo, "Modeling and control of n-paralleled grid-connected inverters with lcl filter coupled due to grid impedance in pv plants," *IEEE Trans. Power Electron.*, vol. 26, no. 3, pp. 770–785, March 2011.

[18] A. Ulbig, T. S. Borsche, and G. Andersson, "Impact of low rotational inertia on power system stability and operation," *IFAC Proceedings Volumes*, vol. 47, no. 3, pp. 7290 – 7297, 2014, 19th IFAC World Congress. [Online]. Available: http://www.sciencedirect.com/science/article/pii/S1474667016427618

[19] Q. C. Zhong, "Power-electronics-enabled autonomous power systems: Architecture and technical routes," *IEEE Trans. Ind. Electron.*, vol. 64, no. 7, pp. 5907–5918, July 2017.

[20] W. Zhang, A. M. Cantarellas, J. Rocabert, A. Luna, and P. Rodriguez, "Synchronous power controller with flexible droop characteristics for renewable power generation systems," *IEEE Trans. Sust. Energy*, vol. 7, no. 4, pp. 1572–1582, Oct. 2016.

[21] J. Jia, G. Yang, and A. H. Nielsen, "A review on grid-connected converter control for short-circuit power provision under grid unbalanced faults," *IEEE Trans. Power Del.*, vol. 33, no. 2, pp. 649–661, April 2018.

[22] N. Bottrell and T. C. Green, "Comparison of current-limiting strategies during fault ride-through of inverters to prevent latch-up and wind-up," *IEEE Trans. Power Electron.*, vol. 29, no. 7, pp. 3786–3797, July 2014.

[23] J. Conroy and R. Watson, "Aggregate modelling of wind farms containing full-converter wind turbine generators with permanent magnet synchronous machines: transient stability studies," *IET Renewable Power Generation*, vol. 3, no. 1, pp. 39–52, March 2009.

[24] N. Bottrell and T. C. Green, "An impedance-based method for the detection of over-load and network faults in inverter interfaced distributed generation," in *2013 15th European Conference on Power Electronics and Applications (EPE)*, Sep. 2013, pp. 1–10.

[25] X. Wang, L. Harnefors, F. Blaabjerg, and P. C. Loh, "A unified impedance model of voltage-source converters with phase-locked loop effect," in *Proc. IEEE ECCE*, Sept 2016, pp. 1–8.

[26] Y. Wang, X. Wang, Z. Chen, and F. Blaabjerg, "Small-signal stability analysis of inverter-fed power systems using component connection method," *IEEE Trans. Smart Grid*, vol. 9, no. 5, pp. 5301–5310, Sep. 2018.

[27] E. Ebrahimzadeh, F. Blaabjerg, X. Wang, and C. Leth Bak, "Efficient approach for harmonic resonance identification of large wind power plants," in *Proc. IEEE PEDG*, June 2016, pp. 1–7.

[28] X. Wang and F. Blaabjerg, "Harmonic stability in power electronic based power systems: Concept, modeling, and analysis," *IEEE Trans. Smart Grid*, vol. 10, no. 3, pp. 2858–2870, 2019.

[29] C. Wan, M. Huang, C. K. Tse, and X. Ruan, "Stability of interacting grid-connected power converters," in *2014 IEEE International Symposium on Circuits and Systems (ISCAS)*, June 2014, pp. 2668–2671.

[30] P. Dang, J. Petzoldt, and T. Ellinger, "Stability analysis of multi-parallel apf systems," in *Proceedings of the 2011 14th European Conference on Power Electronics and Applications*, Aug 2011, pp. 1–8.

[31] X. Wang, F. Blaabjerg, M. Liserre, Z. Chen, J. He, and Y. Li, "An active damper for stabilizing power-electronics-based ac systems," *IEEE Trans. Power Electron.*, vol. 29, no. 7, pp. 3318–3329, July 2014.

[32] B. Kroposki, B. Johnson, Y. Zhang, V. Gevorgian, P. Denholm, B. M. Hodge, and B. Hannegan, "Achieving a 100 % renewable grid: Operating electric power systems with extremely high levels of variable renewable energy," *IEEE Power Energy Mag.*, vol. 15, no. 2, pp. 61–73, March 2017.

[33] E. Ebrahimzadeh, F. Blaabjerg, X. Wang, and C. L. Bak, "Modeling and identification of harmonic instability problems in wind farms," in *Proc. IEEE ECCE*, Sep. 2016, pp. 1–6.

[34] X. Wang, F. Blaabjerg, and W. Wu, "Modeling and analysis of harmonic stability in an ac power-electronics-based power system," *IEEE Trans. Power Electron.*, vol. 29, no. 12, pp. 6421–6432, Dec 2014.

[35] D. Yang, X. Wang, and F. Blaabjerg, "Sideband harmonic instability of paralleled inverters with asynchronous carriers," *IEEE Trans. Power Electron.*, vol. 33, no. 6, pp. 4571–4577, June 2018.

[36] P. Kundur, *Power System Stability and Control*, 1st ed. McGraw-Hill, Inc., 1994, ISBN: 978-0-07-035958-X.

[37] J. O'Sullivan, A. Rogers, D. Flynn, P. Smith, A. Mullane, and M. O'Malley, "Studying the maximum instantaneous non-synchronous generation in an island system—frequency stability challenges in ireland," *IEEE Trans. Power Syst.*, vol. 29, no. 6, pp. 2943–2951, 2014.

[38] K. Creighton, M. McClure, R. Skillen, J. O'Higgens, and T. McCartan, "Increased wind generation in ireland and northern ireland and the impact on rate of change of frequency," *Eirgrid Projects*.

[39] Nahid-Al-Masood, N. Modi, and R. Yan, "Low inertia power systems: Frequency response challenges and a possible solution," in *2016 Australasian Universities Power Engineering Conference (AUPEC)*, 2016, pp. 1–6.

[40] L. H. Kocewiak, B. L. . Kramer, O. Holmstrøm, K. H. Jensen, and L. Shuai, "Resonance damping in array cable systems by wind turbine active filtering in large offshore wind power plants," *IET Renewable Power Generation*, vol. 11, no. 7, pp. 1069–1077, 2017.

[41] N. Tleis, *Power Systems Modelling and Fault Analysis - Theory and Practice*, 1st ed. Elsevier, 2008, ISBN: 978-0-7506-8074-5.

[42] F. Blaabjerg, R. Teodorescu, M. Liserre, and A. V. Timbus, "Overview of control and grid synchronization for distributed power generation systems," *IEEE Trans. Ind. Electron.*, vol. 53, no. 5, pp. 1398–1409, Oct 2006.

[43] Ö. Göksu, R. Teodorescu, C. L. Bak, F. Iov, and P. C. Kjær, "Instability of wind turbine converters during current injection to low voltage grid faults and PLL frequency based stability solution," *IEEE Trans. Power Syst.*, vol. 29, no. 4, pp. 1683–1691, July 2014.

[44] J. Hu, B. Wang, W. Wang, H. Tang, Y. Chi, and Q. Hu, "Small signal dynamics of DFIG-based wind turbines during riding through symmetrical faults in weak AC grid," *IEEE Trans. Energy Convers.*, vol. 32, no. 2, pp. 720–730, June 2017.

[45] N. R. Ullah, T. Thiringer, and D. Karlsson, "Voltage and transient stability support by wind farms complying with the e.on netz grid code," *IEEE Trans. Power Syst.*, vol. 22, no. 4, pp. 1647–1656, Nov 2007.

[46] M. Kayikci and J. V. Milanovic, "Reactive power control strategies for DFIG-based plants," *IEEE Trans. Energy Convers.*, vol. 22, no. 2, pp. 389–396, June 2007.

[47] T. Hadjina and M. Baotić, "Optimization approach to power control of grid side converters during voltage sags," in *Proc. IEEE ICIT*, March 2015, pp. 1106–1111.

[48] X. Du, Y. Wu, S. Gu, H. M. Tai, P. Sun, and Y. Ji, "Power oscillation analysis and control of three-phase grid-connected voltage source converters under unbalanced grid faults," *IET Power Electronics*, vol. 9, no. 11, pp. 2162–2173, 2016.

[49] X. Zhao, J. M. Guerrero, M. Savaghebi, J. C. Vasquez, X. Wu, and K. Sun, "Low-voltage ride-through operation of power converters in grid-interactive microgrids by using negative-sequence droop control," *IEEE Trans. Power Electron.*, vol. 32, no. 4, pp. 3128–3142, April 2017.

[50] S. Omar, A. Helal, and I. Elarabawy, "Stator voltage sensorless DFIG with low voltage ride-through capability using series and parallel grid side converters," in *Proc. IEEE IREC*, March 2016, pp. 1–6.

[51] J. I. Garcia, J. I. Candela, A. Luna, and P. Catalan, "Grid synchronization structure for wind converters under grid fault conditions," in *IECON 2016 - 42nd Annual Conference of the IEEE Industrial Electronics Society*, Oct 2016, pp. 2313–2318.

[52] A. Mojallal and S. Lotfifard, "Enhancement of grid connected pv arrays fault ride through and post fault recovery performance," *IEEE Trans. Smart Grid*, vol. 10, no. 1, pp. 546–555, Jan 2019.

[53] E. Afshari, B. Farhangi, Y. Yang, and S. Farhangi, "A low-voltage ride-through control strategy for three-phase grid-connected pv systems," in *Proc. IEEE PECI*, Feb 2017, pp. 1–6.

[54] I. Erlich, F. Shewarega, S. Engelhardt, J. Kretschmann, J. Fortmann, and F. Koch, "Effect of wind turbine output current during faults on grid voltage and the transient stability of wind parks," in *Proc. IEEE PESGM*, July 2009, pp. 1–8.

[55] D. Dong, J. Li, D. Boroyevich, P. Mattavelli, I. Cvetkovic, and Y. Xue, "Frequency behavior and its stability of grid-interface converter in distributed generation systems," in *Proc. IEEE APEC*, Feb 2012, pp. 1887–1893.

[56] B. Weise, "Impact of k-factor and active current reduction during fault-ride-through of generating units connected via voltage-sourced converters on power system stability," *IET Renewable Power Generation*, vol. 9, no. 1, pp. 25–36, 2015.

[57] Q. Hu, J. Hu, H. Yuan, H. Tang, and Y. Li, "Synchronizing stability of DFIG-based wind turbines attached to weak AC grid," in *Proc. IEEE ICEMS*, Oct 2014, pp. 2618–2624.

[58] D. Dong, B. Wen, D. Boroyevich, P. Mattavelli, and Y. Xue, "Analysis of phase-locked loop low-frequency stability in three-phase grid-connected power converters considering impedance interactions," *IEEE Trans. Ind. Electron.*, vol. 62, no. 1, pp. 310–321, Jan 2015.

[59] J. A. Suul, S. D'Arco, P. Rodríguez, and M. Molinas, "Impedance-compensated grid synchronisation for extending the stability range of weak grids with voltage source converters," *IET Generation, Transmission Distribution*, vol. 10, no. 6, pp. 1315–1326, 2016.

[60] J. Hu, Q. Hu, B. Wang, H. Tang, and Y. Chi, "Small signal instability of PLL-synchronized type-4 wind turbines connected to high-impedance AC grid during LVRT," *IEEE Trans. Energy Conv.*, vol. 31, no. 4, pp. 1676–1687, Dec 2016.

[61] S. Ma, H. Geng, L. Liu, G. Yang, and B. C. Pal, "Grid-synchronization stability improvement of large scale wind farm during severe grid fault," *IEEE Trans. Power Syst.*, vol. 33, no. 1, pp. 216–226, Jan 2018.

[62] H. Wu and X. Wang, "Transient stability impact of the phase-locked loop on grid-connected voltage source converters," in *IEEE Proc. ECCE Asia*, May 2018, pp. 2673–2680.

[63] ——, "An adaptive phase-locked loop for the transient stability enhancement of grid-connected voltage source converters," in *Proc. IEEE ECCE*, Sep. 2018, pp. 5892–5898.

[64] ——, "Transient angle stability analysis of grid-connected converters with the first-order active power loop," in *Proc. IEEE APEC*, March 2018, pp. 3011–3016.

[65] X. He, H. Geng, and G. Yang, "Synchronization stability analysis of grid-tied power converters under severe grid voltage sags," in *Proc. IEEE PEAC*, Nov 2018, pp. 1–6.

[66] S. Ma, H. Geng, L. Liu, G. Yang, and B. C. Pal, "Grid-synchronization stability improvement of large scale wind farm during severe grid fault," *IEEE Trans. Power Syst.*, vol. 33, no. 1, pp. 216–226, Jan 2018.

[67] H. Geng, L. Liu, and R. Li, "Synchronization and reactive current support of PMSG-based wind farm during severe grid fault," *IEEE Trans. Sust. Energy*, vol. 9, no. 4, pp. 1596–1604, Oct 2018.

[68] X. He, H. Geng, R. Li, and B. C. Pal, "Transient stability analysis and enhancement of renewable energy conversion system during LVRT," *IEEE Trans. Sust. Energy*, pp. 1–1, 2019.

[69] H. Wu and X. Wang, "Design-oriented transient stability analysis of pll-synchronized voltage-source converters," *IEEE Trans. Power Electron.*, vol. 35, no. 4, pp. 3573–3589, April 2020.

[70] ——, "Design-oriented transient stability analysis of grid-connected converters with power synchronization control," *IEEE Trans. Ind. Electron.*, vol. 66, no. 8, pp. 6473–6482, Aug 2019.

[71] V. Kaura and V. Blasko, "Operation of a phase locked loop system under distorted utility conditions," *IEEE Trans. Ind. Appl.*, vol. 33, no. 1, pp. 58–63, Jan 1997.

[72] R. Teodorescu, M. Liserre, and P. Rodriguez, *Grid Converters for Photovoltaic and Wind Power Systems*, 1st ed. Wiley, 2011, ISBN: 9780470057513.

[73] P. Rodriguez, A. Luna, I. Candela, R. Mujal, R. Teodorescu, and F. Blaabjerg, "Multiresonant frequency-locked loop for grid synchronization of power converters under distorted grid conditions," *IEEE Trans. Ind. Electron.*, vol. 58, no. 1, pp. 127–138, Jan 2011.

[74] P. Rodriguez, A. Luna, R. S. Munoz-Aguilar, I. Etxeberria-Otadui, R. Teodorescu, and F. Blaabjerg, "A stationary reference frame grid synchronization system for three-phase grid-connected power converters under adverse grid conditions," *IEEE Trans. Power Electron.*, vol. 27, no. 1, pp. 99–112, Jan 2012.

[75] R. Teodorescu and F. Blaabjerg, "Flexible control of small wind turbines with grid failure detection operating in stand-alone and grid-connected mode," *IEEE Trans. Power Electron.*, vol. 19, no. 5, pp. 1323–1332, Sept 2004.

[76] V. Diedrichs, A. Beekmann, and S. Adloff, "Loss of (angle) stability of wind power plants - the underestimated phenomenon in case of very low circuit ratio," *10th International Workshop on Large-Scale Integration of Wind Power into Power Systems as well as on Transmission Networks for Offshore Wind Farms*, pp. 395–402, Jul. 2011.

[77] R. Lasseter, Z. Chen, and D. Pattabiraman, "Grid-forming inverters: A critical asset for the power grid," *IEEE J. Emerg. Sel. Topics Power Electron.*, pp. 1–1, 2019.

[78] L. Zhang, L. Harnefors, and H. P. Nee, "Power-synchronization control of grid-connected voltage-source converters," *IEEE Trans. Power Syst.*, vol. 25, no. 2, pp. 809–820, May 2010.

[79] A. Rodríguez-Cabero, J. Roldán-Pérez, and M. Prodanovic, "Virtual impedance design considerations for virtual synchronous machines in weak grids," *IEEE Trans. Emerg. Sel. Topics Power Electron.*, pp. 1–1, 2019.

[80] L. Huang, H. Xin, H. Yang, Z. Wang, and H. Xie, "Interconnecting very weak ac systems by multiterminal vsc-hvdc links with a unified virtual synchronous control," *IEEE Trans. Emerg. Sel. Topics Power Electron.*, vol. 6, no. 3, pp. 1041–1053, Sep. 2018.

[81] S. Mukherjee, P. Shamsi, and M. Ferdowsi, "Improved virtual inertia based control of a grid connected voltage source converter with fault ride-through ability," in *Proc. IEEE NAPS*, Sept 2016, pp. 1–5.

[82] K. O. Oureilidis and C. S. Demoulias, "A fault clearing method in converter-dominated microgrids with conventional protection means," *IEEE Trans. Power Electron.*, vol. 31, no. 6, pp. 4628–4640, June 2016.

[83] K. Shi, W. Song, P. Xu, R. Liu, Z. Fang, and Y. Ji, "Low-voltage ride-through control strategy for a virtual synchronous generator based on smooth switching," *IEEE Access*, vol. 6, pp. 2703–2711, 2018.

[84] M. Lu, X. Wang, P. C. Loh, and F. Blaabjerg, "Resonance interaction of multiparallel grid-connected inverters with lcl filter," *IEEE Trans. Power Electron.*, vol. 32, no. 2, pp. 894–899, Feb 2017.

[85] L. P. Kunjumuhammed, B. C. Pal, C. Oates, and K. J. Dyke, "The adequacy of the present practice in dynamic aggregated modeling of wind farm systems," *IEEE Trans. Sust. Energy*, vol. 8, no. 1, pp. 23–32, Jan 2017.

[86] N. Nimpitiwan, G. T. Heydt, R. Ayyanar, and S. Suryanarayanan, "Fault current contribution from synchronous machine and inverter based distributed generators," *IEEE Trans. Power Del.*, vol. 22, no. 1, pp. 634–641, Jan 2007.

[87] Y. Gu, N. Bottrell, and T. C. Green, "Reduced-order models for representing converters in power system studies," *IEEE Trans. Power Electron.*, vol. 33, no. 4, pp. 3644–3654, April 2018.

[88] C. M. Rergis, A. R. Messina, and R. J. Betancourt, "Fourier-based accurate reduced-order model for linear power systems applications," in *2016 IEEE PES Transmission Distribution Conference and Exposition-Latin America (PES T D-LA)*, Sep. 2016, pp. 1–6.

[89] S. Ghosh, N. Senroy, and S. Kamalasadan, "Reduced order modeling of wind farms for inclusion in large power system simulations for primary frequency response application," in *2014 North American Power Symposium (NAPS)*, Sep. 2014, pp. 1–6.

[90] L. P. Kunjumuhammed, B. C. Pal, C. Oates, and K. J. Dyke, "Electrical oscillations in wind farm systems: Analysis and insight based on detailed modeling," *IEEE Trans. Sust. Energy*, vol. 7, no. 1, pp. 51–62, Jan 2016.

[91] A. M. S. Al-bayati, F. Mancilla-David, and J. L. Domínguez-Garcíal, "Aggregated models of wind farms: Current methods and future trends," in *2016 North American Power Symposium (NAPS)*, Sep. 2016, pp. 1–6.

[92] A. Sangwongwanich, "Grid-Friendly High-Reliability Photovoltaic Systems," Ph.D. dissertation, Faculty of Engineering and Science at Aalborg University, 2018.

[93] P. M. Anderson and A. A. Fouad, *Power System Control and Stability*, 2003.

[94] J. Z. Zhou, H. Ding, S. Fan, Y. Zhang, and A. M. Gole, "Impact of short-circuit ratio and phase-locked-loop parameters on the small-signal behavior of a VSC-HVDC converter," *IEEE Trans. Power Del.*, vol. 29, no. 5, pp. 2287–2296, Oct 2014.

[95] H. Berndt, M. Hermann, H. D. Kreye, R. Reinisch, U. Scherer, and J. Vanzetta, "Transmissioncode 2007 - network and system rules of the german transmission system operators," Verband der Netzbetreiber, Tech. Rep., 2007.

[96] Ö. Göksu, "Control of Wind Turbines during Symmetrical and Asymmetrical Grid Faults," Ph.D. dissertation, Faculty of Engineering and Science at Aalborg University, 2012.

[97] K. Lentijo and D. F. Opila, "Minimizing inverter self-synchronization due to reactive power injection on weak grids," in *Proc. IEEE ECCE*, Sept 2015, pp. 1136–1142.

[98] J.-J. E. Slotine and W. Li, *Applied Nonlinear Control*, 1st ed. Pearson Educational, 1991, ISBN: 0-13-040890-5.

[99] S. H. Strogatz, "Nonlinear dynamics and chaos: With applications to physics, biology, chemistry, and engineering." Perseus Books, 1994, ch. 6, pp. 145–163, ISBN: 0-201-54344-3.

[100] S. Golestan, J. M. Guerrero, J. C. Vasquez, A. M. Abusorrah, and Y. Al-Turki, "A study on three-phase FLLs," *IEEE Trans. Power Electron.*, vol. 34, no. 1, pp. 213–224, Jan 2019.

[101] VDE, "VDE-AR-N 4110: Technical requirements for the connection and operation of customer installations to the medium-voltage network (TCC medium-voltage)," 2017.

[102] ——, "VDE-AR-N 4120: Technical requirements for the connection and operation of customer installations to the high-voltage network (TCC high-voltage)," 2015.

[103] S. Shah and P. Sensarma, "Auto-synchronization of lc filter based front-end converter with parallel inverters based weak distorted island grid using voltage injection," in *IECON 2012 - 38th Annual Conference on IEEE Industrial Electronics Society*, Oct 2012, pp. 3388–3393.

[104] B. Wen, D. Dong, D. Boroyevich, R. Burgos, P. Mattavelli, and Z. Shen, "Impedance-based analysis of grid-synchronization stability for three-phase paralleled converters," *IEEE Trans. Power Electron.*, vol. 31, no. 1, pp. 26–38, Jan 2016.

[105] R. Rosso, M. Andresen, S. Engelken, and M. Liserre, "Analysis of the interaction among power converters through their synchronization mechanism," *IEEE Trans. Power Electron.*, vol. 34, no. 12, pp. 12 321–12 332, Dec 2019.

[106] L. Huan, H. Xin, W. Dong, and F. Dörfler, "Impacts of grid structure on pll-synchronization stability of converter-integrated power systems," *arXiv:1903.05489v2*, Nov 2019.

[107] D. Dong, B. Wen, P. Mattavelli, D. Boroyevich, and Y. Xue, "Grid-synchronization modeling and its stability analysis for multi-paralleled three-phase inverter systems," in *IEEE Proc. APEC*, March 2013, pp. 439–446.

[108] J. Zhao, M. Huang, and X. Zha, "Transient stability analysis of grid-connected vsis via pll interaction," in *2018 IEEE International Power Electronics and Application Conference and Exposition (PEAC)*, Nov 2018, pp. 1–6.

[109] J. Martínez-Turégano, S. Añó-Villalba, G. Chaques-Herraiz, S. Bernal-Perez, and R. Blasco-Gimenez, "Model aggregation of large wind farms for dynamic studies," in *IECON 2017 - 43rd Annual Conference of the IEEE Industrial Electronics Society*, Oct 2017, pp. 316–321.

[110] Xunwen Su, Yunbo Liu, Haiming Song, and Dianguo Xu, "Comparison between the two equivalent methods of collector system for wind farms," in *2015 International Conference on Estimation, Detection and Information Fusion (ICEDIF)*, Jan 2015, pp. 354–358.

[111] E. Muljadi, C. P. Butterfield, A. Ellis, J. Mechenbier, J. Hochheimer, R. Young, N. Miller, R. Delmerico, R. Zavadil, and J. C. Smith, "Equivalencing the collector system of a large wind power plant," in *2006 IEEE Power Engineering Society General Meeting*, 2006, pp. 9 pp.–.

[112] L. H. Kocewiak, "Harmonics in large offshore wind farms," Ph.D. dissertation, Faculty of Engineering and Science at Aalborg University, 2012.

[113] C. F. Jensen, "Harmonic background amplification in long asymmetrical high voltage cable systems," *Electric Power Systems Research*, vol. 160, pp. 292 – 299, 2018.

[114] J. K. Barre, "Method and apparatus for controlling a power converter during low (zero)-voltage ride-through conditions," European Patent EP 2 652 858 B1, Oct. 11, 2017.

[115] M. Altin, Ö. Göksu, P. Sørensen, A. Morales, J. Fortmann, and F. J. Buendia, "Phase angle calculation dynamics of type-4 wind turbines in rms simulations during severe voltage dips," *IET Renewable Power Generation*, vol. 10, no. 8, pp. 1069–1186, 2016.

[116] T. Paulraj and P. Rajkumar, "Voltage unbalance mitigation using positive sequence series compensator," *IOSR Journal of Electrical and Electronics Engineering*, vol. 9, no. 3, pp. 98–103, 2014.

[117] A. D. Paquette and D. M. Divan, "Virtual impedance current limiting for inverters in microgrids with synchronous generators," *IEEE Trans. Ind. Appl.*, vol. 51, no. 2, pp. 1630–1638, March 2015.

[118] S. H. Strogatz, "From kuramoto to crawford: exploring the onset of synchronization in populations of coupled oscillators," *Physica. D, Nonlinear Phenomena*, vol. 143, pp. 1–20, 2000.

[119] J. W. Simpson-Porco, F. Dörfler, and F. Bullo, "Droop-controlled inverters are kuramoto oscillators," vol. 45, pp. 264–269, 2012.

[120] F. Dörfler, M. Chertkov, and F. Bullo, "Synchronization in complex oscillator networks and smart grids," *Proceedings of the National Academy of Sciences*, vol. 110, no. 6, pp. 2005–2010, 2013. [Online]. Available: https://www.pnas.org/content/110/6/2005

[121] F. Dörfler, M. Chertkov, and F. Bullo, "Synchronization assessment in power networks and coupled oscillators," in *2012 IEEE 51st IEEE Conference on Decision and Control (CDC)*, Dec 2012, pp. 4998–5003.

[122] F. Dörfler and F. Bullo, "Synchronization and transient stability in power networks and non-uniform kuramoto oscillators," in *SIAM Journal on Control and Optimization*, vol. 50, June 2012, pp. 1616–1642.

[123] J. Dragon, M. Coumont, and J. Hanson, "Applicability of non-uniform kuramoto oscillators to transient stability analysis - a power systems perspective," in *2015 European Control Conference (ECC)*, July 2015, pp. 229–234.

ISSN (online): 2446-1636
ISBN (online): 978-87-7210-641-0 AALBORG UNIVERSITY PRESS